Human *FN1* is regulated by the heat-shock response

A thesis submitted in fulfilment of the requirements for the degree of

Doctor of Philosophy (PhD)

of

Rhodes University

Karim Dhanani

Department of Biochemistry and Microbiology

January 2015

Abstract

Heat shock protein 90 (Hsp90) and heat shock factors (HSFs) are known to be involved in the epigenetic regulation of several fundamental oncogenic genes. Fibronectin (FN) is an extracellular matrix (ECM) glycoprotein which plays key roles in cell adhesion and migration. Hsp90 binds directly to FN and Hsp90 inhibition has been shown to regulate FN protein levels and matrix formation. Where inhibition of Hsp90 with a C-terminal inhibitor (novobiocin) induced the loss of FN matrix, treatment with an N-terminal inhibitor (geldanamycin) increased FN matrix levels. GA treatment induced a strong dose and time dependent increase in *FN1* promoter activity and increased total FN mRNA respectively. By contrast, NOV showed no increase in the promoter activity and no change in the expression of FN mRNA. As GA is known to induce the stress response, we investigated the relationship between the cell stress machinery and the transcriptional regulation of FN. Three putative heat shock elements (HSEs) were identified in the *FN1* promoter. The loss of two of the three identified putative HSEs resulted in a loss in the basal transcriptional activity of the *FN1* promoter in our reporter model. This was in addition to the loss of the induction of transcriptional activity with GA treatment observed with the full-length promoter. Binding of HSF1 to one of the putative HSEs, which was identified as potentially functional from the truncation analysis, was confirmed using ChIP. The occupancy of this HSE by HSF1 was shown to increase with GA treatment. These data support the hypothesis that *FN1* is a functional HSF1 target gene. The 5' promoter regions of seven additional ECM protein encoding genes were analysed and mRNA levels were detected by quantitative RT-PCR upon treatment with GA. Collagen 4 $\alpha 2$ and laminin $\beta 3$ mRNA were found to increase in the presence of GA, whereas collagen 4 $\alpha 3$ and osteopontin showed no change. Similarly to *FN1*, these data

indicate that a subset of ECM genes may be under the regulation of the HSF1 mediated heat-shock response. This may have implications for our understanding of ECM dynamics in cancer, where the clinical application of Hsp90 inhibitors is intended. Additionally, our data provide a potential underpinning for the role of the HSF1 mediated heat-shock response in several fibrotic and metabolic stress related pathologies.

Declaration

I herewith declare that I have produced this thesis without the prohibited assistance of third parties and without making use of aids other than those specified; notions taken over directly or indirectly from other sources have been identified as such. This thesis has not previously been presented in identical or similar form to any other South African or foreign examination board.

The thesis work was conducted from January 2012 to December 2014 under the supervision of Dr Adrienne Edkins at Rhodes University.

Grahamstown, 6140
South Africa

Acknowledgements

I would like to acknowledge the following people without whom this work would not have been conducted: Dr Adrienne Edkins for her dedication to professional and rigorous research which is an example to the group under her leadership. We disproportionately benefit from her tireless support. The members of the BioBRU research group and especially Dr Jo-Anne De la Mare, who create an enjoyable and positive working environment every day. The Department of Biochemistry & Microbiology, and particularly Sagaran Abboo and Margot Brooks for their kind assistance and guidance of every student and eventual researcher. My partner Isabel for providing daily motivation and a horizon to work towards. Finally my parents, without whom I would never have considered, let alone reached, the first day of University.

Contents

List of Figures

List of Tables

List of Abbreviations

17-AAG 17-N-Allylamino-17- demethoxygeldanamycin (Tanespimycin)

17-DMAG 17-Dimethylaminoethylamino-17-demethoxygeldanamycin

ACTB Actin beta

AEBSF 4- benzenesulfonyl fluoride hydrochloride

AKT Alpha serine/threonine-protein kinase

AMP Adenosine monophosphate

AMPK 5' AMP-activated protein kinase

ANOVA Analysis of variance

AP-1 Activator protein 1

ATP Adenosine triphosphate

BLAST The Basic Local Alignment Search Tool

BLASTn Nucleotide BLAST

Bp Base pair

BSA Bovine serum albumin

CAF Carcinoma associated fibroblasts

Cdc37 Cell division cycle 37

cDNA Complementary DNA

ChIP Chromatin immunoprecipitation

COL4A2 Collagen, type IV, alpha 2

COL4A3 Collagen, type IV, alpha 3

COX-2 Cyclooxygenase 2

CRE cAMP response element

Cyp40 Cyclophilin 40

D2A1 Mouse breast cancer cells

DMEM Dulbecco's Modified Eagle's Medium

DMSO Dimethyl sulfoxide

DNA Deoxyribonucleic acid

DNAseI Deoxyribonuclease 1

DTT Dithiothreitol

ECM Extracellular matrix

ED-A Extradomain A

ED-B Extradomain B

EDTA Ethylene-diamine-tetraacetic acid

ELMO1 Engulfment and cell motility protein 1

ELN Elastin

EMSA Electrophoretic mobility shift assay

ERK Extracellular-signal-regulated kinases

EV Empty vector

FAK Focal adhesion kinase

FBS Fetal bovine serum

FKBP12 FK506/rapamycin binding protein

FN Fibronectin

FUT4 Fucosyltransferase 4

GA Geldanamycin

GAPDH Glyceraldehyde-3-phosphate dehydrogenase

GEO Gene expression omnibus

GHKL (Gyrase, Hsp90, Histidine Kinase, MutL

Grp94 Glucose regulated protein 94 kDa

GTPase Guanosine triphosphate hydrolysis enzyme

H3 Histone 3

HCC Hepatocellular carcinoma

HEK293FT Human embryonic kidney 293 cells

HeLa Helacyton gartleri: cervical cancer cell line

HER-2 Human epidermal growth factor receptor 2

HIF1A Hypoxia-inducible factor 1-alpha

HOP Hsp70-Hsp90 organising protein

HR Heptad repeat

HRP Horseradish peroxidase

HPRT1 Hypoxanthine phosphoribosyltransferase 1

Hs578T Tripple negative breast cancer cells derived from cells taken from A.J. Hackett

HSF Heat shock factor

HSF1 Heat shock factor 1

HSP Heat shock protein

Hsp27 Heat shock protein 27 kDa

Hsp40 Heat shock protein 40 kDa

Hsp70 Heat shock protein 70 kDa

Hsp90 Heat shock protein 90 kDa

HSP90AA1 Heat shock protein 90kDa alpha

HSP90AB1 Heat shock protein 90kDa alpha

HSPA1A Heat shock 70kDa protein 1A

HSPB1 Heat shock 27kDa protein 1

IC50 Half maximal inhibitory concentration

IF Immunofluorescence

IgG Immunoglobulin G

III9 Fibronectin type III repeat 9

IIICS Fibronectin type III variable region

IV Intravenous

LAMB3 Laminin Beta 3

LAMC2 Laminin gamma 2

LEF-TCF Lymphoid enhancer-binding factor/Transcription factor

LRP Lipoprotein receptor-related proteins

MAPK Mitogen-activated protein kinases

MBF Macrobiophotonics

MEF Murine embryonic fibroblast

miR-1 MicroRNA 1

MMP Matrix metalloproteinase

mRNA Messenger RNA

mTOR Mammailian target of rapamycin

mTORC1 Mammailian target of rapamycin complex 1

MW Molecular weight

NCBI National Center for Biotechnology Information

NEAT1 Nuclear enriched abundant transcript 1

NEV Normalised expression value

NF-1 Nuclear factor 1

NOV Novobiocin

p70S6K1 Serine/threonine kinase that phosphorylates S6

PBS Phosphate buffered saline

PCR Polymerase chain reaction

pHSE Putative heat-shock element

PP5 Protein phosphatase 5

PPIA Protein phosphatase 1

PSA Penicillin-streptomycin-amphotericin B

PTM Post-translational modification

qRT-PCR / qPCR Quantitative real-time polymerase chain reaction

RAS Rat sarcoma

RCF Relative centrifugal force

RE Restriction enzyme

RNA Ribonucleic acid

RNAi RNA interference

RNAPolII RNA polymerase II

RT-PCR Reverse transcription polymerase chain reaction

SDS Sodium dodecyl sulfate

Ser Serine

siRNA Small interfering RNA

SIRT1 Sirtuin1

Sirtuin1 Silent mating type information regulation 2 homolog

SP1 Specificity protein 1

SPP1 Secreted phosphoprotein 1 (Osteopontin)

SV40 Simian virus 40

T4 Bacteriophage T4

TBS Tris-buffered saline

TBST Tris-buffered saline with Tween 20

TGFβ Transforming growth factor beta

TMB 3,3,5,5-Tetramethylbenzidine

TPA Tissue plasminogen activator

TRAP1 TNF receptor-associated protein 1

TRiC TCP-1 ring complex

TSS Transcription start site

V/C Vehicle control

VTN Vitronectin

WB Western blot

WST-1 Water soluble tetrazolium salt 1

ZNF333 Zinc finger protein 333

1

Literature Review

1.1 The heat-shock response

In 1962, the Italian scientist Ferruccio Ritossa identified a puffing pattern on the chromosomes of *Drosophila buschii*, supposedly after a colleague (C. Golgi) increased the incubator temperature. More than 50 years later the cell-stress response remains a focus of active biomedical research. Several kinds of stresses are proteotoxic, including temperature, pH, oxidative stress, infection and high concentrations of some heavy metals(1). Under stressful conditions, cells make use of an adaptive response to abrogate the harmful effects this has to the normal cell biological function. This response, the heat-shock, or cell stress, response operates though the detection of damaged proteins and an up-regulation of heat-shock protein (HSP) levels via the activation of heat-shock transcription factors (HSFs), of which HSF1 is the best characterised. HSPs are comprised mostly by molecular chaperones, with a small number of proteases, which serve to counteract the negative effects of the proteotoxic stress on the normal functioning of cellular processes. HSPs are conventionally named according to their molecular weight. Chaperone HSPs such as heat-shock protein 90 kDa (Hsp90), and heat-shock protein 70 kDa (Hsp70) do this by promoting the maintenance of the correct conformational structure of client proteins. The cross-protection of cellular processes against a variety of stresses using a single conserved mechanism in this way is termed 'hormesis'(2)

1.2 Hsp90

Hsp90 is the most ubiquitously produced molecular chaperone in mammalian cells, and exists in four different isoforms. Hsp90α is the stress inducible cytosolic form of Hsp90, Hsp90β is the constitutively expressed cytosolic form which shares 85 % sequence identity to the α isoform(3). The endoplasmic reticulum isoform of Hsp90 (Grp94) and a mitochondrial isoform of Hsp90, TNF receptor-associated protein 1 (TRAP1) are also constitutively expressed in normal cells. Hsp90 is a highly evolutionarily conserved member of a small protein family called GHKL ATPases which are characterised by their common ATP binding pocket, which is different from the ATP-binding pocket of protein kinases(4). Other members of the GHKL family include MutL, DNA Gyrase and histidine kinase(5).

Hsp90 forms a complex network of interactions with co-chaperones and client proteins which together facilitate the correct function and turnover of proteins involved in many cellular activities(6)(7). Hsp90 is a key facilitator in cellular homoeostasis and is involved in the stabilisation and activation of more than 300 client proteins, many of which are essential for constitutive cell signalling and adaptive responses to stress(4)(8). Hsp90 with Hsp70 and co-chaperones together form the Hsp90 chaperone machine, which facilitates transient, low-affinity protein-protein interactions which promote the correct conformation of client proteins. Hsp70 binds the nascent polypeptide chains and Hsp90 binds later in the client folding process(9). Together with Hsp70 and the co-chaperone CHIP, the Hsp90 chaperone machine works in concert with the Hsp70-Hsp40 chaperone system and the ubiquitin-proteosome system, directing misfolded proteins for degradation(5). It is estimated that as many as 10 % of all cytosolic proteins interact with Hsp90 during their normal proteomic cycling. Hsp90 has also been demonstrated to have extracellular functions(10)(11), including chaperoning cell-surface receptors such as HER-2(12), a role in the activation of the extracellular proteinase MMP2(13), and a role in the stabilisation of the fibronectin (FN) ECM(14).

1.2.1 The Hsp90 cycle

Functional cytosolic Hsp90 exists as a homodimer, with each subunit consisting of three functional domains: an N-terminal ATPase domain, a middle domain (M-domain), and

a C-terminal dimerisation domain(15). Hsp90 monomers are bound together at the C-terminal dimerisation domain(16). The Hsp90 cycle is a description of the mechanism of action for most Hsp90-client interactions(17)(18). During and between client protein binding, Hsp90 undergoes large conformational changes. An open conformation of Hsp90 is stable in the absence of ATP binding to the N-terminal binding pocket(18). Client proteins bind the M-domain and upon ATP binding, a peptide lid closes over the binding pocket which enables the adoption of a closed conformation, in which the N-terminal domains are dimerised(18)(19). This conformational change, with additional client-co-chaperone interactions, supports the maturation of bound client proteins. As the N-terminal ATPase hydrolyses the bound ATP, Hsp90 returns to the open conformation and the client protein is released(18).

The recruitment of client proteins and the regulation of Hsp90 ATPase activity is controlled by co-chaperones in a client specific manner(20) and each stage in the Hsp90 cycle involves a different complex of chaperones and co-chaperones(20)(4). Client proteins begin the Hsp90 cycle in the 'early complex' bound to Hsp70, which is complexed with Hsp40 and Hsp90(21)(22). Hsp70/Hsp90 organising protein (Hop) binds to Hsp90 at one of two tetratricopeptide (TPR) binding sites, inhibiting its ATPase activity and stabilising it in the open conformation(23). Hop facilitates the transfer of the client protein from Hsp70 to Hsp90. The second TPR binding site on Hsp90 is then occupied by Prolyl isomerase (PPIase) proteins such as Cyp40 or Fkbp52, forming the 'intermediate complex'. ATP then binds to the N-terminal ATPase domain of Hsp90 and the protein adopts the closed conformation(4)(21). The 'late complex' is then formed with the binding of p23, which stabilises the closed conformation of Hsp90 and promotes the release of Hop(23). Following ATP hydrolysis by Hsp90, p23 and the client protein are released from the complex as Hsp90 returns to its open conformation(4)(6).

The Hsp90 cycle has major differences in co-chaperone constituents depending on the class of client protein that is bound. For example, in the maturation of kinase Hsp90 client proteins, the Hsp70-client-Hsp90-Hop complex is stabilised by a kinase specific co-chaperone Cdc37(24). Aha1, and ATPase activator and the phophotase Pp5 are also co-chaperones involved in the kinase-specific Hsp90 cycle, where they promote the release of Cdc37, Hop and ADP from the Hsp90 complex(25)(26).

1.3 Heat-shock transcription factors

The mammalian HSF family has four members; HSF1, HSF2, HSF3 and HSF4(27);(28). These transcription factors demonstrate tissue specific expression of target genes and are not all involved in the cell stress response(29)(30). HSF1 has been demonstrated to be the master regulator of the stress response(31)(32). HSF1 monomers are 529 amino acid residues in length and contain five conserved functional domains, namely, the DNA binding domain(33), three hydrophobic heptad repeats (HR-A, HR-B and HR-C), and a C-terminal activation domain. HR-A and HR-B facilitate the formation of homotrimers(34), although heterotrimers with HSF2 has also been reported(35). The HR-C domain serves to suppress spontaneous trimerisation of HSF1 monomers before the post translational modifications required for activation have been made to the activation domain(36).

1.4 Hsp90 and the regulation of the heat-shock response

Activation of the cell stress response is regulated at multiple stages by physical interactions and post-translational modifications of HSF1(2)(37). The most widely accepted mechanism describing the initiation of the heat-shock response is termed the 'titration model'(28)(27). This model explains the process of activation and attenuation of HSF1 activity in terms of a negative feedback loop, with the level of Hsp employment acting as the sensor for stress (Figure 1.1). The model was proposed following the identification of a low-affinity interaction between HSF1 monomers and the Hsp90 complex members including Hsp90, Hsp70, Hsp40, FKBP52 and p23(38)(39)(40)(41). The accumulation of misfolded proteins under stressful conditions results in competitive binding between the Hsp90 and bound HSF1 monomers. As the HSF1 monomers are released they form homotrimers. This process has been shown to occur spontaneously(42), but the regulatory involvement of co-chaperones FKBP52, p23(38) and CHIP(43) in this process has been demonstrated. It has recently been elucidated that the chaperonin complex TRiC also binds HSF1 monomers under normal conditions, and this interaction is disrupted similarly to the Hsp90 complex-HSF1 interaction(44).

A number of modifications to HSF1 serve to activate or to repress its transactivating capacity, and add an additional layer to the regulation of the heat-shock

response(45)(42). The aquisition of DNA binding ability of HSF1 is regulated by post-translational modifications of the C-terminal activator domain and another regulatory domain located in the trimerisation domain(46)(28). Although these processes are not fully understood, it has been shown to involve acetylation, phosphorylation, dephosphrylation and sumoylation, as well as positive and negative regulatory interactions with a number of chaperones and co-chaperones(37)(40)(47)(48)(49).

Activated HSF1 are translocated to the nucleus whereupon they bind regulatory regions of target genes at nGAAn inverted repeat motifs called heat-shock elements (HSEs). Although HSF1 monomers are found in both the cytoplasm and the nucleus(27), the rapid translocation of oligomerised HSF1 to the cell nucleus and the formation of nuclear stress granules are an established feature of the cell stress response(50)(51)(52). Once bound to HSEs, HSF1 aids in the recruitment of RNAPolII initiation complexes and increases the transcription rate of target genes(53)(54)(55). The primary targets of HSF1 mediated transcription are the heat-shock proteins, including the inducible isoform of Hsp90, *HSP90AA1* (Hsp90α) and Hsp70, *HSPA1A* (Hsp72). During heat-shock, Hsp90 has been shown to increase from approximately 1 % of total cellular protein to almost 6 %(56). Some studies have indicated that the initial signal for the activation of the heat-shock response is the loss of correct conformation by outer membrane porin proteins(57)(58).

In addition to the chaperone mediated regulation of HSF1 activation, the transcription factor has been demonstrated to contain redox sensitive thiol groups which enable intrinsic HSF1 stress sensing(60)(61). One of the essential stress-induced phosphorylation sites of HSF1, required for transactivation activity is Ser326(47). This residue has recently be shown to be directly phosphorylated by the mammalian target of rapamycin complex 1 (mTORC1)(62). Dai *et al.* (2012) reported that the knock-out of the tumour suppressor NF1 in a MEF cell lines resulted in the the activation of HSF1 and the acquisition of stress tolerance. The mechanism of HSF1 activation in this case was thought to be related to aberrant MAPK signalling caused by the loss of NF1(63).

The regulation of the heat-shock response has been investigated primarily in cell culture models to date, leaving the mechanisms by which the stress response might be coordinated across an organism largely unexplored. Some work conducted in *C. elegans* has demonstrated that the heat-shock response is under neuronal control(64)(65)(66).

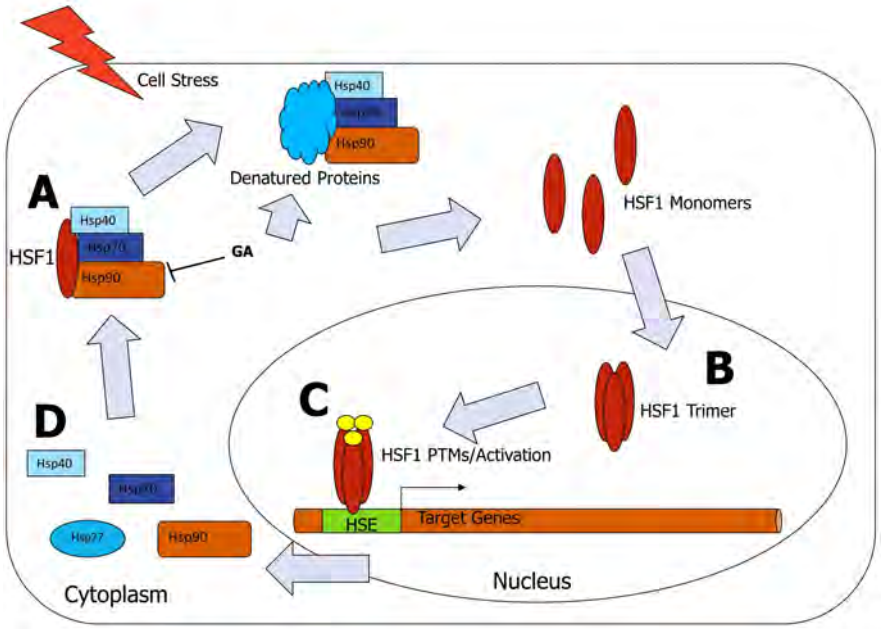

Figure 1.1: The titration model of the HSF1 mediated heat-shock response. - An increase in the levels of misfolded proteins under proteotoxic stress results in competitive binding between the misfolded proteins and HSF1 monomers at the Hsp90 chaperone complex(40) (**A**) and TRiC complex(44) (not shown). The HSF1 monomers are released from Hsp90, and undergo spontaneous trimerisation and translocation to the nucleus(27) (**B**). HSF1 is post-translationaly modified(48)(59) (**C**). Active HSF1 may bind regulatory regions of target genes at nGAAn inverted repeat motifs, called heat-shock elements(54)(55) (HSEs). HSF1 aids in the recruitment of RNAPolII initiation complexes and increases the transcription rate of target genes which include genes for HSPs(53)(54)(55) (**D**).

Additionally, it has been shown that transcriptional feedback between somatic tissues enables chaperone responses independent of neurons, in a cell-non-autonomous manner(67).

As the HSF1 transcriptional programme increases the levels of unemployed molecular chaperones, HSF1-Hsp90 interactions are re-established(39)(40). These interactions reduce the levels of active HSF1 and attenuate the heat-shock response. This negative feedback is essential to the maintenance of proteostasis in the absence of stress, and also ensures that the extent of the heat-shock response is proportional to the stress experienced by the cell. Post-translational modifications including phosphorylation of Ser303 and Ser307 and sumoylation of Lys298 also serve to negatively regulate the heat shock response. The loss of DNA binding capability of HSF1 is associated with the acetlyation of Lys80 in the DNA binding domain, and during the activation process the deacetylase sirtuin-1 (SIRT1) is responsible for deacetylation of this residue(68).

1.4.1 HSF1 target gene identification

A beginning to the systematic identification of the genome-wide target genes and the effects of the transcriptional programming thereof began with Trinklein *et al.* (2004). By combining data from micro-arrays and chromatin immunoprecipitation (ChIP) of HSF1 from three different human cell lines, information on the relationship between stress-inducibility and HSF1 binding was able to be determined. Some interesting and unexpected results were obtained using this approach. Although many heat inducible genes were indeed bound by HSF1, a number of stress inducible genes lacked both HSEs and HSF1 binding. Additionally, only about half of the promoters with predicted HSEs were found to be bound by HSF1(55). Several genes that were bound by HSF1 were not stress inducible(55). These findings showed that there must be other regulatory mechanisms at work during stressful conditions in mammalian systems, and that HSF1 is potentially involved in the transcriptional regulation of target genes that are not necessarily involved in the canonical heat-shock response(55). Page and colleagues later used a similar approach using ChIP-array to compare gene expression profiles of cells with and without siRNA knock-down of HSF1 in HeLa cervical cancer cells(69). As with Trinklein *et al.* (2004) there was not a strong correlation found between HSF1 promoter binding and mRNA expression. However the data did demonstrate the expected significant involvement of HSF1 in the regulation of genes involved in protein

folding, and a wide-ranging transcriptional program that was regulated either directly or indirectly by HSF1, supporting earlier findings(69). Similarly to earlier studies in human models, the association of HSF to target genes in *Drosophila melanogaster* were studied by Gonsalves *et al.* (2011) using ChIP-array. Reflecting the earlier findings, not all of the genes associated with HSF binding sites changed transcriptional levels following heat-shock, and some genes that were stress responsive were not identified as containing HSF binding sites(53).

1.4.2 HSF1 in cancer

The potential involvement of HSF1 in driving cancerous transcriptional programmes was investigated by Dai *et al.* (2007). Making use of a mouse HSF1 knock-out model and cell line models, the authors showed that HSF1 is required for oncogenic transformation caused by p53 and RAS mutations as it controls a wide range of transcriptional effects that together support the oncogenic lifestyle post-mutation(70). This finding is perhaps not surprising given that many cancers over-express molecular chaperones. As there is selection pressure against unstable protein intermediates in signalling cascades, high levels of molecular chaperones facilitate maintenance of the transformed state(71), and HSF1 is the effector of this change. The heat-shock response may be induced due to intracellular conditions created by the transformation, and subsequently maintained by stress factors created by the tumour itself. As we have seen from prior work(55); (69), HSF1 modulates the expression of proteins involved many different cellular processes, and it is therefore not surprising to find that many of these are likely to support the cell indirectly during times of stress, such as metabolism or translation. A study making use of a large number of clinical samples, indicating that high nuclear HSF1 levels in cancer correlated with poor survival rates, supports the hypothesis that the HSF1 transcriptional programme contributes to the progression of cancer(72). Feng *et al.* (2012) also used clinical datasets to show that high HSF1 levels are correlated with poor patient survival, and subsequently demonstrating in hepatocellular carcinoma (HCC) cell lines and a mouse model that over-expression of HSF1 promoted tumour migration and invasion(73).

Jin *et al.* (2011) demonstrated that metabolism related HSF1 target genes are also key to cancer progression in liver carcinoma using a conditional HSF1 knock-out HCC model. It was shown that loss of HSF1 resulted in an increase in AMPK activation

and increased insulin sensitivity(74). Several HSF1 dependent cancerous cell lines were used by Santagata *et al.* (2013) to investigate a potential regulation of protein synthesis pathways by HSF1. It was found that the chemical inhibition of protein synthesis resulted in the loss of HSE occupancy by HSF1, and existing transcriptome data showed that HSF1 inactivation is linked to loss of expression of translational machinery(75).

Further data pertaining to the role HSF1 plays in malignancy was reported by Mendillo and colleagues(76). A comparison of the transcriptome between a high and a low metastatic potential cell line under HSF1 knock-down conditions, with and without heat-shock was used to identify a subset of genes which are regulated by HSF1 only in highly malignant cells and which are independent of heat-shock(76). The genes identified in this subset were involved in a range of cellular processes including cell-cycle regulation, signalling, metabolism, adhesion and translation. They also involved genes for important molecular chaperones(76). The determination of HSF1 dependent changes in the transcriptome that are independent of the oncogenic transformation and heat shock is very interesting, as this would suggest an unknown regulatory mechanism involved in HSF1 DNA binding, or some other more fundamental regulatory difference between the low and high metastatic capability parent cell lines(76). Additionally it has recently been shown that transforming growth factor beta (TGF-β) and stromal cell-derived factor 1 (SDF-1) induce HSF1 activation in cancer associated fibroblasts, which drives a transcriptional programme similar to heat-shock, which serves to support the neighbouring tumour cells by creating a favourable micro-environment(77). The specific genes found to be activated in stromal cells included genes involved in the extracellular matrix (ECM) and cell adhesion. Fucosyltransferase (FUT4), an enzyme involved in the synthesis of the tumour associated antigen LeY and known to be related to cell proliferation was reported by Yang *et al.* (2014) to be a target gene for both HSF1 and SP1 using ChIP and gel-shift assays. Additionally it was shown that MAPK and AKT signalling are involved in the HSF1 and SP1 mediated regulation of FUT4(78).

1.5 Hsp90 and HSF1 as therapeutic targets in cancer

Mutations in a number of different proteins, usually signalling intermediates such as kinases, are the proximal cause of oncogenic transformation. Many of these mutated proteins are inherently unstable. Hsp90 is up-regulated in many cancers and can act

to stabilise these activated oncoproteins. In addition, due to often radically different transcriptional programmes operated by cancerous cells, and environmental conditions within tumours, constitutive proteotoxic stress is common and must be overcome if the cancer is to survive(71). For these reasons functionally active Hsp90 and its associated multi-protein complex is essential in most cancers(79). In fact tumours are often described as 'Hsp90 addicted'. Hsp90 chaperones a large number of oncoproteins from different families, including kinases, transcription factors, and cell-surface receptors. It has therefore been suggested as a prime target for cancer treatment(80)(81). Hsp90 inhibition typically leads to proteosomal degradation of client proteins(7)(80). Due to its involvement in multiple signal transduction pathways and cellular processes, inhibition would therefore result in the loss of core biological functions such as cell proliferation and migration in the affected cells(82). In addition, due to the pleiotropic nature of Hsp90 function, there would be limited opportunity for cells to evolve resistance, although compensatory mechanisms are present due to redundancy in signalling pathways. The strategy of targeting Hsp90 in cancer has been widely reviewed(81)(83)(84)(80)(85).

A natural organic product, geldanamycin (GA) was the first identified Hsp90 inhibitor, and was shown to bind at the N-terminal ATP-binding site(86). This interaction was shown to block the ATP-dependent Hsp90 cycle, and cause client proteins to be released and ultimately degraded(87)(88). In cancer this eventually leads to cell-cycle arrest and apoptosis(89). While geldanamycin is considered unsuitable for therapeutic use due to high toxicity, rational drug design has been used to develop derivatives such as 17-AAG that are under clinical evaluation[1] and these are summarised in Table 1.1(90)(81)(80)(91)(92)(93). Another inhibitor of Hsp90, novobiocin (NOV), a coumermycin antibiotic has been shown to bind a pocket in the C-terminal dimerisation domain of Hsp90(94)(95), and is thought to act by preventing the formation of the active Hsp90 complex. Whereas GA prevents the formation of the closed

[1]Phase I: Testing within a small group of people (2080) to evaluate safety, determine safe dosage ranges, and begin to identify side effects. Phase I trials are not expected to identify all side effects. Phase II: Testing with a larger group of people (100300) to determine efficacy and to further evaluate safety. Phase III: Testing with large groups of people (1,000 3,000) to confirm the drug's effectiveness, monitor side effects, compare it to commonly used treatments, and collect information that will allow it to be marketed.

conformation of Hsp90, C-terminal Hsp90 inhibitors hold the protein in a conformation thought to represent the client-release stage of the Hsp90 cycle(96). As with GA, derivatives of NOV have been synthesised with the goal of increasing its therapeutic potential(97). Both of these classes of Hsp90 inhibitors have been invaluable research tools(98)(99), enabling the elucidation of the mechanisms by which Hsp90 and its co-chaperones perform their cellular functions. Unlike the N-terminal inhibitors however, NOV inhibition of Hsp90 does not lead to the universal degradation of client proteins, but does result in cell-cycle arrest and apoptosis while mitigating the induction of the heat-shock response caused by N-terminal Hsp90 inhibitors(100)(101)(102).

It was demonstrated that among the effects of GA N-terminal inhibition on Hsp90 was the induction of the heat-shock response(40)(120), as would be expected when interactions between HSF1 and Hsp90 are disrupted. Indeed this effect has been considered to be of potential therapeutic value in protein aggregation diseases such as Parkinson's, Huntington's and Alzheimer's disease where HSF1 activation may ameliorate aspects of protein aggregation(121)(122)(123)(124)(125)(126). N-terminal ATPase activity has also been shown to be required for the disassembly of activated HSF1 trimers, and therefore the attenuation of the heat-shock response(127). In cancer however this response represents a challenge to the Hsp90 targeting strategy, as the inhibition results in a concomitant induction of compensatory chaperones(40). It has therefore been suggested that abrogation of the heat-shock response should increase the sensitivity of cancer to Hsp90 inhibition(128).

A number of avenues to preventing HSF1 from activating target genes are available and are being pursued (129)(128). Chou and colleagues found that phosphorylation of Serine 326 on HSF1 is essential for enabling the transactivating capability of HSF1(62). This has subsequently has led to several studies investigating the potential of using mTORC1 inhibitors such as rapamycin or its analogues to prevent HSF1 phosphorylation and thus impede the induction of the heat-shock response during Hsp90 inhibition(130); (131); (132).

1.6 The extracellular matrix

Tissue integrity is maintained by the attachment of constituent cells to a network of secreted proteins, proteoglycans, glycoproteins and polysaccharides(133). The composi-

Table 1.1: N-terminal Hsp90 inhibitors that have been or are currently undergoing clinical trials

Inhibitor	Type	Phase	Administration	Reference
Tanespimycin (17-AAG)	N-Terminal	III	IV	(103)
Retaspimycin (17-AAG) hydrochloride	N-Terminal	III	IV	(104)
Alvespimycin (17-DMAG)	N-Terminal	I	IV	(105)
AUY922	N-Terminal	II	IV	(106)
BIIB021	N-Terminal	II	Oral	(107)
Ganetespib (STA-9090)	N-Terminal	I	IV	(108)
IPI-493	N-Terminal	I	Oral	(109)
SNX-5422	N-Terminal	I	Oral	(110)
BIIB028	N-Terminal	I	IV	(111)
KW-2478	N-Terminal	I	IV	(112)
AT13387	N-Terminal	I	IV/Oral	(113)
XL888	N-Terminal	I	Oral	(114)
HSP990	N-Terminal	I	Oral	(115)
MPC-3100	N-Terminal	I	Oral	(116)
ABI-010	N-Terminal	I	IV	(117)
Debio 0932	N-Terminal	I	Oral	(118)
PU-H71	N-Terminal	I	IV	(119)

tion and structure of the extracellular matrix is cell and tissue specific. In multicellular structures, epithelial, endothelial and stromal cells are involved in the production of the basement membrane (or matrix), a fibrous layer which serves to separate the epithelium, mesothelium and endothelium from connective tissue(134). A primary component of connective tissue is the interstitial matrix, which also exists between the cells comprising tissues themselves. The interstitial matrix is less dense than the basement membrane, and is produced primarily by stromal cells such as fibroblasts(135). Basement membranes are composed of laminins, fibronectin (FN) and type IV collagen, connected to other ECM proteins though linkers. The interstitial matrix by comparison is made up primarily of fibrillar proteins, proteoglycans, and various glycoproteins including FN. Extracellular matrix components interact with both each other and the surrounding cells though cell surface receptors such as integrins via specific binding motifs. These interactions confer the strength and rigidity to tissues and play a role in the assembly and remodelling of the matrix(136)(137). The physical properties of the ECM are an important factor in the micro-environment of the cell. The ECM may promote anchorage of cells to a particular site, or ECM components can either enable or inhibit cell migration by the formation of pathways or barriers respectively(138)(139)(134).

1.6.1 The ECM in determining cell behaviour

A number of biomechanical factors of the ECM such as porosity and elasticity have been shown to play a role in determining cell behaviour. For example: the porosity of the interstitial matrix determines the rate of diffusion of signalling molecules, which is a factor in the formation of concentration gradients(140). The protein composition and modification of the ECM results in changes in polarity. This in turn causes changes in inter-cellular signalling by repressing the free migration of some signalling molecules though the interstitial space (141). Conversely, components of the ECM or breakdown products thereof may play a direct role in signalling (141)(140). The elasticity/rigidity of the ECM also plays role in the determination of cell behaviour. Modifications to focal adhesion binding complex proteins which link the ECM to the actin cytoskeleton often occur in response to mechanical force(142)(143)(144)(145)(146)(147). Topographical features of the ECM have also been shown to influence processes such as cell division(148) and the determination of cell fate in stem cells(149)(150)(151).

Table 1.2: Human pathologies of the extracellular matrix

Pathology	Organ	Tissues Involved	Reference
Cirrhosis	Liver	Connective tissue	(164)(165)
Pulmonary Fibrosis	Lungs	Connective tissue	(166)
Crohn's Disease	Intestine	Connective tissue	(167)(168)(169)
Keloid	Skin	Connective tissue	(170)
Arthrofibrosis	Joints	Connective tissue	(171)(172)
Diabetic retinopathy	Eyes	Basement membrane	(173)(174)
Diabetic nephropathy	Kidneys	Basement membrane	(175)(176)
Scleroderma	Skin	Connective tissue	(177)(178)
Peyronie's disease	Penis	Connective tissue	(179)(180)

The ECM is regularly remodelled in the course of normal protein turnover and in response to changing environmental queues. Remodelling of the ECM involves degradation and deposition processes(152). The degradation of the ECM fibres is primarily undertaken by matrix metalloproteinases (MMPs)(153). The MMPs are a large group of serine proteases encompassing secreted and transmembrane members, which between them are able to degrade a wide range of extracellular proteins (140). Enzymes involved in the remodelling of the ECM are regulated at the transcriptional, translational, post-translational modification levels(154)(155)(156)(157).

A consequence of the interconnected nature of the ECM with surrounding tissue is that a change in ECM properties by one cell will have an effect on the behaviour of nearby cells(158)(159). In normal tissue this is a useful feedback mechanism enabling cells to rapidly adapt to changing environmental conditions(160). However, aberrant cell behaviours may also lead to changes to the turnover and modification of ECM components and this can lead to disease progression(140)(161)(162). Excess levels of ECM proteins due to enhanced expression, or a reduced rate of ECM degradation related to the deregulation of ECM remodelling enzymes, are common in some cancers and are symptomatic of tissue fibrosis(163). Some human diseases related to abnormal ECM dynamics have been summarised in Table 1.2.

1.7 Fibronectin

FN is only present in vertebrates and its evolution is thought to be involved with the emergence of a vasculature lined with endothelial cells(133). FN was the first matrix glycoprotein to be extensively studied, and is an ubiquitous ECM component produced in almost all cell types(181). FN is a multi-domain glycoprotein found intracellularly as a soluble 450 kDa disulphide-linked dimer, and in the extracellular matrix as large insoluble multimers. FN binds cell surfaces and a number of other ECM components including collagen, fibrin, heparin and integrins(182). Integrins are heterodimeric, transmembrane cell adhesion receptors for FN and other extracellular matrix molecules. FN plays a role in a number of cell adhesion and migration processes including embryogenesis, wound healing, blood coagulation, host defence, the maintenance of cell shape, opsonisation(183)(184)(185)(186)(187).

1.7.1 Structure of FN

The FN primary protein structure is based on repeated subunits of homologous type I, II, and III, and three alternatively spliced modules(188)(189). FN dimers are composed from subunits of twelve type I, two type II, and between 15-17 type III module(190)(191). Intra-chain disulphide bonds from between type I and II modules to form dimers, and sets of repeating modules which comprise domains which are bound by other molecules in the extracellular space such as ECM proteins and cell surface bound proteins(192). FN has at least two independent cell adhesion regions with different receptor specificities(193). The primary cell adhesive region is comprised of two amino acid sequences; an Arg-Gly-Asp (RGD) sequence and a Pro-His-Ser-Arg-Asn (PHSRN) sequence located in the III9-II10 region(194)(195)(196). These adhesion sequences only act in concert with each other to facilitate adhesion to cell surface integrins(195). Another cell adhesive region is located near the C-terminal in the alternatively spliced IIICS module(194). The sequences for this region are Leu-Asp-Val (LDV) and Arg-Glu-Asp-Val (REDV)(197)(185). The $\alpha 5\beta 1$ FN-specific integrin binds to the central RGD/PHSRN ('synergy') site. The $\alpha 4\beta 1$ integrin binds to the IIICS site(198)(185).

The assembly of FN into an extracellular matirx is termed fibrillogenesis. FN is secreted by the cell as a soluble dimer which is later rendered insoluble through conformational changes initiated through integrin interactions(199)(200). The binding

of the RGD motif in the III9 module and the so-called synergy sequence in III10 module to the $\alpha5\beta1$ integrin causes conformationals change in the FN molecule that expose self-association sites(199)(200)(201)(202). FN-FN interactions occur at four self-association sites distributed across each subunit(203). The continual addition and extension of FN dimers to growing multimers results in an insoluble FN matrix(190)(202). Integrin-FN clusters also result in the connection of FN to the actin cytoskeleton via receptor cytoplasmic domain interactions(200)(204)(205). Fibrillogenesis has been shown to be regulated by Rho GTPase-MAPK signalling(206)(207) and the focal adhesion kinase (FAK) complex to which FN binds acts as a sensor linking the cytoskeleton with the ECM(208). Several components of the focal adhesion complex are conformationally modified under the effect of mechanical force applied from the ECM(209)(210)(211). The assembled FN matrix is subject to normal protein turnover and to remodelling as a function of cell behaviour(212)(213). These processes require the degradation of the FN fibrils by proteases(157)(214).

In the absence of continual fibrillogenesis, increased levels of FN degradation and a loss of FN matrix are promoted(215). Several MMPs have been found to be involved in the break-down of FN fibrils. The two most important of these are MMP2 and MMP9(140). MMP2, via its C-terminal hemopexin-like domain, interacts exclusively with FN (216). The activation of MMP2 has been shown to result in an increase in cell migration and invasion(13). The final degradation of FN fragments resulting from extracellular proteolysis occurs intracellularly after endocytosis through a caveolin-1dependent processes(217). Lobert *et al.* (2010)(218) demonstrated that in migrating cells FN is endocytosed with the $\alpha5\beta1$ integrin to be degraded in lysosomes following FN-induced ubiquitination of the $\alpha5$ subunit. Endosomal sorting and $\alpha5$ ubiquitination were both shown to be requisite for fibroblast migration. LRP has also been demonstrated by Saliconi and colleagues to bind to FN and act as a catabolic cell surface receptor(187).

1.7.2 FN in disease

FN-receptor interactions play an important role in tumour cell biology(181)(136) and in the progression of a number of diseases including fibrosis(219), synovial related diseases(220) and even Alzheimer's disease(221).

In cancer, high FN levels are associated with increased invasion and metastatic capability in lung cancers and hepatic cancers(136)(222)(223)(224). In a number of other cancer types, however, low levels of FN expression have been found to correlate with migratory capacity(225)(226). Some authors have proposed that the deposition of ECM proteins such as collagen and FN act as a barrier to the growth of tumours(227). MMP2 inhibition has been shown to result in a reduction in tumour growth and metastasis in a mouse ovarian cancer model due to a loss in FN and vitronectin cleavage(228) which supports this propositions. Circulating FN has been shown to be required for tumour growth and angiogenesis(229). In fibrosis and inflammation related diseases, the increased deposition of ECM components including FN is known to be a causative factor in the development of pathological conditions such as cirrhosis of the liver and Crohn's disease(230)(231)(232)

The FN fragments that are the products of FN fibril degradation have been demonstrated to have biological activity alone. Lopez-Armada *et al.* demonstrated that an RGD motif containing fragment of FN could stimulate the production of FN and TNF-α in mesangial cells through interactions with the $\alpha5\beta1$ integrin(233). Yi *et al.* (2001) demonstrated that the III1-C protein fragment (named anastellin by the authors) of FN has antiangiogenic and antimetastatic properties in a mouse model(234). A subsequent study by You *et al.* (2009) found that this fragment stimulates FN matrix remodelling and activates the p38 MAPK pathway, independent of interactions between the fragment and cell surface integrins(235).

1.8 *FN1*

The FN protein in humans is encoded by a single gene called fibronectin 1 (*FN1*). *FN1* is located on chromosome 2 from 216,225,176 bp to 216,300,790 bp. The protein coding region of the FN gene consists of 46 exons and the primary transcript is alternately spliced to create a number of splice variants(189). Alternative splicing of the primary FN mRNA transcript occurs in three regions, corresponding to three regions of the FN molecule. In two of those regions, extra-domain A and B, (ED-A and ED-B) the exon can be included or skipped. These relative proportions of alternatives are cell type and developmentally regulated(188)(181)(236). The splicing of the final region (IIICS) where the exon can be skipped, included or subdivided yielding several variants (five in

humans) is more complex(236). The total number of full length FN variants is therefore 20(237)(189). ED-A inclusion is associated with the formation of long and thick FN fibrils (238) and ED-A and ED-B inclusive FN has been shown to be more expressed in tumour and foetal tissues than in normal tissues(239)(240)(241). In normal tissues the inclusion of extra-domain exons is limited to the cells of the ovary, arterial cartilage and synovial cells(242)(243).

Han *et al.* (2007) demonstrated that FN isoform expression (the regulated splicing of FN mRNAs) is regulated by TGF-β1 and the expression of the splicing factor SRp40. When treated with TGF-β chondrocytes preferentially excluded ED-A and reduced ED-B exon inclusion(238). Gratchev *et al.* (2001) demonstrated that interleukin 4 induction of macrophages lead to an increase in the total levels of FN mRNA and protein. Additionally it was found that ED-A- and ED-B- splice variants were increased under the effects of IL-4(244). Regulation of *FN1* at the transcriptional level has been investigated by several groups for many decades.

1.8.1 *FN1* regulation

A series of publications by Douglas C. Dean and colleagues describe the early analysis of the FN promoter and regulation thereof. The TATAA box is identified at -25 bp, and the CAAT box at -150 bp. Additionally an SP1 transcription factor binding site is identified at -102 bp, along with a CRE motif at -173 bp(245). Later the response of FN synthesis was examined in several cells lines under the effects of three different transcriptional activators(246). It was found that the glucocorticoid dexamethasone induced FN production in a fibrosarcoma cell line due to an observed increase in FN mRNA longevity, whereas TGF-β and forskolin both increased the activity of the *FN1* promoter in most of the cell lines tested(246). The mechanism of the previously identified forskolin induction of FN mRNA was subsequently investigated. Forskolin is an adenylate cyclase activator and a CRE element located at -188 bp to -157 was shown to be responsible for the up-regulation in FN mRNA demonstrated(247). The core promoter of *FN1* was also investigated by Alonso and colleagues who demonstrated that the -170 bp CRE element and the -150 CAAT elements act as a single functional element and display cell line specific occupation patterns(248). A mechanism for the effect of TGF-β previously observed on the levels of FN mRNA was demonstrated by

Gradl *et al.* (1999)(249). β-catenin levels were shown to modulate FN promoter activity via functional LEF-TCF sites identified on the FN promoter. The expression of LEF-1 was shown to modulate *FN1* transcription in fibroblasts, but not epithelial cells, in response to WNT signalling(249).

In recent studies additional processes have been implicated in the regulation of *FN1*, however complete mechanisms for these effects are yet to be elucidated. The interaction of ELMO1 with COX-2 is known to increase the cyclooxygenase activity of COX-2 and this was found to have an effect on FN expression by Yang and colleagues(250). It was shown that this COX-2 related FN up-regulation occurs independent of RAC1(250). Liu *et al.* (2012) demonstrated that the signalling sphingolipid sphingosine-1-phosphate (SP1) is able to affect the up-regulation of FN mRNA and protein under high glucose conditions in rat mesangial cells. It was demonstrated that this occurs through the SP1 receptor and the MAPK pathway, although the authors did not identify the signal effectors that might be involved in this regulation. The S1P2 receptor is reported to be more abundant in diabetic conditions, and it is implied that this is a potential mechanism whereby excess FN ECM is deposited in diabetes related pathologies such as diabetic neuropathy(251).

It has been known that RAS oncogenic transformation reduces the expression of FN(252), and reduced *FN1* expression has been used as a marker in the detection of circulating tumour cells, an experimental early stage cancer diagnostic tool(253). In a paired human lung adenocarcinoma model Yang and colleagues showed that cells with a high metastatic potency had much higher expression levels of *FN1* as determined by qPCR analysis(254). Yang *et al.* (2007)(255) found that in a comparison of tumour and normal tissues *FN1* and other genes involved in focal adhesion formation were an identifying feature of tumour cells, although it was not stated whether the relative expression of *FN1* between these cell types was increased or decreased and to what extent. Similarly Clark *et al.* 2000 reported that in gene expression profiles of highly metastatic cells a number of genes involved in the assembly of the extracellular matrix were up-regulated(256). Wang *et al.* (2011) used the HEpG2 cell line to demonstrate that micro-RNA1 (miR-1) was able to suppresses cell growth and migration due to a direct interaction with FN mRNA, and a similar reduction in cell growth and migration was observed in *FN1* knock-down conditions(257).

FN has been reported to play a pro-survival role in a number of cell lines(258), however the core constituent of cellular homeostasis conservation are the molecular chaperones(7). Research conducted by our group found that a direct interaction between FN and extracellular Hsp90 existed. Decreased levels of both soluble and insoluble FN were observed upon Hsp90 inhibition and Hsp90β knock-down, suggesting a role for Hsp90 in FN matrix stability(14).

1.9 Rationale for this study

Previous work by conducted by our group identified a direct interaction between FN and Hsp90. Decreased levels of both total and extracellular FN matrix were observed upon treatment of cells with the Hsp90 inhibitor NOV and upon depletion of Hsp90 by RNA interference. The effects of NOV or Hsp90 knock-down could be partially rescued by extracellular Hsp90. This suggested a role for Hsp90 in FN matrix stability(14). In the course this work it was noted that GA inhibition of Hsp90 did not produce the same FN matrix phenotype observed with either NOV treatment or knock-down of Hsp90. Whereas Hsp90 knock-down and NOV treatment reduced the FN matrix, GA treatment appeared to cause an increase in the levels of the FN ECM. As GA is known to induce the cell stress response, we decided to investigate whether FN expression was regulated by the cell stress machinery.

1.10 Hypothesis

FN1 expression is modulated by the cell stress response.

1.11 Objectives

- Determination of the effect of GA treatment on FN levels and ECM
- Investigate the effect of GA treatment on FN mRNA levels
- Determine effect of GA treatment on *FN1* promoter activity
- Elucidate mechanistic basis for observations

2

Materials & Methods

2.1 General reagents

Milli-Q water used in this study was prepared using a Millipore Direct Ultrapure System (Merck-Milliopre, USA). Bovine serum albumin (BSA) was obtained from Roche Diagnostics (Switzerland). Polymerase GoTaq Green 2× Master Mix (Promega, USA [Cat No: 9PIM712]) was used in PCR applications unless otherwise stated. Molecular weight markers used in this study include KAPA Universal DNA ladder (KAPA Biosystems, USA [Cat No: KL6302]), a GeneRuler 50 bp Ladder (Thermo Scientific, USA [Cat No: SM0373]) and a pre-stained protein molecular weight marker (Thermo Scientific, USA [Cat No: 26612]). Nuclease Free Water used in various applications was obtained from Qiagen (Netherlands). Application specific reagents are detailed in their respective method description below.

2.2 Cell culture

The Hs578T breast cancer cell line was cultured in Dulbeccos Modified Eagle Medium (DMEM) (Gibco Life technologies, USA) plus 10 % (v/v) Foetal Bovine Serum (FBS) (BioWest, USA), 1mM L-Glutamine (Sigma Aldrich, USA [Cat No: G7513]), 100 U/mL penicillin streptomycin amphotericin (PSA) (Gibco Life technologies, USA) and 2 mM NovoRapid recombinant human insulin (Nordisk pharmaceuticals, Denmark) at 37 °C, with 3.7 % sodium bicarbonate and 9 % CO_2. HEK293FT cell line was maintained in DMEM with 5 % (v/v) FBS, 1mM L-Glutamine (Sigma Aldrich, USA [Cat No: G7513]), 0.1 mM non-essential amino acids (NEAA) (Sigma Aldrich, USA [Cat No:

M7145]), 1 mM sodium pyruvate (Sigma Aldrich, USA [Cat No: S8636]), and 100 U/mL PSA at 37 °C, with 9 % CO_2. Plastic consumables were acquired from NEST Biotechnology Co. (USA), Corning Life Sciences (USA), Greiner Bio-One (USA) and Porvair Sciences (UK). Cell monolayers were lifted for downstream applications with the use of 0.25 % (v/v) Trypsin-ethylenediaminetetraacetic acid (EDTA) (Gibco Life technologies, USA) incubated for 5-10 minutes at 37 °C.

2.3 Cytotoxicity assays

Hs578T cells were seeded in 96-well plates at concentrations of 1 x 10^5 cells/well such that cells were near confluency but not growth inhibited after 72 h. Cells were treated with the vehicle control (geldanamycin/rapamycin: dimethylsulphoxide (DMSO) at 0.2 % (v/v), novobiocin: ethanol at 0.1 % (v/v), or the test compound in increasing doses, from a 10-fold dilution series. After 48 h cells were incubated with WST-1 cell proliferation reagent (Roche, Switzerland) as per the manufacturer's instructions for 4 h at 37 °C. The absorbance at 440 nm was measured using a Synergy Mx Microplate Reader (BioTek Instruments, USA). Data were analysed in GraphPad Prism 4 and IC_{50} values were calculated using non linear regression of dose response curves.

2.4 Fluorescence and confocal microscopy

5 x 10^4 Hs578T cells per well were seeded on sterile glass coverslips in 24-well plates and incubated overnight in cell culture conditions. Cells were then treated as described in the figure legend for each experiment (Figure 3.1, Figure 3.3 and Figure 3.8), and incubated for a further 24 h before the removal of culture medium. Cells were washed once with sterile phosphate-buffered saline (PBS) (137 mM NaCl, 10 mM Na_2HPO_4, 1.76 mM KH_2PO_4 2.7 mM KCl, pH 7.4) and were fixed by submersion in ice-cold methanol for 10 seconds. Coverslips were air-dried completely and subsequently blocked using 1 % (v/v) bovine serum albumin (BSA) in sterile PBS for 45 mins at room temperature. Coverslips were then incubated with primary antibodies diluted in 0.1 % (v/v) BSA/PBS (details and dilutions of antibodies can be found in Table 2.1) overnight. Primary antibody was removed by washing twice for 5 mins with 0.1 %

(v/v) BSA/PBS. Fluorescent secondary antibodies in 1 % (v/v) BSA/PBS were incubated with coverslips protected from light for 1 hour at room temperature before again washing twice for 5 mins with 0.1 % (v/v) BSA/PBS. A brief wash with Hoescht-33342 (1 μg/mL) in Milli-Q water was used to stain cell nuclei and coverslips were mounted onto slides using Dako fluorescent mounting medium. The edges of each coverslip were sealed using clear nail varnish and allowed to dry before visualisation using either a Zeiss Axio Vert.A1 fluorescence microscope or Zeiss LSM 780 confocal microscope using ZEN Black software. Images were analysed with ImageJ 1.42I. GraphPad Prism 4 was used to complete any subsequent statistical analysis. For confocal microscopy, four eight layer 0.4 μm Z-stack images were captured per treatment and these images were processed using Zen Blue software with subsequent analysis conducted using ImageJ 1.42I in combination with statistical analysis on GraphPad Prism 4.

2.5 Immunoblotting

Protein samples were prepared from treated cell monolayers or harvested cell pellets using 5× SDS sample buffer (250 mM Tris-HCl pH 6.8, 10 % [w/v] SDS, 30 % glycerol [v/v], 5 % β-mercaptoethanol [v/v], 0.02 % [v/v] bromophenol blue) and separated using gel electrophoresis as per Laemmli *et al.* (1970)(259). A 4 % (v/v) stacking gel and an 8-12 % (v/v) resolving gel (depending on expected MW of proteins of interest) were used. Samples were electrophoresed at 150 V in 1 x SDS-PAGE running buffer (0.25 mM Tris, 192 mM glycine, 1 % [w/v] SDS). Resolved samples were transferred from PAGE gels to nitrocellulose membranes as per Towbin *et al.* (1979)(260) in western transfer buffer (13 mM Tris-HCl, 100 mM glycine and 20 % [v/v] methanol) using a semi-dry blotting system (SD20 Semi Dry Blotter Maxi, Sigma-Aldrich, USA [Cat No: Z740324]) at 400 mA for 1 h. Membranes were blocked using Blotto solution (Santa Cruz Biotechnology, USA [Cat No: sc-2325]) (5 % [w/v] milk powder, 0.1 % [v/v] Tween-20) in 1 x Tris-buffered saline (TBS) (50 mM Tris, 150 mM NaCl, pH 7.5) for 1 hour and incubated with primary antibody in TBS plus 0.1 % (v/v) Tween-20 (TBS-T), diluted as detailed in (Table 2.1) at 4°C overnight. Membranes were washed 3 times for 10 mins each in fresh TBS-T before incubation with HRP conjugated secondary antibodies in TBS plus 0.1 % Tween-20 for one hour at room temperature. Three final 10 min washes in TBS-T were conducted before signal development using Clarity

Table 2.1: Details of the antibodies used in this study

Cat. Number	Species	Target	Mono/Polyclonal	Dilution
Sigma-Aldrich F0916	Mouse	Fibronectin	Monoclonal	WB - 1:5000
Sigma-Aldrich F0916	Mouse	Fibronectin	Monoclonal	IF - 1:100
Sigma-Aldrich F3648	Rabbit	Fibronectin	Monoclonal	IF - 1:100
Sigma-Aldrich P3430	Mouse	Phospho-Serine	Monoclonal	IF - 1:100
Santa Cruz H-311	Rabbit	HSF1	Polyclonal	ChIP - 2 μg/μL
Santa Cruz H-311	Rabbit	HSF1	Polyclonal	IF - 1:1000
Sigma-Aldrich G8795	Mouse	GAPDH	Monoclonal	WB - 1:5000
Abcam ab16284	Donkey	Mouse IgG	Polyclonal	IF - 1:5000
Abcam ab97110	Donkey	Rabbit IgG	Polyclonal	IF - 1:5000
Invitrogen A10036	Donkey	Mouse IgG	Polyclonal	IF - 1:1000
Abcam ab96875	Donkey	Mouse IgG	Polyclonal	IF - 1:1000
Abcam ab96891	Donkey	Rabbit IgG	Polyclonal	IF - 1:1000

Chemiluminescent Substrate (BioRAD, USA). Either X-Ray development film (Agfa Healthcare, Belgium) or a Chemidoc system (BioRAD, USA) was used to capture chemiluminescent signal.

2.6 Quantitative real-time PCR

5 x 10^4 Hs578T cells, or 1 x 10^5 HEK293FT cells per well were seeded in 24-well plates and incubated in cell culture conditions overnight before treatment in triplicate with compounds or vehicle control solvents as described in the figure legends for qPCR data (Figure 3.2, Figure 3.3, Figure 3.8 and Figure 3.11). At 24 h post-treatment, total RNA was extracted using Direct-zol RNA miniprep kit (Zymo Research, USA). The concentrations of RNA extracted was determined using a Nanodrop 2000 spectrophotometer (Thermo Scientific, USA) and equal amounts of total RNA were added to triplicate cDNA synthesis reactions with a RevertAid First Strand cDNA Synthesis Kit (Thermo Scientific, USA) using Oligo $(dT)_{18}$ primer. qRT-PCR was conducted on the genes of interest as described in the figure legend to the specific experiment (details of qPCR primers used in this study can be found in Table 2.2) using KAPA SYBR FAST qPCR reagents (KAPA Biosystems, USA) as per the manufacturer's instructions with a CFX Connect Real-Time PCR Detection System (BioRAD, USA). Data was analysed in BioRAD CFX Manager 3.1 Software, with additional statistical analysis conducted in GraphPad Prism 4. The DNA obtained from GA and NOV treated Hs578T cells was analysed for stability of a number of housekeeping genes (Figure 5.2). The most stable genes of those tested were *ACTB* and *PPIA* and these were used as controls for all subsequent qPCR assays.

2.7 *In silico* promoter analysis

The genomic sequence for the fibronectin gene (*FN1*) (NCBI: NG_012196.1) was retrieved from the ENCODE human genome build 19 (http://genome.ucsc.edu/ENCODE/). The region from 5000 bp upstream (5'-3') and 1000 bp downstream of the transcription start site (TSS located at 216,211,070 bp of human chromosome 2) was retrieved and analysed for *cis*-element clustering using the Cister algorithm from Boston Universitys ZLab online gene regulation toolkit (http://zlab.bu.edu/ ~mfrith/cister.shtml). The

Table 2.2: Primers used for the qPCR amplification of genes from total RNA extracts

Gene Name	Ref Seq Number	Exon Location	(IDT) Assay Name
ACTB	NM_001101	1 - 2	Hs.PT.39α.22214847
PPIA	NM_021130	4 - 5	Hs.PT.39α.22214851
GAPDH	NM_002046	2 - 3	Hs.PT.39α.22214836
HPRT1	NM_000194	1 - 2	Hs.PT.39α.22214821
FN1	NM_212482	8 - 9	Hs.PT.56α.24776367
FN1 (ED-B)	NM_212482	24 - 26	Hs.PT.56α.39780891
FN1 (ED-A)	NM_212482	32 - 33	Hs.PT.56α.25205031
HSP90AA1	NM_005348	9 - 10	Hs.PT.58.4978327g
HSP90AB1	NM_007355	2 - 3	Hs.PT.58.4825841
HSPB1	NM_001540	1 - 1	Hs.PT.58.39726463.g
HSPA1A	NM_005345	1 - 1	Hs.PT.58.40105845.g
LAMB3	NM_001017402	11 - 12	Hs.PT.58.21203348
LAMC2	NM_018891	1 - 2	Hs.PT.58.19257587
SPP1	NM_001251829	7 - 8	Hs.PT.58.19252426
COL4A2	NM_001846	30 - 31	Hs.PT.58.2924757
COL4A3	NM_000091	13 - 15	Hs.PT.58.3936480
ELN	NM_001081752	32 - 33	Hs.PT.58.4801194
VTN	NM_000638	4 - 5	Hs.PT.58.1205436.g
HSF1	NM_005526	1 - 2	Hs.PT.58.3297105
HIF1A	NM_001530	4 - 6	Hs.PT.58.38473208

same sequence was then analysed using a number of transcription factor binding motif algorithms, with special attention given to the region encompassing the regulatory clustering. TFSearch(261), (http://www.cbrc.jp/papia/howtouse/howtouse_tfsearch.html), PROMO(262)(263) (http://alggen.lsi.upc.es/cgi-bin/promo_v3/promo/promoinit.cgi) and Alibaba2(264) (http://www.gene-regulation.com/pub/programs/alibaba2/index.html) were used in order to identify transcription factor recognitions sequences.

2.8 Luciferase *FN1* reporter assays

The *FN1* promoter sequence from - 1240 bp to + 100 bp was synthesised by GenScript (USA) with flanking restriction endonuclease (RE) digestion sites in a pUC57 vector. This sequence was digested from the pUC57 vector using *Nhe*I and *Bgl*II restriction endonucleases (New England Biolabs, USA) as per the manufacturer's instructions. The same REs were used to digest the pGL4.17 promoterless reporter vector (Promega, USA [Cat No: 9PIE672]). After gel purification of the *FN1* promoter insert and the pGL4.17 backbone, these DNA fragments were ligated overnight using T4 ligase (Promega, USA) to create the pGL4-pFN1 construct (Figure 5.3). Correct orientation of the insert was confirmed by diagnostic RE digestion and 0.8 % (w/v) agarose gel electrophoresis in TAE buffer (40 mM Tris-HCl, 1 mM EDTA). Gels were visualised using a Bio-RAD ChemiDoc XRS+ detection system. The pGL4-pFN1 construct was also confirmed by direct sequencing.

Truncations of the pFN1 sequence of the pGL4-pFN1 vector were produced using PCR with the primers detailed in Table 2.3 which also encoded RE sites enabling sub-cloning of the inserts as before with the full length insert. PCR reactions were set up as follows in GeneAMP PCR reaction tubes (Life Technologies, USA [Cat No: N8010537]): 6.5 μL nuclease free water, 2.5 μL pFN1$_{-810bp}$ (TR1) F or pFN1$_{-380bp}$ (TR2) F primer, 2.5 μL pFN1 TR R primer, 1 μL of pGL4-pFN1 diluted in nuclease free water to a concentration of 100 ng/μL , and 12.5 μL GoTaq Hot Start Green 2X Master Mix. Cycling conditions were as follows: (1) 95 °C (120 secs), (2) 95 °C (30 secs), (3) 55 °C (30 secs), (4) 74 °C (50 secs), (5) step 2 - 4 × 25, (6) 74 °C (300 secs). The PCR products were digested using *Nhe*I and *Bgl*II restriction endonucleases (New England Biolabs, USA) as per the manufacturer's instructions and ligated into the pGL4.17 promoterless reporter vector similarly to the construction of the pGL4-pFN1

vector (Figure 5.3). Endotoxin-free plasmid stocks of these truncations were produced using a EndoFree Plasmid Maxiprep Kit (Qiagen, Netherlands [Cat No: 12362]).

The pCAG-HRP-TM (Addgene: 44441) mammalian expression vector was obtained from Addgene. This vector contained an insert encoding horseradish peroxidase fused to the transmembrane domain of PDGFR under the control of a constitutively active CAG promoter. Endotoxin-free stocks of the pGL4.17 vector, the pGL4-pFN1 construct and pCAG-HRP-TM were made using an EndoFree Plasmid Maxiprep Kit (Qiagen, Netherlands [Cat No: 12362]).

1 x 10^5 HEK293FT cells per well were seeded in 24-well plates and incubated overnight. At 24 h after seeding, the cells were transfected with the pGL4-pFN1 (or truncation constructs if stated in the relevant figure legends) and pCAG-HRP-TM constructs in a 1:1 ratio using X-tremeGENE transfection reagent (Roche, Switzerland) as follows: Vector DNA (for each vector) was diluted to 10 ng/μL in 50 μL/well Opti-MEM reduced-serum media (Life Technologies, USA). 2 μL/well X-tremeGENE transfection reagent was added to the diluted DNA and the mixture was gently agitated and incubated for 30 min. 50 μL of the DNA-X-tremeGENE mixture was then added dropwise to each well, the plate was gently swirled briefly and returned to cell culture conditions. Cells were treated as described in the figure legends (Figure 3.5 and Figure 3.6) for each experiment 24 h following transfection, and were incubated in treatment conditions for 24 h before the luciferase and HRP activities were assayed, unless otherwise stated in the relevant figure legend.

The assay for luciferase and HRP activity in transfected cells was conducted as follows: cells were lysed by incubation for 5 mins in 1 % (v/v) Triton-X100 (Amersham Pharmacia Biotech, UK) in Milli-Q water and the resulting lysate was resuspended in an equal volume of 2× FLAR buffer (adapted from Seibring-van Olst *et al.*, 2012(265)) (40 mM Tricine, 200 μM EDTA, 5.14 mM $MgSO_4$, 34 mM DTT, 250 μM ATP and 100 μM D-luciferin (Promega)). The contents of each 24-well was mixed by pipetting and divided over 3 96-wells in a white 96-well plate (Corning, USA). Luminescence was captured using a Synergy Mx Microplate Reader (BioTek Instruments). 3,3',5,5'-tetramethylbenzidine (TMB) substrate (Sigma-Aldrich, USA) was subsequently added and following a 5 min incubation the reaction was stopped with 2 M H_2SO_4, and the absorbance at 450 nm was measured. Data was analysed and statistical analysis conducted using GraphPad Prism Version 4 software.

Table 2.3: Primers used for the amplification of truncated *FN1* promoter fragments from the pGL4-pFN1 vector

Primer	Sequence (5' to 3')
pFN1$_{-810bp}$ **(TR1) F**	GCTAGCGAACTCCCGGTACTTAGTAG
pFN1$_{-380bp}$ **(TR2) F**	GCTAGCGTCTGGATTCTTAACAGCTGC
pFN1 TR R	AGATCTCACCAAGTTTGCTTCCC

2.9 Chromatin immunoprecipitation

HS578T cells were grown to near confluency in T150 flasks and treated for 24 h with either GA (100 nM) or DMSO, media was removed and the cells were washed once with Hank's balanced salt solution (Sigma-Aldrich, USA [Cat No: T4049]) and lifted using 0.25 % (v/v) trypsin-EDTA. Cells were resuspended in culture medium and pooled in a 50 mL conical tube. Formaldehyde (Sigma-Aldrich, USA [Cat No: T8775]) was added to the cell suspension to a final concentration of 1 % (v/v) and cross-linking was allowed to continue for 10 mins with end-to-end rotation. The reaction was stopped using 0.1 volume of 1.25 M Glycine (Merck, USA) and continuing agitation for 5 mins. The cell suspension was centrifuged at 200 RCF, 4 °C for 10 mins. The supernatant was removed and the cell pellet was resuspended in 50 mL cold sterile PBS before again centrifuging at 200 RCF, 4 °C for 10 mins. The cell pellet was lysed with the addition of cell lysis buffer (Sigma-Aldrich, USA [Cat No: B5938]) plus 1 % (v/v) NP-40, 0.1 M 4-(2-aminoethyl) benzenesulfonyl fluoride (AEBSF) (Sigma-Aldrich, USA [Cat No: A8456]) and 1× protease inhibitor cocktail (Sigma-Aldrich, USA [Cat No: P8340]) and incubation on ice for 20 mins. The lysate was homogenised using 15 strokes of a a 2 mL dounce homogeniser (B pestle) (Sigma-Aldrich, USA [Cat No: T2690]), nuclei were pelleted by centrifugation at 2,500 RCF for 5 mins at 4 °C. Nuclei were resuspended in nuclear lysis buffer (Sigma-Aldrich, USA [Cat No: B6438]) plus 0.1 M AEBSF and 1× protease inhibitor cocktail and incubated on ice for 10 mins. The DNA concentration was determined using a Nanodrop 2000 spectrophotometer and 120 μg chromatin aliquots were made. The shearing of cross-linked chromatin using DNAseI (New England Biolabs, USA [Cat No: EN0521]) was optimised (Figure 5.4), and was used at 0.05 U/μg chromatin for 30 mins. The reaction was stopped using 5 mM EDTA. The prepared chromatin was then used in an Imprint Chromatin Immunoprecipitaton Kit

Table 2.4: Primers used in this study for the amplification of protein-bound DNA isolated during ChIP experiments

Primer	Sequence (5' to 3')
pHSE1 F	AGTTACACACAAAGCAGAGA
pHSE1 R	TTTTCAGGTTGTTCACAGTG
pHSE2 F	TTTTTACACATGCAGGAAAGC
pHSE2 R	GAACTCCCGGTACTTAGTAGA
pHSE3 F	ACAGAAGGGATGCAGAGGACCA
pHSE3 R	GGAAGCAAACTTGGTGAGATCT
Actin F	AGTGTGGTCCTGCGACTTCTAAG
Actin R	CCTGGGCTTGAGAGGTAGAGTGT
ZNF333-3' F	TGCAGCCAGTGTGGGAAAGC
ZNF333-3' R	GTGCTCGTCCGGAAGGGCTTG

(Sigma-Aldrich, USA [Cat No: CHP2]) as per the manufacturer's instructions. The antibodies used to precipitate DNA-protein complexes are detailed in Table 2.1. The resulting purified DNA was analysed via qPCR using KAPA SYBR FAST qPCR reagents as before. The primers used for this analysis are detailed in Table 2.4. qPCR reaction products were analysed using agarose gel electrophoresis and products of interest were confirmed by direct sequencing.

2.10 Reverse transcriptase PCR

1.5 x 10^5 Hs578T cells were seeded in 6-well cell culture plates and incubated in cell culture conditions for 24 hours. Cells were then treated with GA, NOV or the GA vehicle control DMSO. Specific concentrations for each experiment are described in the legend for Figure 3.10. Total RNA was extracted using Direct-zol RNA miniprep kit (Zymo Research, USA). The concentrations of RNA extracted was determined using a Nanodrop 2000 spectrophotometer (Thermo Scientific, USA) and equal amounts of total RNA were added to triplicate cDNA synthesis reactions with a RevertAid First Strand cDNA Synthesis Kit (Thermo Scientific, USA) using Oligo $(dT)_{18}$ primer. Exon flanking primers (detailed in Table 2.5) were used in PCR reactions to amplify the regions of interest from the fibronectin primary transcript. PCR reactions were set

Table 2.5: Exon flanking primers used for the determination of relative proportions of FN splice variants in samples of total RNA extracted from Hs578T cells by RT-PCR.

Primer	Sequence (5' to 3')
III9 F	GCCTGGTACAGAATATGTAGTG
III9 R	ATCCCAGCTGATCAGTAGGCTGGTG
EDB F	TAATATCAGAAAAGTCAATGCCAGTTG
EDB R	AATACTGGTTATAGAATTACCACAACC
EDA F	AGAGCATAGACACTCACTTCATATTT
EDA R	AAACAGAAATGACTATTGAAGGCT
CS1	TTTAAAGCCTGATTCAGACATTCGTT
CS2	GGGAACCGAATATACAATTTATGTCA
CS3	TTCCCCAACTGGTAACCCTT
CS4	TAGTCTACATCTTCCCTGGG

up as follows: 6.5 μL nuclease free water, 2.5 μL of forward primer, 2.5 μL of reverse primer, 1 μL cDNA, and 12.5 μL GoTaq Hot Start Green 2X Master Mix. Cycling conditions were as follows: (1) 95 °C (120 secs), (2) 95 °C (30 secs), (3) 55 °C (30 secs), (4) 74 °C (50 secs), (5) step 2 - 4 $\times$ 25, (6) 74 °C (300 secs). 25 cycles was determined to be non-saturating. The products of each PCR reaction were resolved using agarose gel electrophoresis using a 1.5 % agarose gel and visualised using a Bio-RAD ChemiDoc XRS+ detection system. The relative band intensities were analysed using densitometry in ImageJ 1.42I. The relative exon composition of the FN transcripts were determined from the densitometry data using the calculations described in the RT-PCR splice variant calculations section in the appendix. Additional statistical analysis was conducted using GraphPad Prism Version 4 software.

3

Results

3.1 Geldanamycin, but not novobiocin treatment increases the fibronectin extracellular matrix and fibronectin protein.

The Hs578T cells were selected for use throughout this work as they were found to have constitutively high levels of FN matrix, protein and mRNA when compared with other cell lines screened during preliminary studies (data not shown). The HEK293FT cell line was selected as it was shown to express FN protein and mRNA and is easy to transfect. In order to investigate the effects of Hsp90 inhibition on the FN ECM, Hs587T cells were treated with the Hsp90 inhibitors novobiocin (NOV) at 100 μM and geldanamycin (GA) at 10 nM or the vehicle control DMSO. Both Hsp90 inhibitors were both used at subtoxic concentrations (see Figure 5.1 A & Figure 5.1 B). At 24 hours following treatment, the cells were immunostained for FN (Figure 3.1 A). The confocal images were used to determine the fluorescence intensity of the FN matrix as the mean grey value (MGV) per number of nuclei. The results depicted in Figure 3.1 B are normalised to the average MGV/nuclei in the DMSO treated cells. The microscopy revealed that relative to the vehicle control treated cells, the level of the FN matrix showed a statistically significant increase which was independent of cell number when the cells were treated with GA. By contrast, the FN matrix decreased slightly when the cells were treated with NOV.

It was then necessary to determine whether this increase in the FN matrix was related to an increase in total FN protein or due to some other factor related to FN

extracellular matrix dynamics. The levels of total FN in cells following GA treatment was investigated using immunoblotting. Hs578T and HEK293FT cells were treated with either increasing concentrations of GA or the vehicle control and lysates were probed for total FN (Figure 3.1 C). GAPDH was used as a loading control. These data demonstrate a clear increase in FN when cells are treated with increasing concentrations of GA (Figure 3.1 C). The increase in FN protein levels after treatment with GA in HEK293FT cells was dose dependent at the concentrations tested, whereas the change in the Hs578T cells was in correlation to the concentration of GA until 1 μM is reached. This loss in total FN protein at high concentrations of GA is likely to be related to reduced cell viability (see Figure 5.1 A).

The data in Figure 3.1 when taken together indicate that treatment of Hs578T breast cancer cells with low concentrations of GA resulted in an increase in FN protein abundance and an observable increases in the FN extracellular matrix. Conversely, NOV treatment resulted in a small decrease in the FN extracellular matrix per cell number (Figure 3.1 B), a finding supported by our previous work(14).

3.2 Geldanamycin increases fibronectin mRNA abundance.

In order to determine whether the observed increase in FN protein abundance was related to changes in protein stability or in mRNA abundance, the levels of FN mRNA were analysed in treated Hs578T and HEK293FT cells using quantitative reverse transcriptase PCR (qPCR). Hs578T cells were treated with 100 μM NOV, 10 nM GA or the vehicle control (DMSO) and 24 hours after treatment, RNA was extracted and equal amounts of RNA from each sample was used in cDNA synthesis reactions and subsequent qRT-PCR reactions for FN levels.

The data obtained were analysed using the $\Delta\Delta$Ct (or Livak) method, which compares the relative abundance of the product of interest under test conditions, to the abundance of the same product under control conditions(266). The Livak method also accounts for gene expression changes that are unrelated to the experimental conditions by normalising the values obtained against two housekeeping genes. In four experiments, each with three experimental and three technical replicates, the NOV treated cells showed no statistically significant change in fibronectin mRNA relative to the

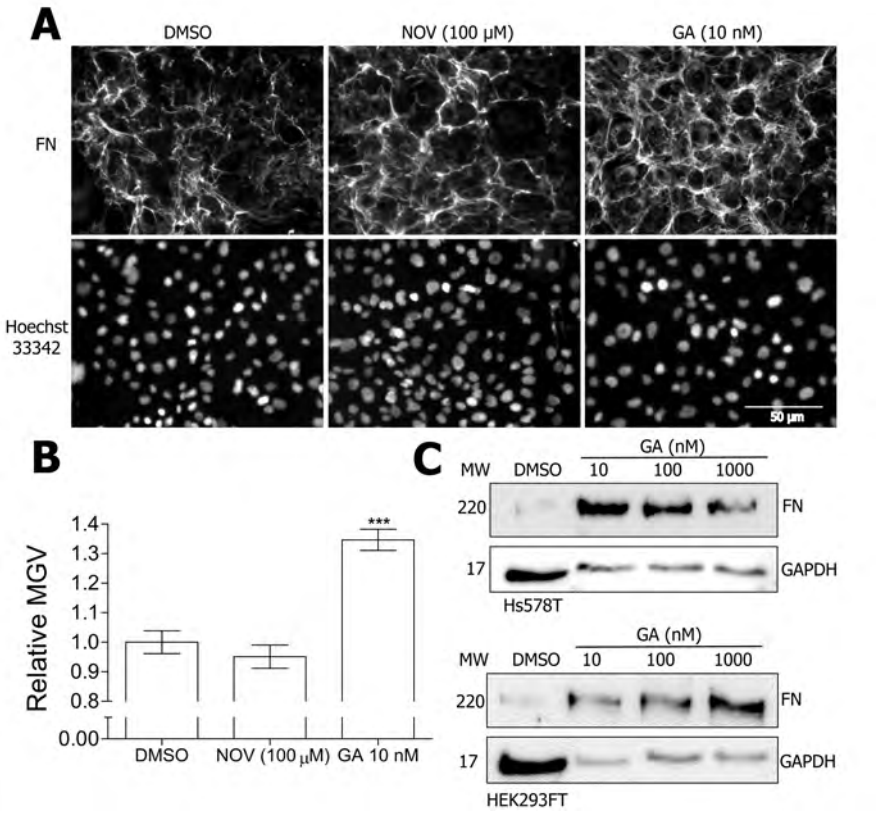

Figure 3.1: Geldanamycin treatment induces fibronectin extracellular matrix and increases fibronectin protein - **(A)** Hs578T cells were treated with 100 μM NOV or 10 nM GA or DMSO (V/C). 24 hours after treatment cells were fixed using methanol and immunostained with mouse anti human FN followed by donkey anti mouse DyLight 488 secondary antibody. Nuclei were stained with Hoechst 33342 (1 mg.mL^{-1}). Images were captured using the 20× objective on a Zeiss Axio Vert.A1 fluorescence microscope and analysed using ZEN Light Blue SP1 (Zeiss, Germany). The scale bar indicates a distance of 50 μm. Fluorescence microscopy images from six fields of view for each treatment were captured and the mean grey values for each field of view was determined using ImageJ 1.42I. **(B)** Average mean grey values (MGV) from duplicate independent experiments. Statistical analysis was performed by comparing inhibitor treated to cells treated with the vehicle control (DMSO) using one way ANOVA with Bonferroni post-test. Images shown are representative of duplicate independent experiments (***p<0.001). **(C)** Hs578T and HEK293FT cells were treated with different concentrations of GA or DMSO, the vehicle control (V/C). 24 hours post treatment, levels of FN protein were analysed by immunoblotting with mouse anti human FN primary antibody.

DMSO treated cells (Figure 3.2 A). The GA treated cells however, did show a statistically significant increase in FN mRNA abundance when compared to the vehicle control, averaging around 10-fold higher than the levels of FN mRNA in the DMSO treated cells (Figure 3.2 A).

The kinetics of the apparent increase in FN mRNA abundance was investigated by preparing RNA after 2, 4, 6 or 8 hours of treatment with 100 nM GA or DMSO. Figure 3.2 B depicts the data from these experiments. There was an increase in the FN mRNA early in the time-course with the peak in the range investigated at 6 hours with an average 1.5-fold increase in FN mRNA, however this increase was not statistically significant.

The dose dependency of the FN mRNA increase in response to GA treatment was subsequently investigated. Hs578T cells (Figure 3.2 C) and HEK293FT cells (Figure 3.2 D) were treated with increasing concentrations of GA or the vehicle control for 24 hours. The data for the Hs578T cells showed a small decrease in the FN mRNA at 1 nM GA, and a dose dependent increase in the abundance of FN mRNA with 10 nM and 100 nM GA (Figure 3.2 C). Figure 3.2 D shows a similar trend for the FN mRNA levels in the HEK293FT cells, although the increase at 100 nM was statistically significant compared to the DMSO treated cells.

3.3 Geldanamycin, but not novobiocin, induces the canonical heat-shock response.

The extracellular matrix, protein and mRNA levels of fibronectin had been found to be responsive to GA treatment, but not NOV treatment. A known effect of the inhibition of Hsp90 by GA is the induction of the cell stress (or the heat-shock) response(267). We investigated if the conditions under which we had observed the induction of FN would be sufficient to induce the cell stress response in Hs5678T and HEK293FT cells. mRNA was prepared from both cell lines after 24 hours of 100 nM GA or DMSO treatment, as this appeared to be the concentration at which the increase in FN mRNA was highest in both cell lines (Figure 3.2). The RNA samples were measured using qPCR for changes in the mRNA levels for known cell stress responsive genes: Hsp90α (*HSP90AA1*), Hsp70 (*HSPA1A*), and Hsp27 (*HSPB1*)(55). These data were analysed using the ΔCt method comparing the treated samples to those treated with the vehicle control, data for the the

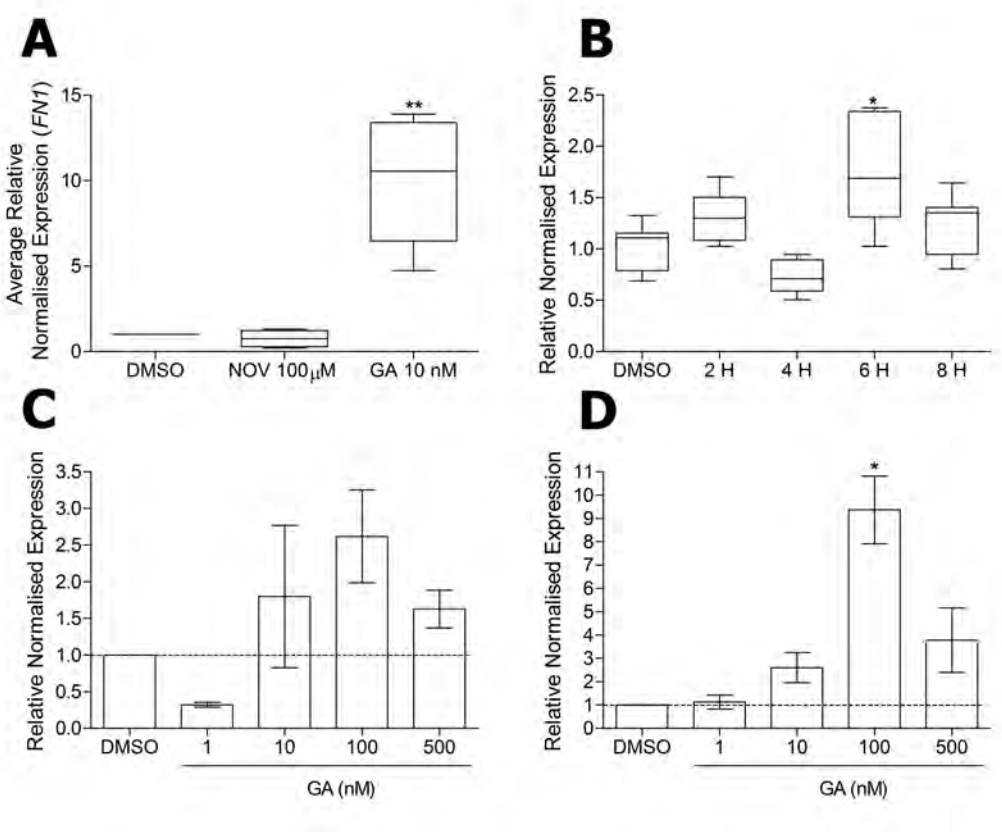

Figure 3.2: *FN1* mRNA levels are increased by geldanamycin treatment in a dose dependent manner - (A) Hs578T cells were treated for 24 hours with either 100 μM NOV or 10 nM GA, with DMSO acting as the control. Values are representative of the averaged normalised expression values (NEV) from four independent biological replicates each with triplicate experimental and technical replicates (**$p<0.01$). Statistical analysis was conducted on the NEVs (average Ct values $p<0.0001$) using a one way ANOVA and comparing the treated samples to the DMSO treated samples with a Tukey post-test. **(B)** Hs578T cells were treated for different periods of time with 100 nM GA or the DMSO vehicle control (8H). Data was analysed as before and values are representative of the NEVs values from three independent biological replicates with triplicate experimental and technical replicates (*$p<0.05$). Statistical analysis was conducted on the NEVs using a one way ANOVA and comparing the GA treated samples to the DMSO treated samples with a Tukey post-test. Hs578T **(C)** and HEK293FT **(D)** cells were each treated for 24 hours with different doses of GA or the vehicle control. Values are representative of the NEVs (*$p<0.01$) from duplicate experiments. In all cases total RNA was extracted and equal amounts of total RNA were used for cDNA synthesis. qPCR was conducted using a CFX Connect Real-Time PCR Detection System (Bio-RAD). Data was analysed using the $\Delta\Delta$Ct method in Bio-RAD CFX Manager 3.1 Software.

control genes are displayed as the non-targeting reference control. Both Hs578T (Figure 3.3 A) and HEK293FT (Figure 3.3 B) cells showed statistically significant increases in the Hsp90α and Hsp70 mRNA in the GA treated cells compared to the vehicle control. Where the HEK293FT cells demonstrated a statistically significant increase in Hsp27 mRNA abundance, the Hs578T cells did not.

The localisation of HSF1 to the nucleus(50), its phosphorylation and the formation of nuclear stress bodies(52)(268) are additional features of the heat-shock response that were investigated using fluorescence and confocal microscopy respectively (Figure 3.3 C and D). In the investigation of the nuclear localisation of HSF1 Hs578T cells were treated with NOV at 100 μM, GA at increasing concentrations, or DMSO. Cells were fixed and immunostained for HSF1. Representative images of the distribution of HSF1 were captured using a Zeiss Axio Vert.A1 fluorescence microscope and analysed using ZEN Light Blue SP1 (Zeiss, Germany). The HSF1 staining in the DMSO treated cells was diffuse, with distribution of HSF1 across the cell nucleus and the cytoplasm (Figure 3.3 C). When the cells were treated with increasing concentrations of GA, the localisation of HSF1 staining became more nuclear with increasing concentrations of GA. There was no change observed in the localisation of HSF1 under NOV treatment which supports our previous findings.

Although HSF1 is known to be phosphorylated under non-stressful conditions, hyperphosphorylation of serine residues on HSF1, such as S326, has been associated with the transcriptional activity of HSF1(27). We investigated changes in the colocalisation of total phosphorylated serine residues (pSerine) and HSF1 as an indicator of HSF1 activation state. After 24 hours of treatment with 100 nM GA or DMSO, Hs578T cells were immunostained for HSF1 and total pSerine. Images were captured using a Zeiss LSM 780 confocal microscope using identical laser settings and analysed using ZEN Black Edition 2012 (Zeiss, Germany). The levels of total HSF1 did not change between the DMSO and GA treated cells, however the total levels of pSerine did increase after treatment with GA (Figure 3.3 D). In the GA treated cells, some granular areas of pSerine staining were detected in the nuclei, and these granules colocalised with HSF1 staining as highlighted by white arrows on Figure 3.3. These colocalision points in the nuclei were not observed in the DMSO treated cells.

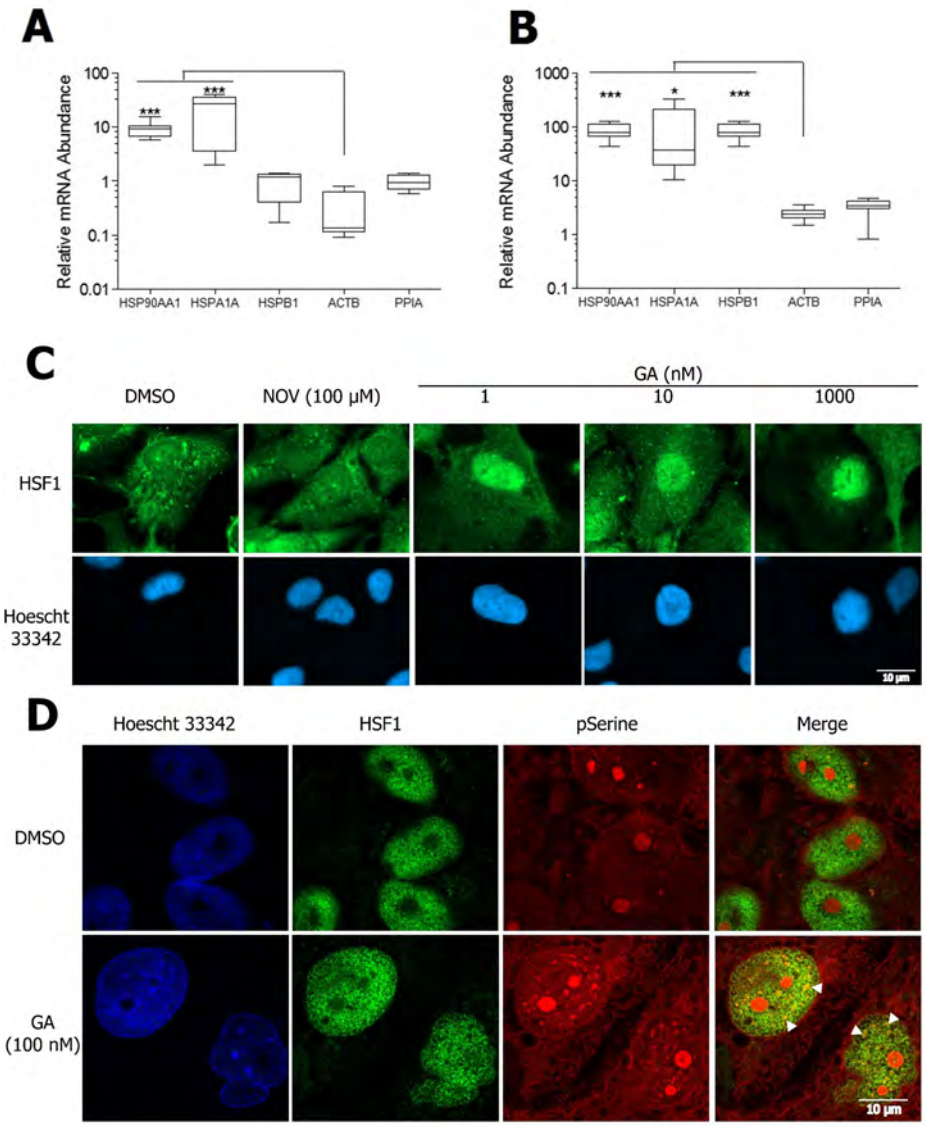

Figure 3.3: Geldanamycin treatment induces the heat-shock response - Hs578T **(A)** and HEK293FT **(B)** cells were treated for 24 hours with 100 nM GA or DMSO. Total RNA was extracted and qPCR was conducted using PPIA and ACTB reference genes. Data were analysed using the ΔCt method and are representative of the averaged relative expression values from three separate biological replicates each with triplicate technical replicates. Statistical analysis was conducted in GraphPad Prism Version 4 using one way ANOVA with a Kruskal-Wallis post test (***$p<0.001$, *$p<0.05$). **(C)** Hs578T cells were treated with 100 μM novobiocin, DMSO or different concentrations of geldanamycin. 2 hours after treatment the cells were immunostained for HSF1 and nuclei were stained with Hoechst 33342 (1 mg.mL^{-1}). Images were captured using the 100× objective on a Zeiss Axio Vert.A1 fluorescence microscope **(D)** Hs578T cells were treated for 24 hours with GA 100 nM or the DMSO vehicle control. The cells were fixed, immunostained for HSF1 and pSerine, and images were captured using the 100× objective on a Zeiss LSM 780 confocal microscope. Scale bars indicate 10 μm. White arrowheads indicate regions of pSerine and HSF1 colocalision in the cell nucleus.

3.4 The *FN1* promoter contains putative heat-shock elements.

Elucidating a possible link between the stress response and the regulation of the FN gene required an analysis of the *FN1* promoter. The genomic sequence for *FN1* (NCBI: NG_012196.1) was retrieved from the ENCODE human genome build 19 (http://genome-.ucsc.edu/ENCODE/). The region from 5000 bp upstream (5'-3') and 1000 bp downstream of the *FN1* transcription start site (TSS, located at 216,211,070 bp on human chromasome 2), was retrieved and analysed for *cis*-element clustering using the Cister algorithm from Boston Universitys ZLab online gene regulation toolkit. The results for this analysis are graphically displayed in Figure 3.4 A. The clustering of known *cis*-regulatory elements such as Sp1, CRE and E2F sites (269), and core promoter motifs such as CCAAT and TATA boxes were identified in the -1500 bp to 500 bp region of the *FN1* sequence analysed, suggesting the presence of the *FN1* promoter (Figure 3.4 A)[1]. The same sequence was analysed for putative heat-shock elements (HSEs) using a number of transcription factor binding motif algorithms, with special attention given to the region encompassing the regulatory clustering from -2000 bp to the TSS (+1). The TFSearch algoritm(261) identified three potential HSEs similar to the canonical HSF1 binding motif (nGAAnnTTCnnGAAn)(55)(27). The locations of the purported HSEs on the *FN1* promoter are shown relative to the TSS (+1) and other key regulatory sites in Figure 3.4 B. These locations described relative to the *FN1* TSS are: pHSE1 (-965 bp to -951 bp), pHSE2 (-806 bp to -787 bp) and pHSE3 (+179 bp to +192 bp) (Figure 3.4 B).

The identification of potential heat-shock factor binding sites on the *FN1* promoter was of interest. We therefore wanted to investigate the effect of GA treatment on the activity of the *FN1* promoter as a prospective mechanism for the effects we had previously observed (Figure 3.1, Figure 3.2). The sequence of *FN1* from - 1240 bp to + 100 bp, encompassing the putative HSEs identified was synthesised and sub-cloned into a promoter-less luciferase reporter vector according to the strategy outlined in appendix Figure 5.3 to create the fibronectin promoter reporter vector pGL4-pFN1.

[1]Posterior probability is the conditional probability assigned to the local cluster of nucleotides of the given binding elements occurring above background frequency.

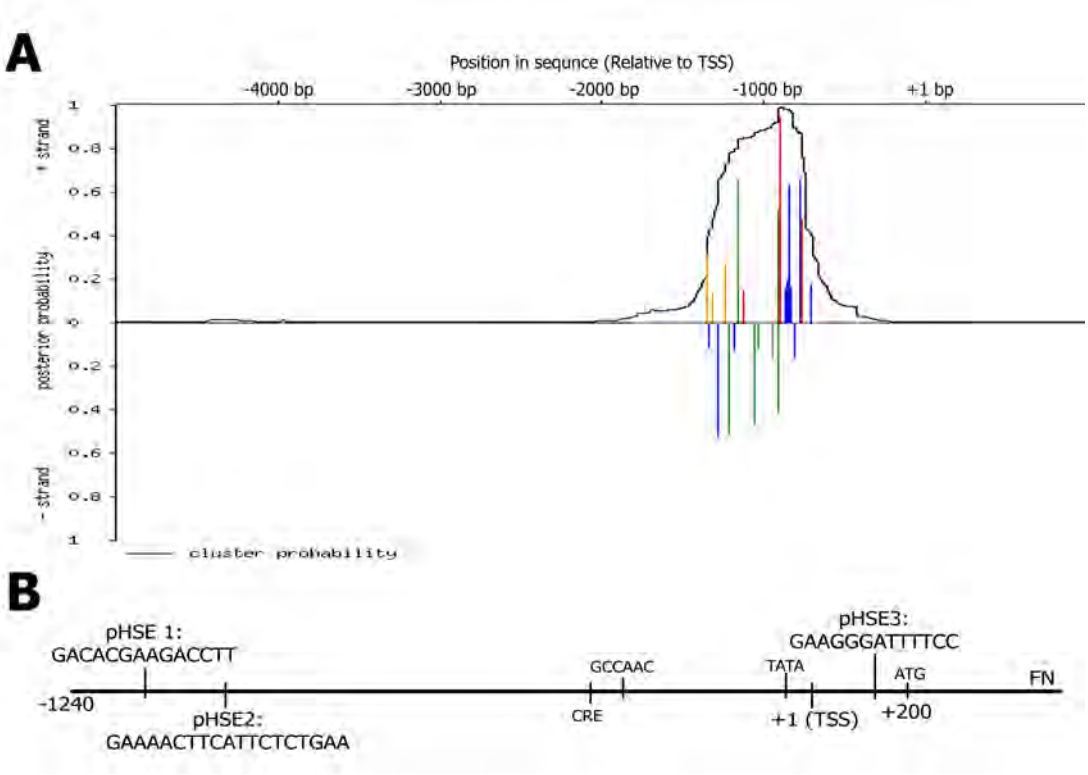

Figure 3.4: The *FN1* promoter contains putative heat-shock elements - The genomic sequence for the fibronectin gene (NCBI: NG_012196.1) was retrieved from the ENCODE human genome build 19 (http://genome.ucsc.edu/ENCODE/). The region from 5000bp upstream (5'-3') and 1000bp downstream of the transcription start site (TSS) (located at 216,211,070 bp on human chromosome 2) was analysed using the Boston Universitys ZLab online gene regulation toolkit in order to identify clusters of common *cis*-regulatory motifs. **(A)** Cister output plot indicating the local posterior probabilities *cis*-regulatory factor clusters on the human fibronectin pre-protein sequence from -4218 bp to +1782 bp. **(B)** The synthesised *FN1* promoter annotated with purported HSEs and key transcription motifs. The CCAAT box (-334 bp)(245) and TATA box (-27 bp)(245) are identified relative to the TSS (+1 bp) and start codon (+ 200 bp).

3.5 Geldanamycin treatment increases the activity of the *FN1* promoter.

In order to investigate the effect of GA on the activity of the *FN1* promoter, transient transfection of the reporter vector into the HEK293FT cell line was used. As previously demonstrated the HEK293FT cell line behaves similarly to the Hs578T breast carcinoma cell line with respect to FN under the test conditions of interest, and the HEK293FT cell line is easily transfected with plasmid DNA.

HEK293FT cells were transfected with pGL4-pFN1, our *FN1* promoter reporter vector and pCAG-HRP-TM, a vector encoding horseradish peroxidase (HRP). Promoterless pGL4.17 vector and non-transfected cells (N/T) were used as negative controls. The luciferase assay was adapted from Seibring-van Olt *et al.* (2012)(265) to make use of the pCAG-HRP-TM vector as a transfection efficiency control. At 24 hours post transfection the cells were treated with either 100 μM NOV, increasing concentrations of GA, or the vehicle control. At a further 24 hours post treatment cells were lysed and the levels of luciferase and HRP activity were measured. Luminescence values were divided by the HRP absorbance and normalised to the DMSO vehicle control (Figure 3.5 A). The DMSO vehicle control shows the baseline level of expression of the pGL4-pFN1 vector luciferase, and hence the basal activity of the *FN1* promoter in untreated HEL293FT cells. All of the other test conditions were normalised to this column. Negative controls showed no luciferase activity as expected, with a very low background expression from the promoter-less pGL4.17 vector (EV). The treatment of the cells with NOV decreased the relative activity of the *FN1* promoter, as did treatment with GA at 1 nM. Higher doses of GA treatment showed an induction of activity of the reporter system with a peak 4.5-fold increase in promoter activity at 100 nM GA. Higher doses of GA reduced the activity of the reporter system relative to this peak, possibly due to cytotoxicity, but values remained above 2-fold higher than the DMSO control. The relative levels of luciferase activity for GA concentrations 10 nM and higher were statistically significant.

The kinetics of the induction of the reporter system activity was investigated using similar assay methodology with staggered treatment times for 100 nM GA. HEK293FT cells were transfected with pGL4-pFN1 and pCAG-HRP-TM, with pGL4.17 acting as

the negative control. The cells were treated 24 hours after transfection at 4 hour intervals from 36 to 8 hours prior to cell lysis and the measurement of luciferase and HRP activities. The data were normalised as before to the HRP transfecton control and then to the vehicle control (Figure 3.5 B). DMSO treated cells represent the baseline activity of the *FN1* promoter luciferase reporter system, and the empty pGL4.17 vector (EV) showed negligible background expression. At 8 hours after GA treatment there was the maximum observed relative activity of the reporter system. The relative activity showed a gradual reduction in luciferase activity between 8 hours and 36 hours after GA treatment, but expression of the reporter system was still 2-fold higher than the basal levels observed with the vehicle control at 36 hours after GA treatment.

3.6 Loss of putative heat-shock elements abrogates stress-responsiveness of the FN1 promoter.

The activity of the cloned region of the *FN1* promoter encompassing putative heat-shock elements was shown to be responsive to GA treatment, and thus it was next necessary to determine whether the potential HSF binding motifs were required for the observed increase in promoter activity in response to GA treatment. In order to investigate this, truncations of the FN promoter were generated by PCR from the pGL4-pFN1 vector and re-cloned into the pGL4.17 reporter vector. These promoter truncations, designated pGL4-pFN1_810 (TR1) and pGL4-pFN1_380 (TR2) (Figure 3.6 A), lacked the two distal putative HSEs located close to -1 kb from the TSS.

HEK293FT cells were transfected with either pGL4-pFN1, pGL4-pFN1_810 (TR1), pGL4-pFN1_380 (TR2), or empty pGL4.17 together with pCAG-HRP-TM. At 24 hours post transfection, cells were treated with either DMSO or GA at 100 nM. A further 24 hours following treatment cells were lysed and processed as previously described with luciferase activity normalised to the HRP transfection control and then normalised to the vehicle control treated full length *FN1* promoter vector. The cells transfected with the full-length cloned promoter sequence demonstrated the expected increase in luciferase activity upon treatment with 100 nM GA. The cells transfected with the empty pGL4 vector showed no significant luciferase activity in thwe presence or absence of GA. Both truncated promoter sequences, however, showed a reduction by more than

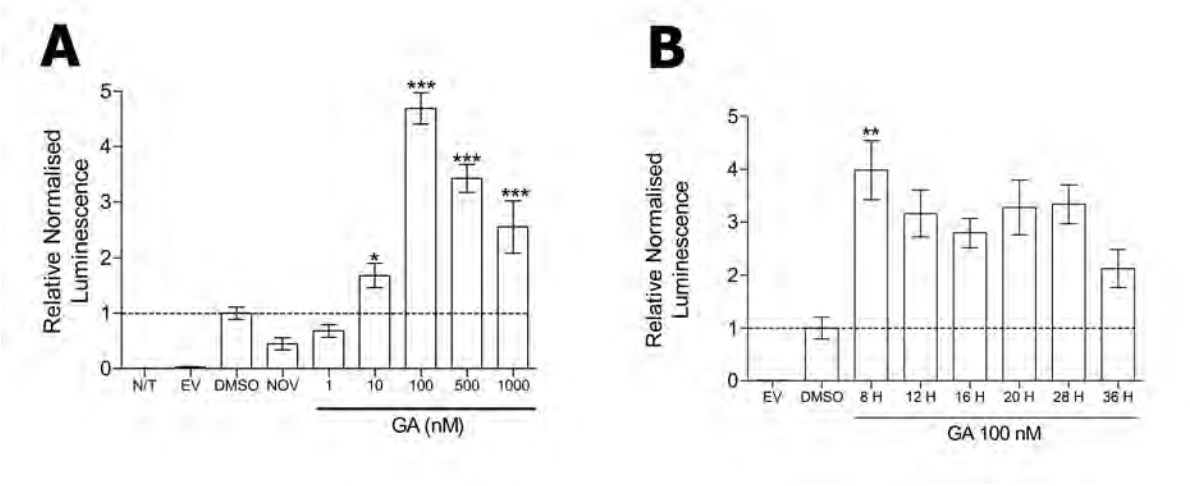

Figure 3.5: ***FN1*** **promoter activity is increased by GA treatment - (A)** HEK293FT cells were transfected with pGL4-pFN1 and pCAG-HRP-TM. Empty pGL4.17 vector (EV) and non-transfected cells (N/T) served as negative controls. 24 hours post transfection the cells were treated with varying doses of GA, 100μM NOV or the vehicle control. 24 hours post treatment cells were assayed for luciferase and HRP activity. Luminescence values were divided by the absorbance and normalised to the DMSO vehicle control. Values shown are representative of 12 biological replicates per treatment with 3 technical replicates per transfection. Data were analysed and statistical analysis was conducted in GraphPad Prism Version 4 by comparing the inhibitor treated cells to the DMSO control using one way ANOVA with Bonferroni post-test (***p<0.001). **(B)** HEK293FT cells were transfected with pGL4-pFN1 and pCAG-HRP-TM. Empty pGL4.17 vector and DMSO treated cells served as negative controls. Beginning at 24 hours post transfection the cells were treated with 100 nM GA at different time points such that after 36 hours when the cells were lysed and the luminescence was captured, the cells had been exposed to GA for time points from 8-36 hours. The luciferase assay was conducted and the data processed as previously described. Values shown are representative of 3 replicates per transfection (**p<0.01). Statistical analysis was conducted in GraphPad Prism Version 4 by comparing the inhibitor treated cells to the DMSO control using one way ANOVA with Kruskal-Wallis post-test.

50 % in basal activity and showed no statistically significant increase in luminescence after 100 nM GA treatment.

These data suggested that the DNA region removed by the first truncation (TR1) contained the motif responsible for the increase in promoter activity observed on GA treatment (Figure 3.6). There was also a loss in basal reporter activity, indicating that one or more sites involved in the constitutive activity of the *FN1* promoter were also eliminated in the first truncation. There was little difference between the relative normalised luminescence values between the cells transfected with the first or the second truncation, potentially indicating that no important regulators of FN gene expression were encompassed by the -810 bp to - 380 bp region of the promoter.

3.7 Heat-shock factor 1 occupies a heat shock element on the fibronectin promoter and occupancy is responsive to geldanamycin treatment.

We had demonstrated that the loss of a DNA sequence spanning the location of two purported HSE motifs resulted in the loss of a GA induced increase in the activity of a *FN1* promoter reporter system. Next it was necessary to test for direct binding of HSF1 to these sequences. qPCR primers were designed against the three regions on the *FN1* promoter containing putative HSEs (Table 2.4). Hs578T cells were treated with either DMSO or 100 nM GA for 24 hours prior to harvesting and processing as described in the methodology chapter. Chromatin immunoprecipitation (ChIP) was conducted using an Imprint UltraChromatin Immunoprecipitation kit (Sigma-Aldrich) on 7.5 million cells per ChIP (around 30 μg chromatin) with mouse anti-RNApolII as an experimental control and rabbit anti-HSF1 as the test condition on both DMSO and GA (100 nM) treated cell chromatin. The protein DNA complexes obtained were un-crosslinked and the DNA was purified as per the manufacturer's instructions. qPCR was conducted on the DNA and the fold enrichment of HSF1 to the purported heat shock element at -965 bp to -951 bp (pHSE1) over the isotype control was determined using the ΔCt method as outlined by Livak and Schmittgen (2001)(266) for both treatment conditions.

The positive control of RNAPolII recruitment to the actin promoter showed binding under both treatment conditions, but no clear change between the GA and DMSO treated cells (Figure 3.7). The negative control (RNAPolII recruitment to *ZNF333* 28kb

3.7 Heat-shock factor 1 occupies a heat shock element on the fibronectin promoter and occupancy is responsive to geldanamycin treatment.

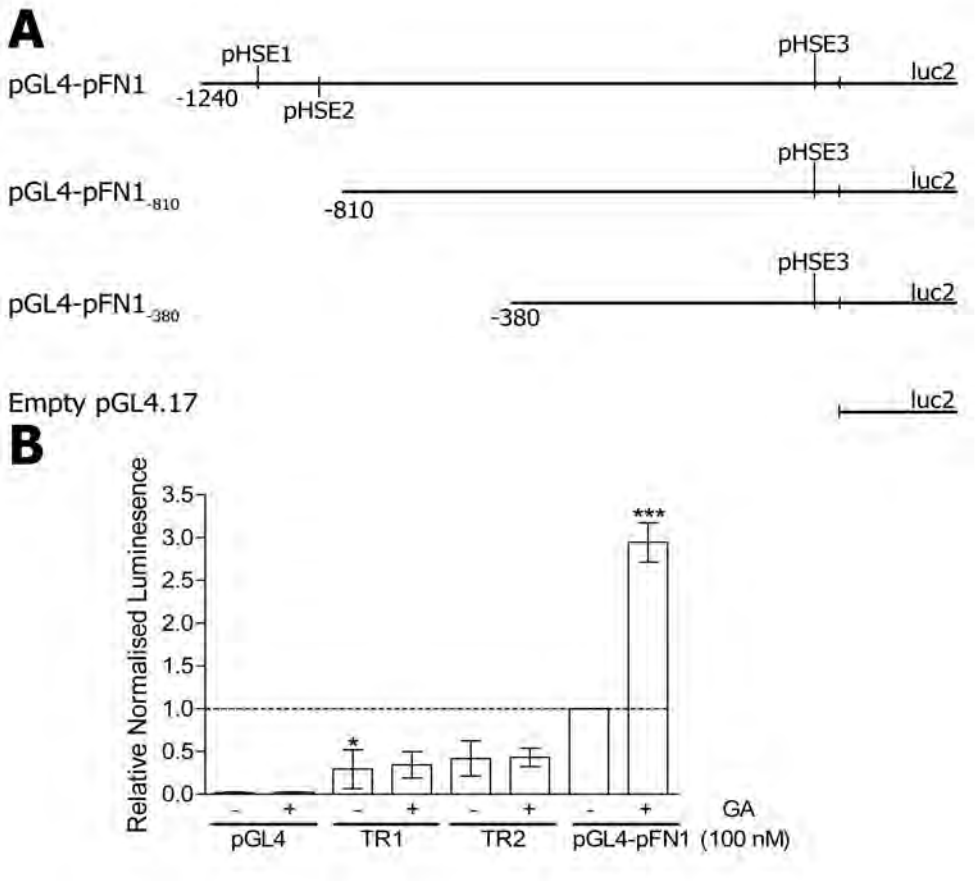

Figure 3.6: GA induced up-regulation of FN1 is dependent on heat shock elements on the promoter. - **(A)** Two truncations of the synthesised *FN1* promoter were made by PCR amplification. New vectors pGL4-pFN1_810 (TR1) and pGL4-pFN1_380 (TR2) were validated by sequencing. **(B)** HEK293FT cells were transfected with pGL4-pFN1, pGL4-pFN1$_{-810}$ (TR1), pGL4-pFN1$_{-380}$ (TR2), or empty pGL4.17 and pCAG-HRP-TM, 24 hours post transfection the cells were treated with 100 nM GA or DMSO. 8 hours following treatment, cells were lysed and a luciferase assay was conducted as before. Values shown are representative of 6 experimental replicates (transfections) per treatment with 3 technical replicates per transfection. Data were analysed and statistical analysis was conducted in GraphPad Prism Version 4 using one way ANOVA with a Dunnett's Multiple Comparison Test (*$p<0.05$, ***$p<0.001$).

downstream of the TSS) showed no binding enrichment for either treatment (Figure 3.7). Recruitment of HSF1 to the pHSE1 site was detected in both the DMSO and GA treated cells (Figure 3.7). A clear increase in enrichment of HSF1 recruitment to HSE1 in the GA treated cells compared to the vehicle control was observed in both replicate experiments. This fold increase was statistically significant in one of the replicate ChIP experiments (Figure 3.7). The product obtained from the HSE1 PCR was confirmed by direct sequencing and found to match the predicted HSE1 (Table 5.1). These data were reproduced in a second independent pull-down experiment from chromatin prepared from the same biological samples. The two other purported HSEs; pHSE2 and pHSE3, were unable to be tested for as the primers designed to amplify these regions produced multiple bands during PCR amplification.

These data confirmed that HSF1 bound at the predicted HSE motif at -965 bp to -951 bp on the *FN1* promoter, and that the occupancy of this HSE was increased by GA treatment.

3.8 Repression of HSF1 activation by mTORC1/FKBP12 inhibition reduces FN1 mRNA.

We demonstrated occupancy of HSE1 on the *FN1* promoter by HSF1, and now wanted to confirm the mechanistic relationship between HSF1 and *FN1* via an independent mechanism. The master nutrient sensor mTORC1 has been shown to directly enable HSF1 transactivation capacity through the phosphorylation of S326(62). We investigated the effects of mTORC1 inhibition on HSF1 activation by microscopy and the levels of FN mRNA by qPCR analysis.

Hs578T cells were treated with either rapamycin (50 nM), GA (100 nM), or both at the given concentrations, with DMSO acting as the vehicle control. It had previously been determined that the rapamycin treatment was at a sub-toxic concentration (appendix Figure 5.1 C). From the same biological samples coverslips were prepared for microscopy and RNA was extracted and processed 24 hours post-treatment, as previously described. qPCR was conducted on the total FN mRNA present and the data were analysed using the ΔCt method to show the levels of FN mRNA relative to the vehicle control (Figure 3.8 A). Compared to the DMSO treated cells, GA treated cells showed a statistically significant increase in the abundance of FN mRNA as we had

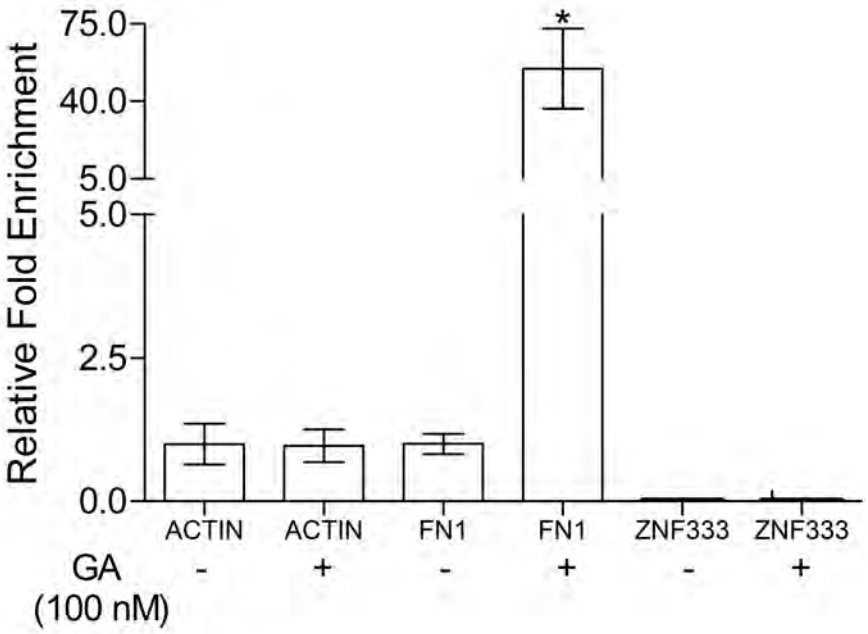

Figure 3.7: Heat-shock factor 1 occupies a heat shock element on the fibronectin promoter and occupancy is responsive to geldanamycin treatment. - Hs578T cells were treated with either 100 nM GA or the vehicle control. 24 hours post-treatment the cells were harvested. Chromatin immunoprecipitation was conducted using the Imprint UltraChromatin Immunoprecipitation Kit (Sigma-Aldrich) as per the manufacturer's instructions. The purified DNA was amplified using qPCR in a CFX Connect Real-Time PCR Detection System (Bio-RAD). The Ct values obtained were used to calculate the fold enrichment of the *FN1* purported heat-shock element relative to the isotype control and input DNA from the anti-HSF1 immunoprecipitation under the two conditions was determined using the ΔCt method(266). These fold increase values were normalised to the DMSO treated sample for each paired ChIP. RNAPolII enrichment on the actin promoter (chr7: 5537367 bp - 5537443 bp) was used as a positive control and the same on the *ZNF333* gene 28kb downstream of the TSS was used as a negative control. Data from one of two independent ChIP experiments with similar results are shown. Data were analysed and statistical analysis was conducted in GraphPad Prism Version 4 using one way ANOVA with Kruskal-Wallis post-test (*$p<0.05$).

previously demonstrated (Figure 3.2). Cells treated with rapamycin alone showed a statistically significant decrease in the abundance of FN mRNA compared to the DMSO treated cells. Treatment of cells with both rapamycin and GA was able to prevent the GA induced increase in FN mRNA and was not statistically different to the DMSO control. No change in the abundance of FN mRNA compared to the DMSO control (Figure 3.8 A).

The Hs578T cells treated with either rapamycin (50 nM), GA (100 nM), both, or DMSO were immunostained as previously described. Representative images are shown in Figure 3.8 C. DMSO treated cells had lower pSerine staining than cells treated with GA or rapamycin. The levels of HSF1 staining did not change greatly across the treatment conditions, however punctate nuclear pSerine staining was observed in the GA treated cells (Figure 3.8 C, white arrows), but not the rapamycin treated cells. In the cells treated with both GA and rapamycin, the punctate staining is observable but reduced. The nuclear punctate pSerine staining can be seen to colocalise with HSF1 in the GA treated cells, and is observable but reduced in the GA and rapamycin treated cells. These points of colocalisation are indicated with arrows (Figure 3.8 C).

Quantitative pixel-on-pixel colocalisation analysis between the pSerine and the HSF1 staining was conducted using the MBF ImageJ 1.42I intensity correlation analysis plug-in on the z-stacked images(270). The average Mander's overlap coefficient (R) for each treatment was normalised to the DMSO treated cells (Figure 3.8 B). This analysis demonstrated statistically significant changes in the Mander's Overlap Coefficient (R) upon either rapamycin or GA treatment alone compared to the vehicle control The rapamycin treatment resulted in a reduction in colocalisation between HSF1 and pSerine (0.841 ± 0.077), whereas GA treatment resulted in an increase (1.072 ± 0.055). Treatment with both compounds did not result in a statistically significant change from the DMSO treated cells (1.005 ± 0.078).

The colocalisation data in Figure 3.8 B mirrors the qPCR data in Figure 3.8 A. These data together indicated that when treating Hs578T cells with GA and rapamycin the increase in FN mRNA observed under the effect of GA alone is abrogated. As HSF1 activation has been shown to be dependent on mTORC1 phosphorylation(62), these data support the interpretation that HSF1 is involved in the regulation of *FN1* expression. Additionally the levels of FN mRNA are reduced relative to the DMSO treated cells under the effect of rapamycin alone (Figure 3.8 A), perhaps suggesting

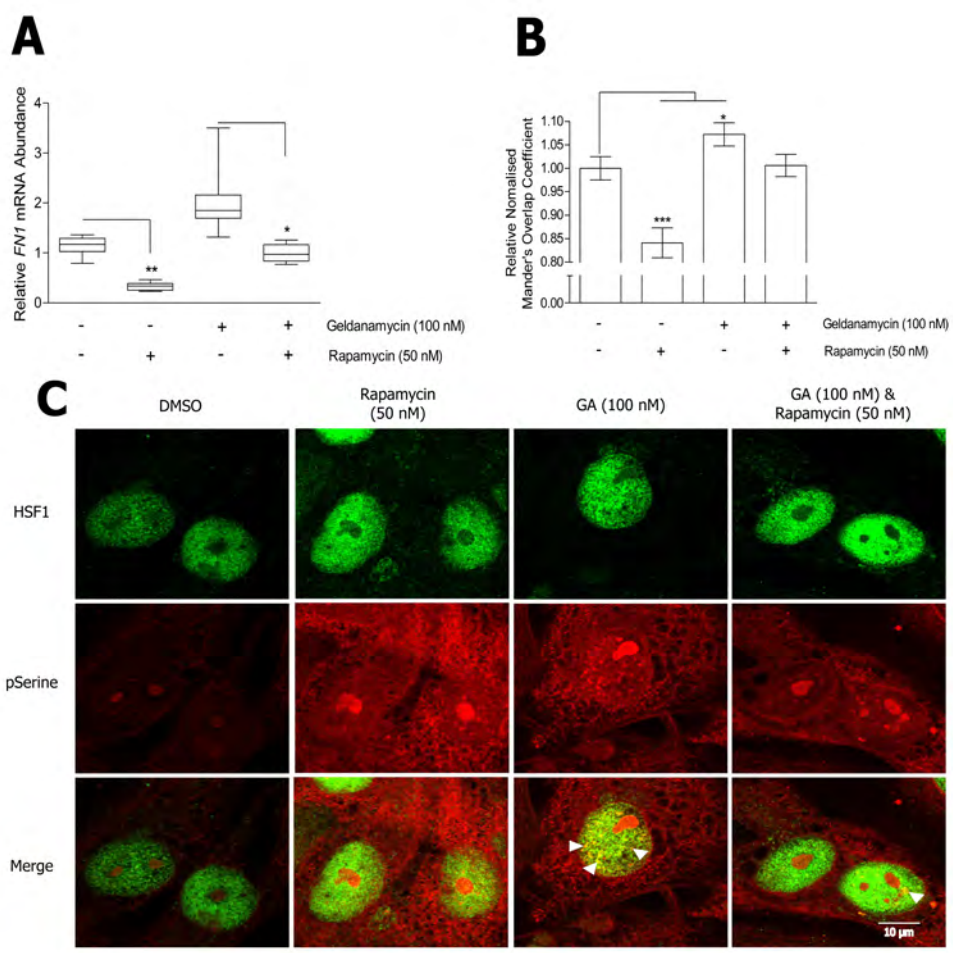

Figure 3.8: Geldanamycin up-regulation of *FN1* is negated by mTORC inhibition - Hs578T cells were treated for 24 hours with GA (100 nM), Rapamycin (50 nM), both or the vehicle control. **(A)** Total RNA was extracted and qPCR was conducted using PPIA as a reference gene. Shown values are representative of the averaged relative mRNA abundance relative to the vehicle control (*p<0.05, **p<0.01) from biological and technical triplicates. Data were analysed and statistical analysis was conducted as before. **(B)** 24 hours after treatment cells were immunostained for HSF1 and pSerine. Images were captured using a Zeiss LSM 780 confocal microscope using the 100× objective. Average Mander's overlap coefficients for each treatment was normalised to the DMSO treated cells for 4 z-stacks per treatment. Representative images are shown in **(C)**. Scale bar indicates a distance of 10 μm. White arrowheads indicate regions of pSerine and HSF1 colocalision in the cell nucleus.

a role for HSF1 in the constitutive expression of the *FN1* gene. A putative role for HSFs in the basal activity of the *FN1* promoter was also supported by the results of the truncation analysis (Figure 3.6).

3.9 Geldnamycin treatment does not change fibronectin splice variant proportions

Fibronectin is a highly alternately spliced gene, containing three alternatively spliced exons which give rise to twenty distinct isoforms of the fibronectin protein(188). The effect of Hsp90 inhibitors on the relative proportions of these isoforms was studied using RT-PCR of the FN mRNA with exon flanking primers, using a protocol adapted from Kilian *et al.* (2004)(271). Figure 3.9 is a schematic representation of the alternately spliced regions in the fibronectin primary transcript and indicates the locations of the primers (listed in Table 2.5) used in this analysis (Figure 3.9 A).

The three alternatively spliced exons are: exon 24 (extra-domain-B / ED-B), exon 32 (extra-domain-A / ED-A) and exon 39 (variable region / IIICS) (Figure 3.9 B). Both exons ED-B and ED-A may be either included or excluded (Figure 3.9 C), whereas the IIICS region may be included completely, excluded completely or partially included in three different ways (which give rise to the 5 putative splice variants described below) (Figure 3.9 D). These partial IIICS inclusions have been previously researched(236), however the precise boundaries between included and excluded regions of the IIICS exon had not been identified. We conducted a systematic sequencing of the PCR products obtained from the splice analysis in order to accurately determine the exon boundaries for the IIICS splice variants. The diagram of the IIICS section in Figure 3.9 demonstrates our results from direct sequencing of the PCR products from the IIICS region in order to identify the locations of the inclusions of the different exon fragments. These data are shown in appendix Figure 5.6.

Exon 39 of the *FN1* primary transcript is 360 bp long and has five splice variants designated IIICS 0 bp, IIICS 192 bp, IIICS 267 bp, IIICS 285 bp and IIICS 360 bp, according to the size of the included fragment (Figure 3.9 D). IIICS 0 bp is the complete exclusion of the exon, and IIICS 360 bp is the complete inclusion. The three partially included fragments are structured as follows: IIICS 192 bp has both a 5' 72 bp and a

3' 90 bp truncation. The IIICS 267 bp splice variant has only the 3' 90 bp truncation, and the IIICS 285 bp splice variant has only the 5' 72 bp truncation (Figure 5.6).

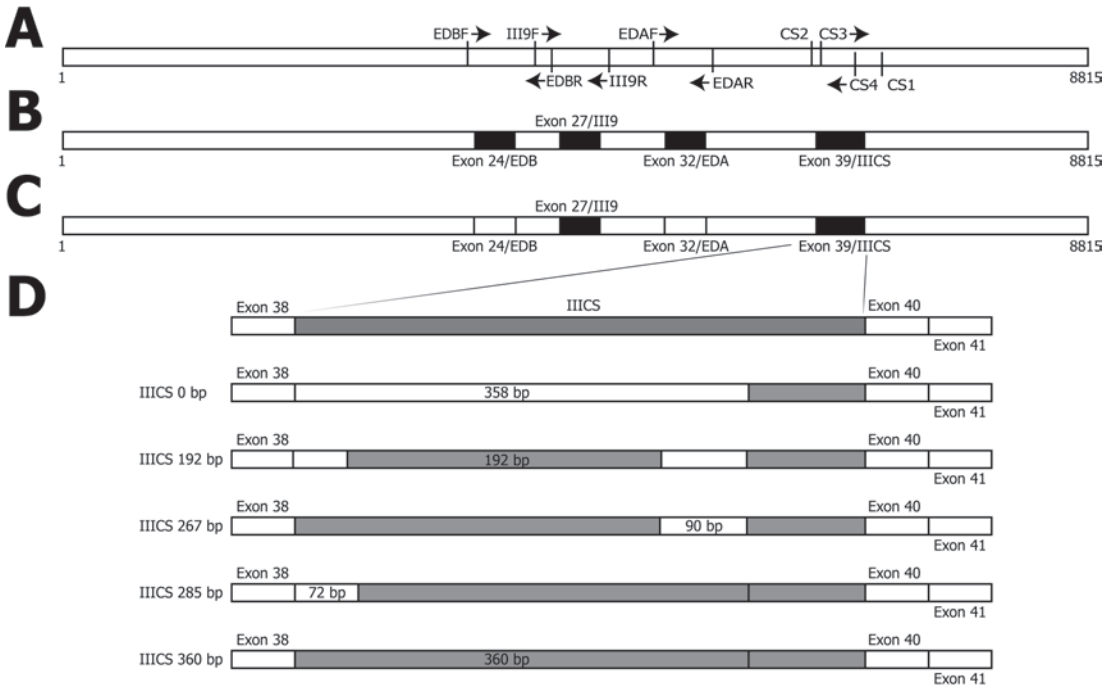

Figure 3.9: ***FN1*** **primary transcript splicing schematic** - **A** Schematic diagram of the FN mRNA primary transcript indicating the locations of the exon flaking primers used to determine relative splice variant composition. There are three alternatively spliced regions in the fibronectin primary transcript; extra domain-B (ED-B), extra domain-A (ED-A) and the IIICS region, highlighted in **B**. The III9 exon is included in all FN splice variants. **C** The ED-B and ED-A exons can either be included or excluded, whereas the IIICS region can be alternately spliced in five ways. **D** The IIICS region can be excluded completely (IIICS 0 bp), included completely (IIICS 360 bp) or partially included; IIICS 192 bp has both a 5' 72 bp and a 3' 90 bp truncation. The IIICS 267 bp splice variant has only the 3' 90 bp truncation, and the IIICS 285 bp splice variant has only the 5' 72 bp truncation.

In order to determine the relative proportions of the fibronectin splice variants under Hsp90 inhibition, the RT-PCR strategy using exon flanking primers (Table 2.5) was used. Hs578T cells were treated with 100 μM NOV, 10 nM GA or the vehicle control (DMSO). RNA was extracted and equal amounts of RNA were used in cDNA synthesis as previously described. The primers were used in five separate PCR reactions per cDNA sample and were conducted such that the reactions were non saturated.

3.9 Geldnamycin treatment does not change fibronectin splice variant proportions

Each PCR reaction yielded multiple bands (see appendix Table 5.2 for primer pairs and corresponding products, and appendix Figure 5.5 for a representative example). The relative intensities of bands in the same lane were analysed using densitometry in ImageJ 1.42I and the percentage composition of each alternately spliced exon was determined. Total FN, which was detected by the III9 exon which is present in all FN splice variants, was assayed as a positive control. Calculations are outlined in the appendix calculations section. The synthesised results for these data are depicted in Figure 3.10.

Figure 3.10 A and B show the change in relative composition of the ED-B and ED-A exons respectively under the effect of Hsp90 inhibitors. In the DMSO treated cells, the Hs578T cell line produced FN with approximately 15 % ED-B+ and 50 % ED-A+. Following NOV treatment, the inclusion of the ED-B exon appears to increase to around 25 % but this apparent increase was not shown to be statistically significant. GA treated cells similarly showed a small increase in the inclusion of ED-B in response to GA but this was also not statistically significant. The relative change in the ED-A exon upon treatment with both Hsp90 inhibitors was a small 5-10 % increase in exon inclusion to approximately 60 % ED-A+ FN mRNA, which was not deemed to be significant.

The relative composition of the IIICS region under the experimental conditions is shown in Figure 3.10 C. The relative IIICS composition for FN under the control conditions showed that the largest fraction was composed of IIICS 267 bp, followed by roughly equal amounts of IIICS 360 bp and IIICS 0 bp and small amounts of IIICS 192 bp, with only trace (<2 %) of IIICS 285 bp. These proportions did not change in any statistically significant manner after treatment with either NOV or GA. Only a minor increase in IIICS 360 bp with a concomitant decrease in the inclusion of the IIICS 267 bp splice variant was observed under GA treatment. A slightly larger (± 10 %) increase in IIICS exclusion (IIICS 0 bp) with a corresponding decrease in IIICS 267 bp and IIICS 360 bp inclusion under the effect of NOV treatment.

We subsequently investigated the change in relative composition of the ED-B and ED-A exons in response to increasing concentrations of GA. Hs578T cells were treated with GA at 1 nM - 1 μM and 24 hours post treatment RNA was extracted and RT-PCR analysis was conducted as previously outlined. The III9 exon which had acted as a positive control in the RT-PCR experiments (as it is included in all FN splice variants)

is plotted in Figure 3.10 D for comparison with the ED-B+ and ED-A+ inclusion data. All values are normalised to the DMSO treated samples for each exon. The abundance of the III9 (total FN) signal increased in a dose dependent manner under the effect of GA, relative to the DMSO control. These results support our previous data (Figure 3.2). The relative inclusion of the ED-B and ED-A exons however, did not change in any statistically significant manner from the vehicle control under the effects increasing concentrations of GA. Verification of all PCR products was accomplished by observation of band sizes and direct sequencing of products (Figure 5.5 & Figure 5.6).

Verification of PCR products was accomplished by observation of band sizes, and direct sequencing of products (Figure 5.5).

3.10 A subset of other extracellular matrix genes are GA responsive.

We next investigated potential responsiveness of a number of other extracellular matrix proteins (ECMs) to GA treatment. The -2000 bp to +1 bp promoter regions of known heat-shock inducible genes (*HSP90AA1*, *HSPA1A*, *HSPB1*(55), stress related transcription factors (*HSF1*, *HIF1A*)(30)(272) and a subset of key extracellular matrix protein genes (lamanin beta 3 [*LAMB3*], lamanin gamma 2 *LAMC2*, collagen 4 alpha 2 [*COL4A2*], collagen 4 alpha 3 [*COL4A3*], elastin [*ELN*], vitronectin [*VTN*] and osteopontin [*SPP1*])(141)(140)(273) were obtained from the Ensemble database and screened for potential HSEs using TFSearch. A summary of the results from this analysis are tabulated in Table 5.3. The locations of predicted HSF binding motifs on the gene promoter regions are highlighted with black boxes in Figure 3.11 A.

Hs578T cells were treated for 24 hours with GA 100 nM or DMSO. Total RNA was extracted and processed as previously described and qPCR was conducted on heat-shock protein genes, stress related transcription factor genes, and ECM genes using ACTB as a reference gene. The data were analysed using the ΔCt method comparing the GA treated samples to the DMSO treated samples. Figure 3.11 B shows that relative to the vehicle control, *HSP90AA1* (50-fold), *HSPA1A* (360-fold) and *HSPB1* (4.5-fold) mRNA were increased after treatment with GA. Both Hsp70 mRNA and Hsp90α mRNA were increased by statistically significant amounts relative to the housekeeping gene (Figure 3.11 B). HIF1α mRNA was also increased (4.5-fold)

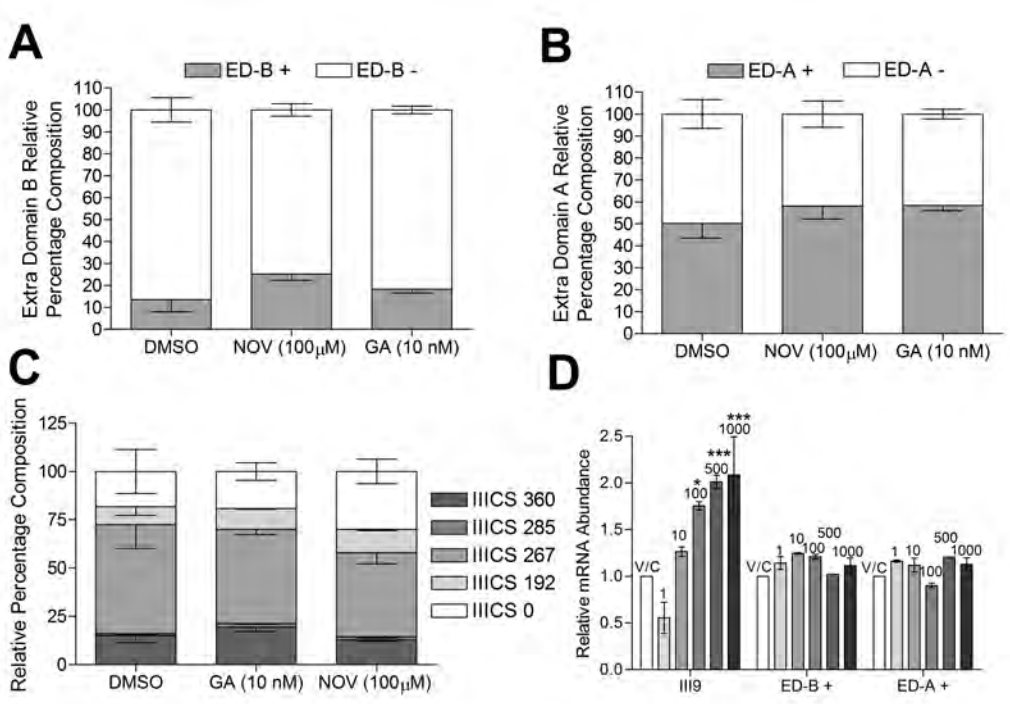

Figure 3.10: ***FN1*** **splice variant proportions are not altered by geldanamycin treatment** - Hs578T cells were treated for 24 hours with GA at 10 nM. Total RNA was extracted and equal amounts of total RNA were used for cDNA synthesis as described previously. PCR analysis of FN extra domain B (ED-B) (**A**) and extra domain A (ED-A) (**B**) transcript isoforms, variable region (IIICS) (**C**), and total fibronectin (III9 - included in all FN mRNA transcripts) (**D**) was conducted using exon flanking primers. ED-B+ indicates mRNA transcripts inclusive of the ED-B exon, whereas ED-B- indicates transcripts excluding the ED-B exon. Labels for ED-A data are analogous to those in **B**. The proportion of ED-B, ED-A and IIICS inclusive transcripts (and the III9 exon abundance) was determined using densitometry and normalised the DMSO vehicle control (V/C). Values are representative of triplicate biological and technical replicates. Statistical analysis was performed using a two way ANOVA with Bonferroni post-test (*$p<0.05$, *** $p<0.001$).

in the GA treated cells relative to the DMSO treated cells but this increase was not shown to be statistically significant. These data are consistent with the stress-inducible nature of these genes(30)(55).

Figure 3.11 C shows the relative fold change of the ECM protein mRNA after GA treatment compared to the DMSO control. *ELN*, *VTN* and *LAMC2* were not detected in either the DMSO treated Hs578T cells or the GA treated cells. *SPP1* mRNA and *COL4A3* mRNA did not change after treatment with GA, however *LAMB3* (3-fold) and FN (2.5-fold) mRNA increased upon GA treatment (Figure 3.11 C). *LAMB3* and *FN1* mRNA were increased statistically significantly under GA treatment compared to the housekeeping gene. These data suggest the FN may not be the only ECM gene responsive to GA treatment.

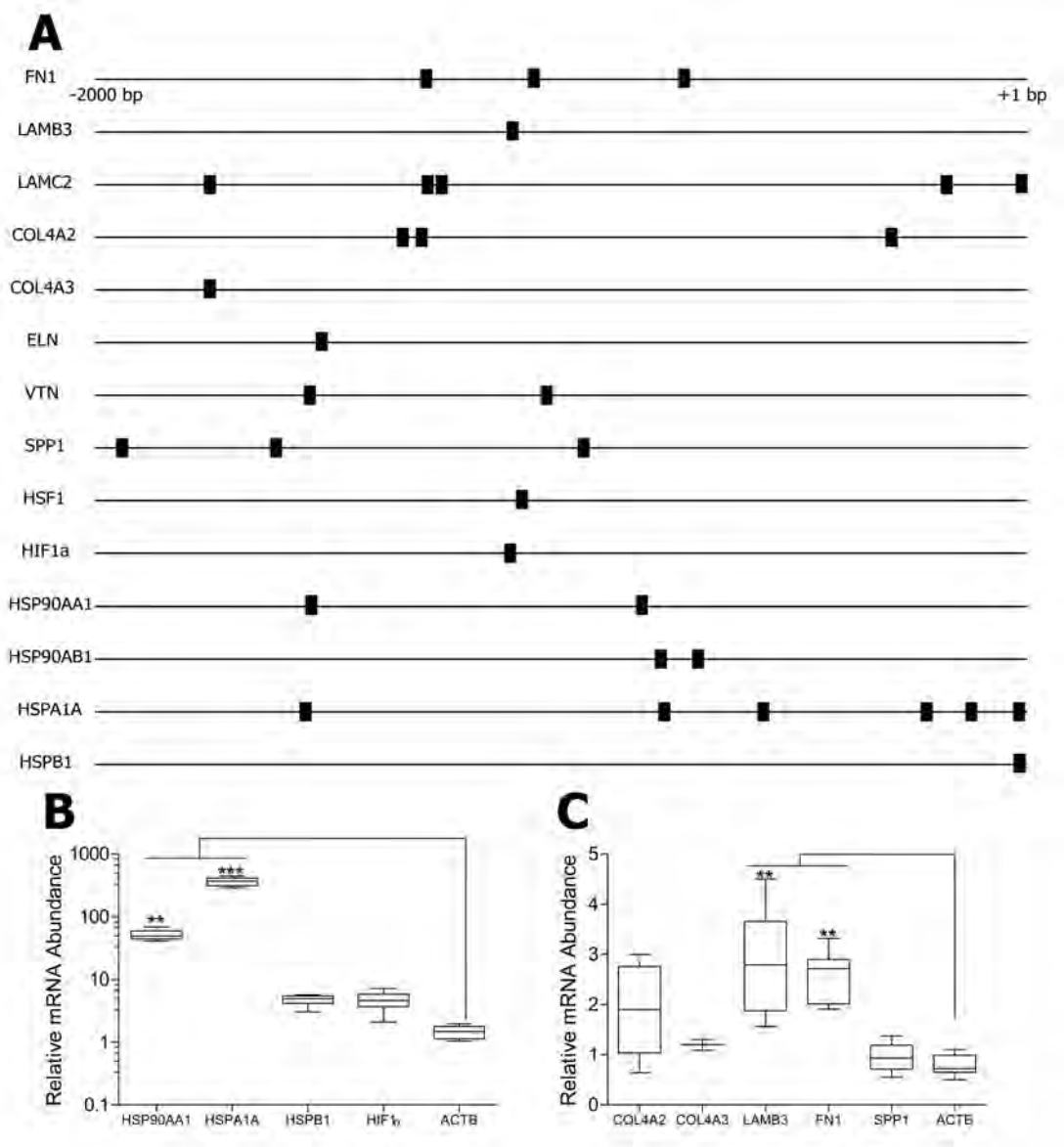

Figure 3.11: A subset of other extracellular matrix genes are stress responsive - **(A)** -2000 bp to +1 bp promoter regions of selected genes were analysed using TFSearch (fibronectin 1 (*FN1*), lamanin β 3 (*LAMB3*), lamanin γ 2 (*LAMC2*), collagen 4 α 2(*COL4A2*), collagen 4 α 3 (*COL4A3*), elastin (*ELN*), vitronectin (*VTN*), osteopontin (*SPP1*), heat-shock factor 1 (*HSF1*), hypoxia inducible factor α (*HIF1α*), heat-shock protein 90 kDa α (*HSP90AA1*), heat-shock protein 90 kDa β (*HSP90AB1*), heat-shock protein 27 kDa (*HSPA1A*)). The locations of predicted heat-shock elements are indicated by black boxes. Hs578T cells were treated for 24 hours with GA 100 nM or DMSO. Total RNA was extracted and qPCR was conducted on known stress inducible genes **(B)** and a selection of extracellular matrix genes **(C)**. Data were analysed and statistical analysis was conducted in GraphPad Prism Version 4 using one way ANOVA with a Kruskal-Wallis post test (**B** **p<0.01, ***p<0.001)(**C** **p<0.01) and are representative of the averaged mRNA abundance relative to the vehicle control from experimental and technical triplicates.

4

Discussion

The data presented in the present study support the conclusion that GA increases the levels of FN protein *via* an HSF1 mediated increase in *FN1* promoter activity. It was demonstrated that GA induces an increase in FN protein levels, FN ECM matrix and FN mRNA (Figure 3.1 & Figure 3.2). It was subsequently found that the human *FN1* promoter contained putative HSEs (Figure 3.4). Moreover, GA was able to induce the heat-shock response in an *in vitro* model identical to that in which the increase in FN mRNA and protein was observed (Figure 3.3). The observed increase in FN mRNA in cells treated with GA was found to correspond to an increase in *FN1* promoter activity (Figure 3.5). This increase was able to be attenuated by the loss of two of the purported HSEs in the *FN1* promoter (Figure 3.6). One of these HSEs was found to be occupied by HSF1 in untreated cells and occupancy was shown to increase in cells treated with GA (Figure 3.7). Additionally, treatment with rapamycin was shown to abrogate the effect of GA on FN mRNA levels (Figure 3.8). Several genes encoding ECM proteins were assayed in untreated cells and in those treated with GA. Two ECM genes (*COL4A2* & *LAMB3*) were found to have elevated mRNA levels in the GA treated cells, similarly to *FN1* (Figure 3.11).

4.1 *FN1* is an HSF1 target gene and is stress responsive

The findings of this study demonstrate that the human *FN1* promoter is bound by HSF1 at an HSE located at -965 bp to -951 bp (Figure 3.7), and that this HSE is functional in the response of the FN promoter activity to the GA-induced heat shock response

(Figure 3.6). HSF1 bound to an HSE sequence in the *FN1* promoter. The pentameric nGAAn HSE sequence has been demonstrated by a number of ChIP-seq experiments to be diverse in structure and location relative to the gene TSS (55)(274)(275)(276). The sequence of the HSE identified on the *FN1* promoter (gGAAagGACacGAAg) (Figure 3.4) differs from the HSE consensus sequence (nGAAnnTTCnnGAAn)(277) in the number of repeats. The *NEAT1* promoter has been shown to contain an HSE which similarly differs from the consensus sequence, and this HSE was shown to be HSF1-bound and responsive to heat-shock(276).

There has been no previous report of HSF1 binding to the FN promoter, and to the best of our knowledge this is also the first report that GA induces FN expression and does so by increasing binding of HSF1 to the *FN1* promoter (Figure 3.2; Figure 3.5; Figure 3.6; Figure 3.7). We have preliminary data to suggest that heat-shock and chemically induced hypoxia (using $CoCl_2$) also induced increases in FN mRNA levels, suggesting that the response may not be limited to treatment with GA (Dhanani 2014 unpublished observations). This would suggest that *FN1* is stress-inducible. It remains to be determined whether other N-terminal inhibitors of Hsp90 also increase FN levels.

The *FN1* promoter is known to be bound by other transcription factors including c-Jun/ATF-2-CRE motif interactions(278)(246)(279), AP-1 binding(280) and TCF/LEF interactions(249).

A number of human HSF1 target genes have been previously identified using similar approaches to those used in our present study. Trinklein *et al.* (2004) reported a study in which *in silico* promoter analysis was combined with microarray data from three different human cells lines in order to identity HSF1 target genes (55). *FN1* was not identified in the published output from this study or supplementary data, however much of the raw data, including cell types studies, is unavailable for many data sets. In the absence of this information, we may only speculate that the cell lines used may not have been constitutive FN producing cells, and thus FN may not have been identified as being responsive to stress.

Some genome-wide studies have been conducted using the *Drosophila melanogaster* model in order to identify HSF1 targets(275)(281)(53). The available data for these studies do not indicate that a Drosophila *FN1* homologue was detected as an HSF1 target. Indeed, the NCBI does not list a homologous gene in Drosophila as it does with the zebrafish and frog, although a protein sharing similar functions and epitopes has

been reported(282). A more focused approach to identifying specific HSF1 target genes has recently been used to identify HSF1 regulated genes in HK-2 human kidney cells, A172 human glioma cells, MCF-7 and MDA-MB-231 human cancer cells (283)(78).

Support for our finding that *FN1* is an HSF1 target gene can be found in expression profiling data from mouse embryonic fibroblast model systems deposited on the NCBI GEO database. HSF1 null MEFs exhibited a reduction in *FN1* mRNA expression compared to WT MEFs (GDS1527(55); GSE65252(77)). In a similar study using Hela cervical cancer cells, which do not constitutively produce a substantial FN matrix or express high levels of FN mRNA, HSF1 siRNA knock-down did not change the levels of *FN1* expression (GSE3697(69)).

Our observation of increased FN matrix and protein may also be an effect of a combination of reduced FN turnover and decreased FN protein degradation. Hsp90 has been shown to chaperone and play a role in the activation of MMP2(13) and MMP9(140), both of which play a role in the proteolytic degradation of the FN extracellular matrix(140)(152). The inhibition, even if partial, of Hsp90 might be sufficient to prevent the efficient turnover of the matrix.

In addition to FN it was shown that two other genes coding for ECM components laminin $\beta 3$ and collagen $4\alpha 2$ demonstrate a similar increase in mRNA abundance upon GA treatment in the Hs578T cell line (Figure 3.11). This is the first report of cell stress response related induction in the mRNA for these ECM proteins. Data from HSF1 null fibroblasts shows a decrease in *COL4A2* compared to normal fibroblasts (GEO data: GDS1527(55)), which again was not reflected in similar data from HeLa cells (GDS1733(69)). No published data to support or contradict the observed effect on *LAMB3* was available. Interestingly, as observed in previous studies(55)(276) there was no correlation between the number of predicted HSEs in the promoter and the GA-induced response, as the osteopontin (*SPP1*) promoter was predicted to contain three HSEs but was not induced under the conditions of our experiments.

HSF1 mediated stress induction of FN and the potential of parallel regulation for collagen and laminin is of interest because together these proteins are major components of the interstitial matrix and the basement membrane(284). Changes in these structures as a result of stress-induced deregulation of ECM components may impact on human diseases. In particular, our results have implications for disease in the following contexts: 1) diseases in which HSF1 activation ia a hallmark (such as cancer),

2) diseases characterised by increases in FN deposition by unknown mechanisms (such as diabetes) and 3), diseases in which GA or derivatives are to be used therapeutically.

4.1.0.1 Cancer and the tumour microenvironment

The cancerous environment is often characterised by a number of proteotoxic stresses arising from nutrient and oxygen deprivation, signalling imbalance and gene overexpression(285)(286). The factors which influence this microenvironment are contributed to by a number of different cell types. These include a heterogenous collection of tumour cells along with a stromal fibroblasts and immune cells. These cells and the ECM they produce comprise the tumour microenvironment(140). In cancerous cells themselves, ECM proteins are often down-regulated, which is seen to increase their migratory potential(287)(288)(289). Deregulated ECM dynamics whether they result in a loss or over deposition of ECM components are considered a hallmark of cancer(140). The deposition of ECM proteins is key to the progression of the metastatic cancers, as this enables angiogenesis and also promotes cell migration(290). The cells of some cancer types, such as intestinal and lung carcinoma exhibit increased FN expression, and this increase is observed particularly at the invading edge of migrating tumours(291)(292).

High levels of HSF1 activation in tumour cells have been associated with increased cell growth and metastasis(73)(75)(70). It is possible that in cancers with constitutively active *FN1*, the pro-invasion and survival effects of high levels of FN deposition under the effects of HSF1 activation will play a role in cancer progression independent of the surrounding milieu.

Cancer associated fibroblasts (CAFs) are the primary ECM producing components of the stroma in most cancers(293). Cells sense differences in physical ECM properties and migrate preferentially toward regions of increased stiffness(294). As FN contributes greatly to the cross-linking of various ECM proteins(295)(296) and therefore the ECM's overall rigidity(296)(204) and because integrin-FN interactions are essential for cell migration(297), it seems likely that increased FN deposition by stromal cells like CAFs in response to stress would will contribute to augmented metastatic capability of a primary tumour. CAFs have been shown to arise from normal fibroblasts via the enhancement of TGF-β and SDF-1 autocrine signalling loops(298). Tumour cells presumably initiate this increase in signalling via the activation of HSF1 common to cancer(299)(300), or via the secretion of large amounts of TGF-β. This enhancement is

also mediated and maintained by HSF1(77); TGF-β is an HSF1 target gene(301)(302), and TGF-β activates HSF1(303). TGF-β is known to increase *FN1* promoter activity in a number of different cell lines(246). It is tempting to speculate that one mechanism by which TGF-β increases FN levels is via the activation of HSF1. This proposed mechanism is illustrated in Figure 4.1.

There is evidence to suggest that cancer cells may create ECM rich regions at distal sites(304)(305). For example Kaplan *et al.* (2005) describe how increased FN expression is required for hematopoietic progenitor cell adhesion(306), and given the central role FN plays in the ECM, increased *FN1* expression may promote the anchorage, migration and development of cancer metastases(307)(308). Indeed it has been demonstrated in animal models that treatment of cancer with GA analogues caused an increase in the incidence of metastases(309)(310).

4.1.0.2 Diabetes

Proteotoxic and oxidative stresses produced by cancers are mirrored in several aspects by nutritional stresses.

HSF1 regulation is now understood to be closely interconnected to nutritional state(68)(311) and the nutrient sensor mTORC1 has been shown to directly regulate HSF1(62).

Insulin signalling is a core constituent in the maintenance of glucose homeostasis in organisms, and promotes mTORC1 activation(312). mTORC1 is the master nutrient sensor and is positioned at a central point in several intracellular signalling cascades involved in cell growth and proliferation(313). Chou *et al.* (2012) demonstrated that HSF1 activation is dependent on phosphorylation of HSF1 S326 by mTORC1(62).

A number of studies have demonstrated that high glucose conditions, such as those observed in diabetes, maintain an active Akt kinase via DJ-1(314)(315), which inactivates PRAS40 to increase the mTORC1 kinase activity (316)(313)(317)(316) and presumably activate HSF1.

Diabetes is also known to present with pathologies associated with excess ECM protein deposition(318). These pathologies include nephropathy of the retina(319) and the kidneys(320) in which thickening of the basement membrane is a hallmark(321)(322)(323).

The mechanism leading to the increased basement membrane is currently poorly described. Sphingosine-1-phosphate (Sp1) has been shown to regulate FN levels in mesangial cells in high glucose conditions(251). This effect on FN levels was shown to involve an S1P2 receptor initiated pathway involving ERK1/2 and p38MAPK(324), however no signal effector has yet been identified. The MAPK pathway is associated with pathways involved in the regulation of cell growth and proliferation such as AKT and mTORC pathways(313), which again would culminate in the activation of HSF1. Interestingly, the primary components of the basement membrane (laminin, collagen and FN) are the proteins observed in this study to be stress-responsive (Figure 3.11). It is tempting to speculate that, given that the GA-mediated induction of FN could be reversed by the mTORC inhibitor rapamycin, the HSF1 mediated increase in ECM proteins might be one possible mechanism to explain the thickening of the basement membrane in high glucose conditions associated with activated mTORC.

4.1.0.3 Implications in other human diseases

A number of other physiological states are known to be linked with diseases caused by an over production of FN and other ECM proteins(325)(326) (see Table 1.2). Infection, smoking and alcohol abuse cause inflammation resulting in eventual fibrosis related pathologies(327)(326)(291). In fact, inflammatory responses are closely connected with metabolic and ER stress conditions already discussed(328). Inflammatory stress responses are known to drive an HSF1 mediated up-regulation of HSPs(329)(330), via the febrile response(331)(332).

Again the relationship between inflammation, HSF1 and FN is prospectively important in the context of conditions such as pulmonary fibrosis, liver cirrhosis, Crohn's disease and rheumatoid arthritis(333)(334). TGF-β1 has been shown to induce FN expression via p38 in a human fetal lung fibroblast model(335), however similar stimuli activate p38MAPK and HSF1 mediated stress responses(336). As HSF1 is activated by TGF-β1(303), the involvement of HSF1 activation in fibrotic conditions with up-regulated FN appears likely. Inflammation is thought to play a crucial role in the development of Alzheimer's disease, and although the role of FN in the development of Alzheimer's disease is unclear, FN deposition in the brain vasculature is known to precede the accumulation of amyloid protein(337)(338)(339).

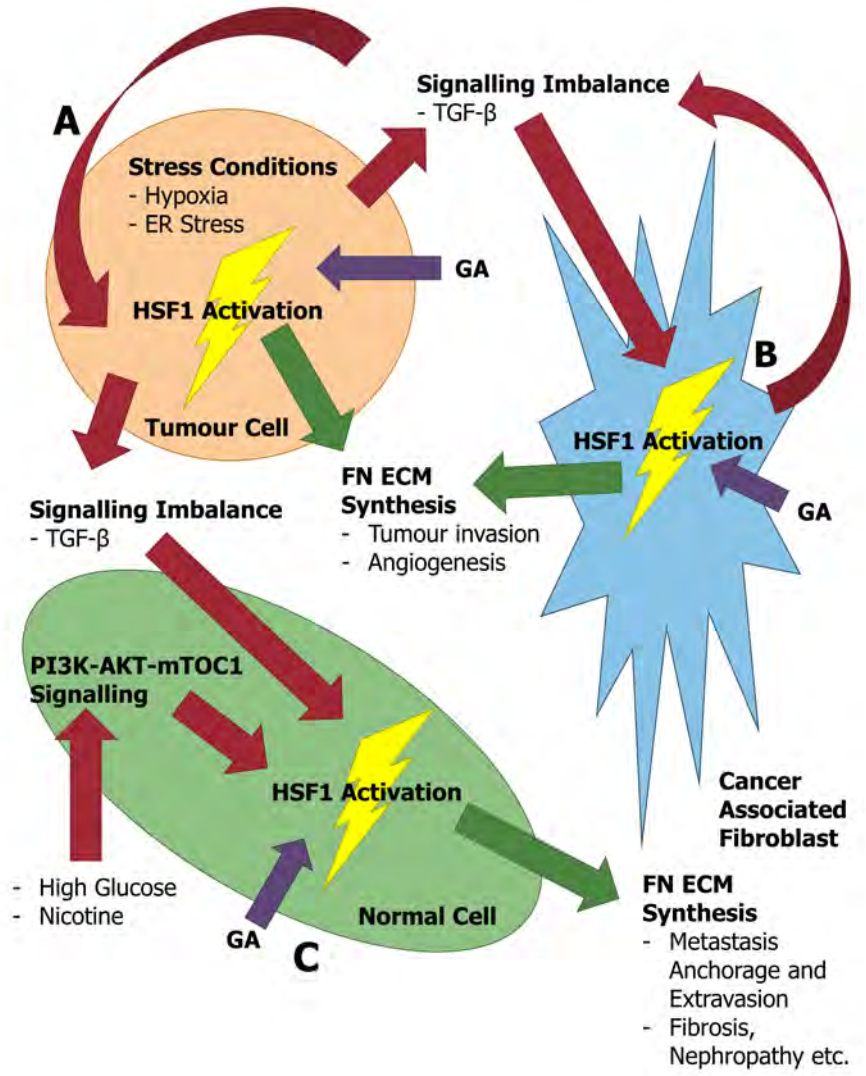

Figure 4.1: Schematic representation of the possible implications for the HSF1 regulation of *FN1* in the cancerous microenvironment and in normal cells. - This model shows that GA activates HSF1 in normal and cancerous cells, and that this might lead to increased deposition of FN in the ECM and promote cell migration. **A** Cancerous cells have been often found to have constitutively active HSF1. This drives a transcriptional programme which supports the malignant phenotype, including the deregulation of the cytokine TGF-β. **B** TGF-β activates HSF1 in stromal cells such as cancer associated fibroblasts, which may lead to an increase in the transcription of *FN1*. In the tumour microenvironment, increased FN deposition by both tumour and stromal cells may serve to promote tumour invasion and angiogenesis. **C** FN deposition by normal cells may also promote the adhesion of circulating tumour cells at secondary sites and support extravasion. Factors that activate the ATK/mTOR signalling pathways such as high glucose conditions and nicotine may also result in an HSF1 mediated increase in the expression of FN. HSF1 mediated FN expression in these conditions might contribute to fibrosis and the thickening of the basement membrane.

4.1.0.4 Implications for the therapeutic application of GA

Hsp90 inhibitors, particularly those targeted to the N-terminus of the protein, are considered candidates in the future treatment of cancer(82), and a number of these compounds are currently in clinical trials (see Table 1.1). The results of the present study have implications for the use of N-terminal Hsp90 inhibitors. We have shown that GA induces FN expression via the cell stress response, and many of the Hsp90 inhibitors currently in clinical trials are thought to have the same effect of inducing the cell stress response(267)(340). Although it would need to be experimentally demonstrated, we predict that these GA analogues will also induce FN expression.

A number of phase 3 clinical trials have been conducted to assess the efficacy of the Hsp90 inhibitor and GA analogue 17-AAG in the treatment of cancers(341)(93). 17-DMAG, another GA analogue which has been assessed(342)(93). These inhibitors have improved binding affinities and therefore reduced IC_{50} values demonstrated in cell culture. The concentrations used *in vivo* in clinical trials is in the range of 20-100 mg/L/24 h(343)(342)(341). 17-AAG *in vivo* concentrations are reported to peak at between 1.7 - 3 μM(344), 200 fold higher than the 10 nM we have shown to increase the levels of FN ECM *in vitro* (Figure 3.1). Regardless of the rate at which these compounds are metabolised, large parts of the body will receive low doses of Hsp90 inhibitors with current clinical administration methodologies. Although these doses will be sub-toxic, the data from our present study (Figure 3.1 & Figure 3.5) indicate that low GA concentrations are sufficient to increase FN promoter activity and FN protein levels. The result of this might be the development of aberrant ECM dynamics and concomitant pathologies in tissues distant from the tumour site. It would be interesting to observe whether current clinical trials yield results indicating changes to the ECM.

Should an Hsp90 inhibitor induced activation of the *FN1* promoter arise result in negative clinical outcomes, the use of C-terminal Hsp90 inhibitors might be a promising alternative to N-terminal Hsp90 inhibition as a therapeutic strategy. Inhibiting Hsp90 without inducing the cell stress response is a current area under investigation(345). The use of NOV derivatives such as coumermycin A1 is still many years from clinical trials but the use of HSF1 inhibitors such as quercetin or emunin(129)(128) in combination with GA analogues could be promising(130)(132)(131).

The use of N-terminal Hsp90 inhibitors in the alleviation of diabetes related symptoms has also been investigated due to the increased levels of insulin sensitivity observed upon HSF1 activation(74). In a mouse model Lee *et al.* (2013) demonstrated that chronic dosing with AUY922 was able to reverse hyperglycemia(346). In light of the findings of our study it might prove beneficial to investigate any fibrotic effects that might arise from treatment regimes using GA analogues in the treatment of diabetes.

The use of N-terminal Hsp90 inhibitors in the treatment of protein aggregation related diseases such as Alzheimer's disease (AD) and Parkinson's disease is another potential future application for N-terminal Hsp90 inhibitors(124)(347). These diseases have been demonstrated to be linked to age related loss in HSF1 expression(348)(59), and a concomitant loss in the ability for cells to prevent protein aggregation(349). In these cases the induction of the heat-shock response is the desired effect of the compound. Activation of HSF1 using N-terminal Hsp90 inhibitors has been demonstrated to decrease -synuclein and ameloid-β aggregation(348) (347)(350)(351)(352). The use of GA analogues in the treatment of AD is yet to be investigated in humans, but given that FN accumulation from vascular endothelial cells might be both a driver of disease development and an effect of treatment, our current findings could inform experimental design. Plasma levels of FN may be used as a diagnostic biomarker for AD(353), and consequently the chronic administration of N-terminal Hsp90 inhibitors might have practical implications such as rendering this marker ineffectual.

A wide array of inflammation and fibrosis related diseases have been investigated in murine models for the potential therapeutic benefits conferred by the anti-inflammatory effects of HSF1 activation(330). Our data demonstrating the activation of HSF1 results in increased FN expression and deposition may have particular bearing on the use of this approach in disease related fibroblasts, as it may exacerbate fibrotic symptoms, or even trigger the development of related fibroses in other tissues in individuals who are predisposed to these conditions by genetics or lifestyle.

4.2 Final Conclusions

The finding that FN is regulated by HSF1 and the cell stress machinery is unexpected given the traditional roles assigned to typical HSF1 target genes. However, upon consideration of the role FN has been shown to play in promoting the survival of cells in

normal conditions(258)(354), in disease states(355)(258), and in cancer where it is a predictor of chemotherapeutic resistance(356)(355), this relationship becomes understandable as part of an ancient and conserved mechanism for cell survival under the effects of chronic stress.

Any potential biological significance of HSF1 mediated FN up-regulation is yet to be determined, and our intention is to prioritise an investigation into this making use of an *in vitro* model. In addition to this, a determination of the extent to which the HSF1 mediated up-regulation of FN in response to stress affects the ECM as a whole and in different cell types must be determined.

In conclusion, our hypothesis has been supported; a role for transcriptional regulation of the *FN1* gene by the cell stress machinery has been demonstrated. Although some work will be required to support our existing data, the evidence we have presented for an HSF1 mediated stress induction of FN is mutually corroborative and is supported by published data from two independent research groups(55)(77).

References

[1] K. Richter, M. Haslbeck, and J. Buchner. **The heat shock response: life on the verge of death**. *Molecular cell*, **40**(2):253–266, 2010. 1

[2] R. I. Morimoto. **Dynamic remodeling of transcription complexes by molecular chaperones**. *Cell*, **110**(3):281–284, 2002. 1, 4

[3] S. K. Wandinger, K. Richter, and J. Buchner. **The Hsp90 chaperone machinery.** *The Journal of biological chemistry*, **283**(27):18473–18477, 2008. 2

[4] J. Li, J. Soroka, and J. Buchner. **The Hsp90 chaperone machinery: conformational dynamics and regulation by co-chaperones.** *Biochimica et biophysica acta*, **1823**(3):624–635, 2012. 2, 3

[5] R. Zhao and W. A. Houry. **Hsp90: a chaperone for protein folding and gene regulation**. *Biochemistry and cell biology*, **83**(6):703–710, 2005. 2

[6] A. Röhl, J. Rohrberg, and J. Buchner. **The chaperone Hsp90: changing partners for demanding clients**. *Trends in biochemical sciences*, **38**(5):253–262, 2013. 2, 3

[7] M. Taipale, D. F. Jarosz, and S. Lindquist. **HSP90 at the hub of protein homeostasis: emerging mechanistic insights**. *Nature reviews Molecular cell biology*, **11**(7):515–528, 2010. 2, 10, 20

[8] S. Alarcon, M. Mollapour, M.-J. Lee, S. Tsutsumi, S. Lee, Y. Kim, T. Prince, A. Apolo, G. Giaccone, W. Xu, et al. **Tumor-intrinsic and tumor-extrinsic factors impacting hsp90-targeted therapy**. *Current molecular medicine*, **12**(9):1125, 2012. 2

[9] J. Frydman. **Folding of newly translated proteins in vivo: the role of molecular chaperones**. *Annual review of biochemistry*, **70**(1):603–647, 2001. 2

[10] M. W. Hance, K. D. Nolan, and J. S. Isaacs. **The double-edged sword: conserved functions of extracellular hsp90 in wound healing and cancer.** *Cancers*, **6**(2):1065–1097, 2014. 2

[11] K. Sidera and E. Patsavoudi. **Extracellular HSP90**. *Cell Cycle*, **7**(11):1564–1568, 2008. 2

[12] K. Sidera, M. Gaitanou, D. Stellas, R. Matsas, and E. Patsavoudi. **A critical role for HSP90 in cancer cell invasion involves interaction with the extracellular domain of HER-2**. *Journal of Biological Chemistry*, **283**(4):2031–2041, 2008. 2

[13] J. D. Sims, M. Jessica, and D. G. Jay. **Extracellular heat shock protein (Hsp)70 and Hsp90 assist in matrix metalloproteinase-2 activation and breast cancer cell migration and invasion.** *PloS one*, **6**(4), 2011. 2, 16, 59

[14] M. C. Hunter, K. L. O'Hagan, A. Kenyon, K. C. Dhanani, E. Prinsloo, and A. L. Edkins. **Hsp90 binds directly to fibronectin (FN) and inhibition reduces the extracellular fibronectin matrix in breast cancer cells.** *PloS one*, **9**(1), 2014. 2, 20, 33

[15] L. H. Pearl and C. Prodromou. **Structure, function, and mechanism of the Hsp90 molecular chaperone**. *Advances in protein chemistry*, **59**:157–186, 2002. 3

[16] J. Li and J. Buchner. **Structure, function and regulation of the hsp90 machinery**. *Biomedical journal*, **36**(3):106, 2013. 3

[17] C. Graf, M. Stankiewicz, G. Kramer, and M. P. Mayer. **Spatially and kinetically resolved changes in the conformational dynamics of the Hsp90 chaperone machine**. *The EMBO journal*, **28**(5):602–613, 2009. 3

[18] A. K. Shiau, S. F. Harris, D. R. Southworth, and D. A. Agard. **Structural Analysis of E. coli hsp90 Reveals Dramatic Nucleotide-Dependent Conformational Rearrangements**. *Cell*, **127**(2):329–340, 2006. 3

[19] M. M. Ali, S. M. Roe, C. K. Vaughan, P. Meyer, B. Panaretou, P. W. Piper, C. Prodromou, and L. H. Pearl. **Crystal structure of an Hsp90–nucleotide–p23/Sba1 closed chaperone complex**. *Nature*, **440**(7087):1013–1017, 2006. 3

[20] C. Ratzke, M. N. Nguyen, M. P. Mayer, and T. Hugel. **From a ratchet mechanism to random fluctuations evolution of Hsp90's mechanochemical cycle**. *Journal of molecular biology*, **423**(3):462–471, 2012. 3

[21] L. Neckers, M. Mollapour, and S. Tsutsumi. **The complex dance of the molecular chaperone Hsp90**. *Trends in biochemical sciences*, **34**(5):223–226, 2009. 3

[22] M. Hessling, K. Richter, and J. Buchner. **Dissection of the ATP-induced conformational cycle of the molecular chaperone Hsp90**. *Nature structural & molecular biology*, **16**(3):287–293, 2009. 3

[23] C.-T. Lee, C. Graf, F. J. Mayer, S. M. Richter, and M. P. Mayer. **Dynamics of the regulation of Hsp90 by the co-chaperone Sti1**. *The EMBO journal*, **31**(6):1518–1528, 2012. 3

[24] M. Taipale, I. Krykbaeva, M. Koeva, C. Kayatekin, K. D. Westover, G. I. Karras, and S. Lindquist. **Quantitative analysis of HSP90-client interactions reveals principles of substrate recognition**. *Cell*, **150**(5):987–1001, 2012. 3

[25] M. Retzlaff, F. Hagn, L. Mitschke, M. Hessling, F. Gugel, H. Kessler, K. Richter, and J. Buchner. **Asymmetric activation of the hsp90 dimer by its cochaperone aha1**. *Molecular cell*, **37**(3):344–354, 2010. 3

[26] M. S. Roe, M. M. Ali, P. Meyer, C. K. Vaughan, B. Panaretou, P. W. Piper, C. Prodromou, and L. H. Pearl. **The Mechanism of Hsp90 Regulation by the Protein Kinase-Specific Cochaperone p50 cdc37.** *Cell*, **116**(1):87–98, 2004. 3

[27] M. Akerfelt, R. I. Morimoto, and L. Sistonen. **Heat shock factors: integrators of cell stress, development and lifespan.** *Nature reviews. Molecular cell biology*, **11**(8):545–555, 2010. 4, 5, 6, 37, 39

[28] J. Anckar and L. Sistonen. **Heat shock factor 1 as a coordinator of stress and developmental pathways.** *Advances in experimental medicine and biology*, 2007. 4, 5

[29] A. Vihervaara, C. Sergelius, J. Vasara, M. A. Blom, A. N. Elsing, R. Pia, and L. Sistonen. **Transcriptional response to stress in the dynamic chromatin environment of cycling and mitotic cells.** *Proceedings of the National Academy of Sciences of the United States of America*, **110**(36):E3388–E3397, 2013. 4

[30] L. Pirkkala, P. Nykänen, and L. Sistonen. **Roles of the heat shock transcription factors in regulation of the heat shock response and beyond**. *The FASEB Journal*, **15**(7):1118–1131, 2001. 4, 53, 55, 91

[31] R. D. McMillan, X. Xiao, L. Shao, K. Graves, and I. J. Benjamin. **Targeted disruption of heat shock transcription factor 1 abolishes thermotolerance and protection against heat-inducible apoptosis**. *Journal of Biological Chemistry*, **273**(13):7523–7528, 1998. 4

[32] Y. Zhang, L. Huang, J. Zhang, D. Moskophidis, and N. F. Mivechi. **Targeted disruption of hsf1 leads to lack of thermotolerance and defines tissue-specific regulation for stress-inducible Hsp molecular chaperones**. *Journal of cellular biochemistry*, **86**(2):376–393, 2002. 4

[33] F. F. Damberger, J. G. Pelton, C. J. Harrison, H. Nelson, and D. E. Wemmer. **Solution structure of the DNA-binding domain of the heat shock transcription factor determined by multidimensional heteronuclear magnetic resonance spectroscopy**. *Protein Science*, **3**(10):1806–1821, 1994. 4

[34] P. K. Sorger and H. Nelson. **Trimerization of a yeast transcriptional activator via a coiled-coil motif**. *Cell*, **59**(5):807–813, 1989. 4

[35] A. Sandqvist, J. K. Björk, M. Åkerfelt, Z. Chitikova, A. Grichine, C. Vourc'h, C. Jolly, T. A. Salminen, Y. Nymalm, and L. Sistonen. **Heterotrimerization of heat-shock factors 1 and 2 provides a transcriptional switch in response to distinct stimuli**. *Molecular biology of the cell*, **20**(5):1340–1347, 2009. 4

[36] S. K. Rabindran, R. I. Haroun, J. Clos, J. Wisniewski, and C. Wu. **Regulation of heat shock factor trimer formation: role of a conserved leucine zipper**. *Science*, **259**(5092):230–234, 1993. 4

[37] R. I. Morimoto. **Regulation of the heat shock transcriptional response: cross talk between a family of heat shock factors, molecular chaperones, and negative regulators**. *Genes & Development*, **12**, 1998. 4, 5

[38] S. Bharadwaj, A. Ali, and N. Ovsenek. **Multiple components of the HSP90 chaperone complex function in regulation of heat shock factor 1 in vivo**. *Molecular and cellular biology*, **19**(12):8033–8041, 1999. 4

[39] Y. Shi, D. D. Mosser, and R. I. Morimoto. **Molecular-chaperones as HSF1-specific transcriptional repressors**. *Genes & development*, **12**(5):654–666, 1998. 4, 7

[40] J. Zou, Y. Guo, T. Guettouche, D. F. Smith, and R. Voellmy. **Repression of heat shock transcription factor HSF1 activation by HSP90 (HSP90 complex) that forms a stress-sensitive complex with HSF1**. *Cell*, **94**(4):471–480, 1998. 4, 5, 6, 7, 11

[41] A. Ali, S. Bharadwaj, R. OCarroll, and N. Ovsenek. **HSP90 interacts with and regulates the activity of heat shock factor 1 in Xenopus oocytes**. *Molecular and cellular biology*, **18**(9):4949–4960, 1998. 4

[42] A. Vihervaara and L. Sistonen. **HSF1 at a glance**. *Journal of cell science*, **127**(2):261–266, 2014. 4, 5

[43] Q. Dai, C. Zhang, Y. Wu, H. McDonough, R. A. Whaley, V. Godfrey, H.-H. Li, N. Madamanchi, W. Xu, L. Neckers, et al. **CHIP activates HSF1 and confers protection against apoptosis and cellular stress**. *The EMBO journal*, **22**(20):5446–5458, 2003. 4

[44] D. W. Neef, A. M. Jaeger, R. Gomez-Pastor, F. Willmund, J. Frydman, and D. J. Thiele. **A Direct Regulatory Interaction between Chaperonin TRiC and Stress-Responsive Transcription Factor HSF1**. *Cell reports*, **9**(3):955–966, 2014. 4, 6

[45] M. P. Kline and R. I. Morimoto. **Repression of the heat shock factor 1 transcriptional activation domain is modulated by constitutive phosphorylation.** *Molecular and cellular biology*, **17**(4):2107–2115, 1997. 5

[46] B. Chu, F. Soncin, B. D. Price, M. A. Stevenson, and S. K. Calderwood. **Sequential phosphorylation by mitogen-activated protein kinase and glycogen synthase kinase 3 represses transcriptional activation by heat shock factor-1**. *Journal of Biological Chemistry*, **271**(48):30847–30857, 1996. 5

[47] T. Guettouche, F. Boellmann, W. S. Lane, and R. Voellmy. **Analysis of phosphorylation of human heat shock factor 1 in cells experiencing a stress**. *BMC biochemistry*, **6**(1):4, 2005. 5

[48] C. I. Holmberg, V. Hietakangas, A. Mikhailov, J. O. Rantanen, M. Kallio, A. Meinander, J. Hellman, N. Morrice, C. MacKintosh, R. I. Morimoto, J. E. Eriksson, and L. Sistonen. **Phosphorylation of serine 230 promotes inducible transcriptional activity of heat shock factor 1**. *The EMBO Journal*, 2001. 5, 6

[49] I. Shamovsky and E. Nudler. **New insights into the mechanism of heat shock response activation**. *Cellular and Molecular Life Sciences*, **65**(6):855–861, 2008. 5

[50] J. T. Westwood, J. Clos, and C. Wu. **Stress-induced oligomerization and chromosomal relocalization of heat-shock factor**. *Nature*, **353**(6347):822–827, 1991. 5, 37

[51] R. Baler, G. Dahl, and R. Voellmy. **Activation of human heat shock genes is accompanied by oligomerization, modification, and rapid translocation of heat shock transcription factor HSF1.** *Molecular and cellular biology*, **13**(4):2486–2496, 1993. 5

[52] C. I. Holmberg, S. A. Illman, M. Kallio, A. Mikhailov, and L. Sistonen. **Formation of nuclear HSF1 granules varies depending on stress stimuli**. *Cell stress & chaperones*, **5**(3):219, 2000. 5, 37

[53] S. E. Gonsalves, A. M. Moses, Z. Razak, F. Robert, and J. Westwood. **Whole-genome analysis reveals that active heat shock factor binding sites are mostly associated with non-heat shock genes in Drosophila melanogaster.** *PloS one*, **6**(1), 2011. 5, 6, 8, 58

[54] J. S. Hahn, Z. Hu, D. J. Thiele, and V. R. Iyer. **Genome-wide analysis of the biology of stress responses through heat shock transcription factor.** *Molecular and cellular biology*, **24**(12):5249–5256, 2004. 5, 6

[55] N. D. Trinklein, J. I. Murray, S. J. Hartman, D. Botstein, and R. M. Myers. **The role of heat shock transcription factor 1 in the genome-wide regulation of the mammalian heat shock response.** *Molecular biology of the cell*, **15**(3):1254–1261, 2004. 5, 6, 7, 8, 35, 39, 53, 55, 58, 59, 66, 91

[56] L. E. Hightower. **Heat shock, stress proteins, chaperones, and proteotoxicity**. *Cell*, **66**(2):191–197, 1991. 5

[57] D. Y. Kim, E. Kwon, J. Choi, H.-Y. Hwang, and K. K. Kim. **Structural basis for the negative regulation of bacterial stress response by RseB**. *Protein science*, **19**(6):1258–1263, 2010. 5

[58] S. Hasenbein, M. Meltzer, P. Hauske, M. Kaiser, R. Huber, T. Clausen, and M. Ehrmann. **Conversion of a regulatory into a degradative protease**. *Journal of molecular biology*, **397**(4):957–966, 2010. 5

[59] J. Anckar and L. Sistonen. **Regulation of HSF1 function in the heat stress response: implications in aging and disease**. *Annual review of biochemistry*, **80**:1089–1115, 2011. 6, 65

[60] S. G. Ahn and D. J. Thiele. **Redox regulation of mammalian heat shock factor 1 is essential for Hsp gene activation and protection from stress.** *Genes & development*, **17**(4):516–528, 2003. 5

[61] Y. Wang. **Regulation of the heat shock response by thiol-reactive compounds in the yeast Saccharomyces cerevisiae**. 2012. 5

[62] S. D. Chou, T. Prince, J. Gong, and S. K. Calderwood. **mTOR is essential for the proteotoxic stress response, HSF1 activation and heat shock protein synthesis.** *PloS one*, **7**(6), 2012. 5, 11, 46, 48, 61

[63] C. Dai, S. Santagata, Z. Tang, J. Shi, J. Cao, H. Kwon, R. T. Bronson, L. Whitesell, S. Lindquist, et al. **Loss of tumor suppressor NF1 activates HSF1 to promote carcinogenesis**. *The Journal of clinical investigation*, **122**(10):3742–3754, 2012. 5

[64] V. Prahlad, T. Cornelius, and R. I. Morimoto. **Regulation of the cellular heat shock response in Caenorhabditis elegans by thermosensory neurons**. *Science*, **320**(5877):811–814, 2008. 5

[65] D. A. Clark, C. V. Gabel, H. Gabel, and A. D. Samuel. **Temporal activity patterns in thermosensory neurons of freely moving Caenorhabditis elegans encode spatial thermal gradients**. *The Journal of neuroscience*, **27**(23):6083–6090, 2007. 5

[66] P. v Oosten-Hawle and R. I. Morimoto. **Transcellular chaperone signaling: an organismal strategy for integrated cell stress responses**. *The Journal of experimental biology*, **217**(1):129–136, 2014. 5

[67] P. v Oosten-Hawle, R. S. Porter, and R. I. Morimoto. **Regulation of organismal proteostasis by transcellular chaperone signaling.** *Cell*, **153**(6):1366–1378, 2013. 7

[68] S. D. Westerheide, J. Anckar, S. M. Stevens, L. Sistonen, and R. I. Morimoto. **Stress-inducible regulation of heat shock factor 1 by the deacetylase SIRT1.** *Science (New York, N.Y.)*, **323**(5917):1063–1066, 2009. 7, 61

[69] T. J. Page, D. Sikder, L. Yang, L. Pluta, R. D. Wolfinger, T. Kodadek, and R. S. Thomas. **Genome-wide analysis of human HSF1 signaling reveals a transcriptional program linked to cellular adaptation and survival**. *Molecular BioSystems*, **2**, 2006. 7, 8, 59

[70] C. Dai, L. Whitesell, A. B. Rogers, and S. Lindquist. **Heat shock factor 1 is a powerful multifaceted modifier of carcinogenesis.** *Cell*, **130**(6):1005–1018, 2007. 8, 60

[71] P. Workman, F. Burrows, L. Neckers, and N. Rosen. **Drugging the cancer chaperone HSP90**. *Annals of the New York Academy of Sciences*, **1113**(1):202–216, 2007. 8, 10

[72] S. Santagata, R. Hu, N. U. Lin, M. L. Mendillo, L. C. Collins, S. E. Hankinson, S. J. Schnitt, L. Whitesell, R. M. Tamimi, S. Lindquist, and T. A. Ince. **High levels of nuclear heat-shock factor 1 (HSF1) are associated with poor prognosis in breast cancer.** *Proceedings of the National Academy of Sciences of the United States of America*, **108**(45):18378–18383, 2011. 8

[73] F. Fang, R. Chang, and L. Yang. **Heat shock factor 1 promotes invasion and metastasis of hepatocellular carcinoma in vitro and in vivo**. *Cancer*, **118**(7):1782–1794, 2012. 8, 60

[74] X. Jin, D. Moskophidis, and N. F. Mivechi. **Heat Shock Transcription Factor 1 Is a Key Determinant of HCC Development by Regulating Hepatic Steatosis and Metabolic Syndrome**. *Cell Metabolism*, **14**(1), 2011. 9, 65

[75] S. Santagata, M. L. Mendillo, Y.-c. Tang, A. Subramanian, C. C. Perley, S. P. Roche, B. Wong, R. Narayan, H. Kwon, M. Koeva, et al. **Tight coordination of protein translation and HSF1 activation supports the anabolic malignant state**. *Science*, **341**(6143), 2013. 9, 60

[76] M. L. Mendillo, S. Santagata, M. Koeva, G. W. Bell, R. Hu, R. M. Tamimi, E. Fraenkel, T. A. Ince, L. Whitesell, and S. Lindquist. **HSF1 drives a transcriptional program distinct from heat shock to support highly malignant human cancers.** *Cell*, **150**(3):549–562, 2012. 9

[77] S. Ruth, S. Santagata, M. L. Mendillo, L. M. Sholl, B. Irit, A. H. Beck, D. Dora, M. Koeva, S. M. Stemmer, L. Whitesell, and S. Lindquist. **The reprogramming of tumor stroma by HSF1 is a potent enabler of malignancy.** *Cell*, **158**(3):564–578, 2014. 9, 59, 61, 66

[78] X. Yang, J. Wang, S. Liu, and Q. Yan. **HSF1 and Sp1 Regulate FUT4 Gene Expression and Cell Proliferation in Breast Cancer Cells**. *Journal of Cellular Biochemistry*, **115**, 2014. 9, 59

[79] L. Whitesell and S. L. Lindquist. **HSP90 and the chaperoning of cancer**. *Nature Reviews Cancer*, **5**(10):761–772, 2005. 10

[80] J. Trepel, M. Mollapour, G. Giaccone, and L. Neckers. **Targeting the dynamic HSP90 complex in cancer**. *Nature Reviews Cancer*, 2010. 10

[81] L. Neckers and P. Workman. **Hsp90 molecular chaperone inhibitors: are we there yet?** *Clinical Cancer Research*, **18**(1):64–76, 2012. 10

[82] P. Workman. **Overview: translating Hsp90 biology into Hsp90 drugs**. *Current cancer drug targets*, **3**(5):297–300, 2003. 10, 64

[83] M. B. Almeida, J. L. d Nascimento, A. M. Herculano, and C. M. E. **Molecular chaperones: toward new therapeutic tools.** *Biomedicine & pharmacotherapy*, **65**(4):239–243, 2011. 10

[84] L. H. Pearl, C. Prodromou, and P. Workman. **The Hsp90 molecular chaperone: an open and shut case for treatment.** *The Biochemical journal*, **410**(3):439–453, 2008. 10

[85] A. A. Khalil, N. F. Kabapy, S. F. Deraz, and C. Smith. **Heat shock proteins in oncology: diagnostic biomarkers or therapeutic targets?** *Biochimica et biophysica acta*, **1816**(2):89–8104, 2011. 10

[86] C. E. Stebbins, A. A. Russo, C. Schneider, N. Rosen, F. U. Hartl, and N. P. Pavletich. **Crystal structure of an Hsp90–geldanamycin complex: targeting of a protein chaperone by an antitumor agent**. *Cell*, **89**(2):239–250, 1997. 10

[87] T. W. Schulte, M. V. Blagosklonny, C. Ingui, and L. Neckers. **Disruption of the Raf-1-Hsp90 molecular complex results in destabilization of Raf-1 and loss of Raf-1-Ras association**. *Journal of Biological Chemistry*, **270**(41):24585–24588, 1995. 10

[88] E. G. Mimnaugh, C. Chavany, and L. Neckers. **Polyubiquitination and proteasomal degradation of the p185c-erbB-2 receptor protein-tyrosine kinase induced by geldanamycin**. *Journal of Biological Chemistry*, **271**(37):22796–22801, 1996. 10

[89] I. Hostein, D. Robertson, F. DiStefano, P. Workman, and P. A. Clarke. **Inhibition of signal transduction by the Hsp90 inhibitor 17-allylamino-17-demethoxygeldanamycin results in cytostasis and apoptosis**. *Cancer Research*, **61**(10):4003–4009, 2001. 10

[90] R. Garcia-Carbonero, A. Carnero, and L. Paz-Ares. **Inhibition of HSP90 molecular chaperones: moving into the clinic**. *The lancet oncology*, **14**(9):e358–e369, 2013. 10

[91] K. Jhaveri, T. Taldone, S. Modi, and G. Chiosis. **Advances in the clinical development of heat shock protein 90 (Hsp90) inhibitors in cancers**. *Biochimica et Biophysica Acta (BBA)-Molecular Cell Research*, **1823**(3):742–755, 2012. 10

[92] T. Taldone, A. Gozman, R. Maharaj, and G. Chiosis. **Targeting Hsp90: small-molecule inhibitors and their clinical development**. *Current opinion in pharmacology*, **8**(4):370–374, 2008. 10

[93] M. A. Biamonte, R. V. d Water, J. W. Arndt, R. H. Scannevin, D. Perret, and W.-C. Lee. **Heat shock protein 90: inhibitors in clinical trials**. *J. Med. Chem*, **53**(1):3–17, 2010. 10, 64

[94] M. G. Marcu, A. Chadli, I. Bouhouche, M. Catelli, and L. M. Neckers. **The heat shock protein 90 antagonist novobiocin interacts with a previously unrecognized ATP-binding domain in the carboxyl terminus of the chaperone**. *Journal of Biological Chemistry*, **275**(47):37181–37186, 2000. 10

[95] S. Chaudhury, T. R. Welch, and B. S. Blagg. **Hsp90 as a target for drug development**. *ChemMedChem*, **1**(12):1331–1340, 2006. 10

[96] B.-G. Yun, W. Huang, N. Leach, S. D. Hartson, and R. L. Matts. **Novobiocin induces a distinct conformation of Hsp90 and alters Hsp90-cochaperone-client interactions**. *Biochemistry*, **43**(25):8217–8229, 2004. 11

[97] J. R. Porter, C. C. Fritz, and K. M. Depew. **Discovery and development of Hsp90 inhibitors: a promising pathway for cancer therapy**. *Current opinion in chemical biology*, **14**(3):412–420, 2010. 11

[98] K. Moulick, J. H. Ahn, H. Zong, A. Rodina, L. Cerchietti, E. M. G. DaGama, E. Caldas-Lopes, K. Beebe, F. Perna, K. Hatzi, et al. **Affinity-based proteomics reveal cancer-specific networks coordinated by Hsp90**. *Nature chemical biology*, **7**(11):818–826, 2011. 11

[99] J.-P. Lambert, G. Ivosev, A. L. Couzens, B. Larsen, M. Taipale, Z.-Y. Lin, Q. Zhong, S. Lindquist, M. Vidal, R. Aebersold, et al. **Mapping differential interactomes by affinity purification coupled with data-independent mass spectrometry acquisition**. *Nature methods*, 2013. 11

[100] L. Galam, M. K. Hadden, Z. Ma, Q.-Z. Ye, B.-G. Yun, B. S. Blagg, and R. L. Matts. **High-throughput assay for the identification of Hsp90 inhibitors based on Hsp90-dependent refolding of firefly luciferase**. *Bioorganic & medicinal chemistry*, **15**(5):1939–1946, 2007. 11

[101] S. B. Matthews, G. A. Vielhauer, C. A. Manthe, V. K. Chaguturu, K. Szabla, R. L. Matts, A. C. Donnelly, B. S. Blagg, and J. M. Holzbeierlein. **Characterization of a novel novobiocin analogue as a putative C-terminal inhibitor of heat shock protein 90 in prostate cancer cells**. *The Prostate*, **70**(1):27–36, 2010. 11

[102] S. N. Shelton, M. E. Shawgo, S. B. Matthews, Y. Lu, A. C. Donnelly, K. Szabla, M. Tanol, G. A. Vielhauer, R. A. Rajewski, R. L. Matts, et al. **KU135, a novel novobiocin-derived C-terminal inhibitor of the 90-kDa heat shock protein, exerts potent antiproliferative effects in human leukemic cells**. *Molecular pharmacology*, **76**(6):1314–1322, 2009. 11

[103] S. Modi, A. Stopeck, H. Linden, D. Solit, S. Chandarlapaty, N. Rosen, G. D'Andrea, M. Dickler, M. E. Moynahan, S. Sugarman, et al. **HSP90 inhibition is effective in breast cancer: a phase II trial of tanespimycin (17-AAG) plus trastuzumab in patients with HER2-positive metastatic breast cancer progressing on trastuzumab**. *Clinical Cancer Research*, **17**(15):5132–5139, 2011. 12

[104] W. K. Oh, M. D. Galsky, W. M. Stadler, S. Srinivas, F. Chu, G. Bubley, J. Goddard, J. Dunbar, and R. W. Ross. **Multicenter phase II trial of the heat shock protein 90 inhibitor, retaspimycin hydrochloride (IPI-504), in patients with castration-resistant prostate cancer**. *Urology*, **78**(3):626–630, 2011. 12

[105] J. Lancet, I. Gojo, M. Burton, M. Quinn, S. Tighe, K. Kersey, Z. Zhong, M. Albitar, K. Bhalla, A. Hannah, et al. **Phase I study of the heat shock protein 90 inhibitor alvespimycin (KOS-1022, 17-DMAG) administered intravenously twice weekly to patients with acute myeloid leukemia**. *Leukemia*, **24**(4):699–705, 2010. 12

[106] S. A. Eccles, A. Massey, F. I. Raynaud, S. Y. Sharp, G. Box, M. Valenti, L. Patterson, A. d Haven Brandon, S. Gowan, F. Boxall, et al. **NVP-AUY922: a novel heat shock protein 90 inhibitor active against xenograft tumor growth, angiogenesis, and metastasis**. *Cancer research*, **68**(8):2850–2860, 2008. 12

[107] K. Lundgren, H. Zhang, J. Brekken, N. Huser, R. E. Powell, N. Timple, D. J. Busch, L. Neely, J. L. Sensintaffar, Y.-c. Yang, et al. **BIIB021, an orally available, fully synthetic small-molecule inhibitor of the heat shock protein Hsp90**. *Molecular Cancer Therapeutics*, **8**(4):921–929, 2009. 12

[108] K. Wong, M. Koczywas, J. Goldman, E. Paschold, L. Horn, J. Lufkin, R. Blackman, F. Teofilovici, G. Shapiro, and M. Socinski. **An open-label phase II study of the Hsp90 inhibitor ganetespib (STA-9090) as monotherapy in patients with advanced non-small cell lung cancer (NSCLC)**. In *ASCO Meeting Abstracts*, **29**, pages 7500–7500, 2011. 12

[109] G. Floris, R. Sciot, A. Wozniak, T. Van Looy, J. Wellens, G. Faa, E. Normant, M. Debiec-Rychter, and P. Schöffski. **The Novel HSP90 inhibitor, IPI-493, is highly effective in human gastrostrointestinal stromal tumor xenografts carrying heterogeneous KIT mutations**. *Clinical Cancer Research*, **17**(17):5604–5614, 2011. 12

[110] A. Rajan, R. J. Kelly, J. B. Trepel, Y. S. Kim, S. V. Alarcon, S. Kummar, M. Gutierrez, S. Crandon, W. M. Zein, L. Jain, et al. **A phase I study of PF-04929113 (SNX-5422), an orally bioavailable heat shock protein 90 inhibitor, in patients with refractory solid tumor malignancies and lymphomas**. *Clinical Cancer Research*, **17**(21):6831–6839, 2011. 12

[111] D. Hong, R. Said, G. Falchook, A. Naing, S. Moulder, A.-M. Tsimberidou, G. Galluppi, N. Dakappagari, C. Storgard, R. Kurzrock, et al. **Phase I study of BIIB028, a selective heat shock protein 90 inhibitor, in patients with refractory metastatic or locally advanced solid tumors**. *Clinical Cancer Research*, **19**(17):4824–4831, 2013. 12

[112] T. Nakashima, T. Ishii, H. Tagaya, T. Seike, H. Nakagawa, Y. Kanda, S. Akinaga, S. Soga, and Y. Shiotsu. **New molecular and biological mechanism of antitumor activities of KW-2478, a novel nonansamycin heat shock protein 90 inhibitor, in multiple myeloma cells**. *Clinical Cancer Research*, **16**(10):2792–2802, 2010. 12

[113] B. Graham, J. Curry, T. Smyth, L. Fazal, R. Feltell, I. Harada, J. Coyle, B. Williams, M. Reule, H. Angove, et al. **The heat shock protein 90 inhibitor, AT13387, displays a long duration of action in vitro and in vivo in non-small cell lung cancer**. *Cancer science*, **103**(3):522–527, 2012. 12

[114] K. H. Paraiso, H. E. Haarberg, E. Wood, V. W. Rebecca, Y. A. Chen, Y. Xiang, A. Ribas, R. S. Lo, J. S. Weber, V. K. Sondak, et al. **The HSP90 inhibitor XL888 overcomes BRAF inhibitor resistance mediated through diverse mechanisms**. *Clinical Cancer Research*, **18**(9):2502–2514, 2012. 12

[115] B. Lamottke, M. Kaiser, M. Mieth, U. Heider, Z. Gao, Z. Nikolova, M. R. Jensen, J. Sterz, I. v Metzler, and O. Sezer. **The novel, orally bioavailable HSP90 inhibitor NVP-HSP990 induces cell cycle arrest and apoptosis in multiple myeloma cells and acts synergistically with melphalan by increased cleavage of caspases**. *European journal of haematology*, **88**(5):406–415, 2012. 12

[116] S.-H. Kim, A. Bajji, R. Tangallapally, B. Markovitz, R. Trovato, M. Shenderovich, V. Baichwal, P. Bartel, D. Cimbora, R. McKinnon, et al. **Discovery of (2 S)-1-[4-(2-{6-Amino-8-[(6-bromo-1, 3-benzodioxol-5-yl) sulfanyl]-9 H-purin-9-yl} ethyl) piperidin-1-yl]-2-hydroxypropan-1-one (MPC-3100), a Purine-Based Hsp90 Inhibitor**. *Journal of medicinal chemistry*, **55**(17):7480–7501, 2012. 12

[117] Q. Fu, J. Sun, W. Zhang, X. Sui, Z. Yan, and Z. He. **Nanoparticle albumin-bound (NAB) technology is a promising method for anti-cancer drug delivery**. *Recent patents on anti-cancer drug discovery*, **4**(3):262–272, 2009. 12

[118] N. Isambert, A. Hollebecque, Y. Berge, H. v Ingen, S. Brienza, A. Destaillats, J.-C. Soria, P. Fumoleau, and J.-P. Delord. **A phase I study of Debio 0932, an oral HSP90 inhibitor, in patients with solid tumors**. In *Journal Of Clinical Oncology*, **30**. Amer. Soc. Clincial Oncology, 2012. 12

[119] E. Caldas-Lopes, L. Cerchietti, J. H. Ahn, C. C. Clement, A. I. Robles, A. Rodina, K. Moulick, T. Taldone, A. Gozman, Y. Guo, et al. **Hsp90 inhibitor PU-H71, a multimodal inhibitor of malignancy, induces complete responses in triple-negative breast cancer models**. *Proceedings of the National Academy of Sciences*, **106**(20):8368–8373, 2009. 12

[120] H. R. Kim, H. S. Kang, and H. D. Kim. **Geldanamycin induces heat shock protein expression through activation of HSF1 in K562 erythroleukemic cells**. *IUBMB life*, **48**(4):429–433, 1999. 11

[121] D. M. Roth, D. M. Hutt, J. Tong, M. Bouchecareilh, N. Wang, T. Seeley, J. F. Dekkers, J. M. Beekman, D. Garza, L. Drew, E. Masliah, R. I. Morimoto, and W. E. Balch. **Modulation of the Maladaptive Stress Response to Manage Diseases of Protein Folding.** *PLoS biology*, **12**(11), 2014. 11

[122] T. F. Outeiro, E. Kontopoulos, S. M. Altmann, I. Kufareva, K. E. Strathearn, A. M. Amore, C. B. Volk, M. M. Maxwell, J.-C. Rochet, P. J. McLean, et al. **Sirtuin 2 inhibitors rescue α-synuclein-mediated toxicity in models of Parkinson's disease**. *science*, **317**(5837):516–519, 2007. 11

[123] P. K. Auluck and N. M. Bonini. **Pharmacological prevention of Parkinson disease in Drosophila**. *Nature medicine*, **8**(11):1185–1186, 2002. 11

[124] A. Sittler, R. Lurz, G. Lueder, J. Priller, M. K. Hayer-Hartl, F. U. Hartl, H. Lehrach, and E. E. Wanker. **Geldanamycin activates a heat shock response and inhibits huntingtin aggregation in a cell culture model of Huntingtons disease**. *Human molecular genetics*, **10**(12):1307–1315, 2001. 11, 65

[125] W. Luo, A. Rodina, and G. Chiosis. **Heat shock protein 90: translation from cancer to Alzheimer's disease treatment?** *BMC neuroscience*, **9**(Suppl 2):S7, 2008. 11

[126] C. Ross and M. Poirier. **Protein aggregation and neurodegenerative disease.** *Nature medicine*, **10**:S10–7, 2004. 11

[127] R. Conde, Z. R. Belak, M. Nair, R. F. O'Carroll, and N. Ovsenek. **Modulation of Hsf1 activity by novobiocin and geldanamycin**. *Biochemistry and Cell Biology*, **87**(6):845–851, 2009. 11

[128] L. Whitesell and S. Lindquist. **Inhibiting the transcription factor HSF1 as an anticancer strategy.** *Expert opinion on therapeutic targets*, **13**(4):469–478, 2009. 11, 64

[129] N. Nagai, A. Nakai, and K. Nagata. **Quercetin suppresses heat shock response by down-regulation of HSF1**. *Biochemical and biophysical research communications*, **208**(3):1099–1105, 1995. 11, 64

[130] Y. Chen, J. Chen, A. Loo, S. Jaeger, and L. Bagdasarian. **Targeting HSF1 sensitizes cancer cells to HSP90 inhibition**. 2013. 11, 64

[131] S. H. Millson and P. W. Piper. **Insights from yeast into whether the rapamycin inhibition of heat shock transcription factor (Hsf1) can prevent the Hsf1 activation that results from treatment with an Hsp90 inhibitor**. *Oncotarget*, **5**(13):5054, 2014. 11, 64

[132] J. Acquaviva, S. He, J. Sang, D. L. Smith, M. Sequeira, C. Zhang, R. C. Bates, and D. A. Proia. **mTOR inhibition potentiates HSP90 inhibitor activity via cessation of HSP synthesis.** *Molecular cancer research : MCR*, **12**(5):703–713, 2014. 11, 64

[133] C. A. Whittaker, K.-F. Bergeron, J. Whittle, B. P. Brandhorst, R. D. Burke, and R. O. Hynes. **The echinoderm adhesome**. *Developmental biology*, **300**(1):252–266, 2006. 11, 15

[134] S. Özbek, P. G. Balasubramanian, R. Chiquet-Ehrismann, R. P. Tucker, and J. C. Adams. **The evolution of extracellular matrix**. *Molecular biology of the cell*, **21**(24):4300–4305, 2010. 13

[135] M. Egeblad, E. S. Nakasone, and Z. Werb. **Tumors as organs: complex tissues that interface with the entire organism**. *Developmental cell*, **18**(6):884–901, 2010. 13

[136] S. K. Akiyama, K. Olden, and K. M. Yamada. **Fibronectin and integrins in invasion and metastasis**. *Cancer and Metastasis Reviews*, **14**(3):173–189, 1995. 13, 16, 17

[137] I. Wierzbicka-Patynowski and J. E. Schwarzbauer. **The ins and outs of fibronectin matrix assembly.** *Journal of cell science*, **116**(Pt 16):3269–3276, 2003. 13

[138] J. Huxley-Jones, J. W. Pinney, J. Archer, D. L. Robertson, and R. P. Boot-Handford. **Back to basics–how the evolution of the extracellular matrix underpinned vertebrate evolution**. *International journal of experimental pathology*, **90**(2):95–100, 2009. 13

[139] H. Hutter, B. E. Vogel, J. D. Plenefisch, C. R. Norris, R. B. Proenca, J. Spieth, C. Guo, S. Mastwal, X. Zhu, J. Scheel, et al. **Conservation and novelty in the evolution of cell adhesion and extracellular matrix genes**. *Science*, **287**(5455):989–994, 2000. 13

[140] P. Lu, K. Takai, V. M. Weaver, and Z. Werb. **Extracellular matrix degradation and remodeling in development and disease**. *Cold Spring Harbor perspectives in biology*, **3**(12):a005058, 2011. 13, 14, 16, 53, 59, 60, 91

[141] R. O. Hynes. **The extracellular matrix: not just pretty fibrils.** *Science (New York, N.Y.)*, **326**(5957):1216–1219, 2009. 13, 53, 91

[142] V. Kölsch, T. Seher, G. J. Fernandez-Ballester, L. Serrano, and M. Leptin. **Control of Drosophila gastrulation by apical localization of adherens junctions and RhoGEF2**. *Science*, **315**(5810):384–386, 2007. 13

[143] R. Windoffer, A. Kölsch, S. Wöll, and R. E. Leube. **Focal adhesions are hotspots for keratin filament precursor formation**. *The Journal of cell biology*, **173**(3):341–348, 2006. 13

[144] D. J. Montell. **Morphogenetic cell movements: diversity from modular mechanical properties**. *Science*, **322**(5907):1502–1505, 2008. 13

[145] R. Fernandez-Gonzalez, S. d. M. Simoes, J.-C. Röper, S. Eaton, and J. A. Zallen. **Myosin II dynamics are regulated by tension in intercalating cells**. *Developmental cell*, **17**(5):736–743, 2009. 13

[146] P.-A. Pouille, P. Ahmadi, A.-C. Brunet, and E. Farge. **Mechanical signals trigger Myosin II redistribution and mesoderm invagination in Drosophila embryos**. *Science signaling*, **2**(66):ra16, 2009. 13

[147] C. C. DuFort, M. J. Paszek, and V. M. Weaver. **Balancing forces: architectural control of mechanotransduction**. *Nature reviews Molecular cell biology*, **12**(5):308–319, 2011. 13

[148] M. Théry, V. Racine, A. Pépin, M. Piel, Y. Chen, J.-B. Sibarita, and M. Bornens. **The extracellular matrix guides the orientation of the cell division axis**. *Nature cell biology*, **7**(10):947–953, 2005. 13

[149] D. H. Kim, P. P. Provenzano, C. L. Smith, and A. Levchenko. **Matrix nanotopography as a regulator of cell function.** *The Journal of cell biology*, **197**(3):351–360, 2012. 13

[150] A. J. Engler, S. Sen, H. L. Sweeney, and D. E. Discher. **Matrix elasticity directs stem cell lineage specification**. *Cell*, **126**(4):677–689, 2006. 13

[151] P. M. Gilbert, K. L. Havenstrite, K. E. Magnusson, A. Sacco, N. A. Leonardi, P. Kraft, N. K. Nguyen, S. Thrun, M. P. Lutolf, and H. M. Blau. **Substrate elasticity regulates skeletal muscle stem cell self-renewal in culture**. *Science*, **329**(5995):1078–1081, 2010. 13

[152] M. Egeblad and Z. Werb. **New functions for the matrix metalloproteinases in cancer progression**. *Nature Reviews Cancer*, **2**(3):161–174, 2002. 14, 59

[153] T. E. Cawston and D. A. Young. **Proteinases involved in matrix turnover during cartilage and bone breakdown**. *Cell and tissue research*, **339**(1):221–235, 2010. 14

[154] S. Caudroy, M. Polette, B. Nawrocki-Raby, J. Cao, B. P. Toole, S. Zucker, and P. Birembaut. **EMMPRIN-mediated MMP regulation in tumor and endothelial cells**. *Clinical & experimental metastasis*, **19**(8):697–702, 2002. 14

[155] H. Munshi and M. Stack. **Reciprocal interactions between adhesion receptor signaling and MMP regulation**. *Cancer and Metastasis Reviews*, **25**(1):45–56, 2006. 14

[156] D. Schroen and C. Brinckerhoff. **Nuclear hormone receptors inhibit matrix metalloproteinase (MMP) gene expression through diverse mechanisms.** *Gene expression*, **6**(4):197–207, 1995. 14

[157] J. D. Mott and Z. Werb. **Regulation of matrix biology by matrix metalloproteinases**. *Current opinion in cell biology*, **16**(5):558–564, 2004. 14, 16

[158] H. Yu, J. K. Mouw, and V. M. Weaver. **Forcing form and function: biomechanical regulation of tumor evolution**. *Trends in cell biology*, **21**(1):47–56, 2011. 14

[159] D. T. Butcher, T. Alliston, and V. M. Weaver. **A tense situation: forcing tumour progression**. *Nature Reviews Cancer*, **9**(2):108–122, 2009. 14

[160] M. S. Samuel, J. I. Lopez, E. J. McGhee, D. R. Croft, D. Strachan, P. Timpson, J. Munro, E. Schröder, J. Zhou, V. G. Brunton, et al. **Actomyosin-mediated cellular tension drives increased tissue stiffness and β-catenin activation to induce epidermal hyperplasia and tumor growth**. *Cancer cell*, **19**(6):776–791, 2011. 14

[161] T. R. Cox and J. T. Erler. **Remodeling and homeostasis of the extracellular matrix: implications for fibrotic diseases and cancer**. *Disease models & mechanisms*, **4**(2):165–178, 2011. 14

[162] E. Arriazu, M. R. d Galarreta, F. J. Cubero, M. Varela-Rey, M. P. P. d Obanos, T. M. Leung, A. Lopategi, A. Benedicto, I. Abraham-Enachescu, and N. Nieto. **Extracellular Matrix and Liver Disease**. *Antioxidants & redox signaling*, 2014. 14

[163] C. Frantz, K. M. Stewart, and V. M. Weaver. **The extracellular matrix at a glance**. *Journal of cell science*, **123**(24):4195–4200, 2010. 14

[164] D. Schuppan. **Structure of the extracellular matrix in normal and fibrotic liver: collagens and glycoproteins.** In *Seminars in liver disease*, **10**, pages 1–10, 1990. 14

[165] J. P. Iredale, A. Thompson, and N. C. Henderson. **Extracellular matrix degradation in liver fibrosis: Biochemistry and regulation**. *Biochimica et Biophysica Acta (BBA)-Molecular Basis of Disease*, **1832**(7):876–883, 2013. 14

[166] D. J. Tschumperlin, J. C. Jones, and R. M. Senior. **The fibrotic matrix in control: does the extracellular matrix drive progression of idiopathic pulmonary fibrosis?** *American journal of respiratory and critical care medicine*, **186**(9):814–816, 2012. 14

[167] M. Pruteanu, N. P. Hyland, D. J. Clarke, B. Kiely, and F. Shanahan. **Degradation of the extracellular matrix components by bacterial-derived metalloproteases: Implications for inflammatory bowel diseases**. *Inflammatory bowel diseases*, **17**(5):1189–1200, 2011. 14

[168] C. Breynaert, J. Cremer, C. Perrier, M. Ferrante, S. Vermeire, P. Rutgeerts, J. Ceuppens, K. Geboes, and G. Van Assche. **Extracellular Matrix Protein Expression in Chronic Relapsing Dextran Sodium Sulphate Colitis Reflects Transmural Remodeling in Human Crohn's Disease**. *Gastroenterology*, **144**(5):S669–S670, 2013. 14

[169] C. Bonnans, J. Chou, and Z. Werb. **Remodelling the extracellular matrix in development and disease**. *Nature Reviews Molecular Cell Biology*, **15**(12):786–801, 2014. 14

[170] G. Sidgwick and A. Bayat. **Extracellular matrix molecules implicated in hypertrophic and keloid scarring**. *Journal of the European Academy of Dermatology and Venereology*, **26**(2):141–152, 2012. 14

[171] J. Zeichen, M. Van Griensven, I. Albers, P. Lobenhoffer, and U. Bosch. **Immunohistochemical localization of collagen VI in arthrofibrosis**. *Archives of orthopaedic and trauma surgery*, **119**(5-6):315–318, 1999. 14

[172] W. Efird, P. Kellam, S. Yeazell, P. Weinhold, and L. E. Dahners. **An evaluation of prophylactic treatments to prevent post traumatic joint stiffness**. *Journal of Orthopaedic Research*, **32**(11):1520–1524, 2014. 14

[173] M. Brownlee. **Biochemistry and molecular cell biology of diabetic complications**. *Nature*, **414**(6865):813–820, 2001. 14

[174] E. Ioachim, M. Stefaniotou, S. Gorezis, E. Tsanou, K. Psilas, and N. Agnantis. **Immunohistochemical study of extracellular matrix components in epiretinal membranes of vitreoproliferative retinopathy and proliferative diabetic retinopathy.** *European journal of ophthalmology*, **15**(3):384–391, 2004. 14

[175] F. N. Ziyadeh. **The extracellular matrix in diabetic nephropathy**. *American journal of kidney diseases*, **22**(5):736–744, 1993. 14

[176] S. Kolset, F. Reinholt, and T. Jenssen. **Diabetic nephropathy and extracellular matrix**. *Journal of Histochemistry & Cytochemistry*, page 0022155412465073, 2012. 14

[177] F. K. Tan, F. C. Arnett, S. Antohi, S. Saito, A. Mirarchi, H. Spiera, T. Sasaki, O. Shoichi, K. Takeuchi, J. P. Pandey, et al. **Autoantibodies to the extracellular matrix microfibrillar protein, fibrillin-1, in patients with scleroderma and other connective tissue diseases**. *The Journal of Immunology*, **163**(2):1066–1072, 1999. 14

[178] A. Akhmetshina, C. Dees, M. Pileckyte, G. Szucs, B. M. Spriewald, J. Zwerina, O. Distler, G. Schett, and J. H. Distler. **Rho-associated kinases are crucial for myofibroblast differentiation and production of extracellular matrix in scleroderma fibroblasts**. *Arthritis & Rheumatism*, **58**(8):2553–2564, 2008. 14

[179] A. I. El-Sakka, H. M. Hassoba, R. J. Pillarisetty, R. Dahiya, and T. F. Lue. **Peyronie's disease is associated with an increase in transforming growth factor-beta protein expression**. *The Journal of urology*, **158**(4):1391–1394, 1997. 14

[180] W. J. Hellstrom and T. J. Bivalacqua. **Peyronie's disease: etiology, medical, and surgical therapy**. *Journal of andrology*, **21**(3):347–354, 2000. 14

[181] L. J. **Fibronectin in malignancy.** *Seminars in cancer biology*, **12**(3):187–195, 2002. 15, 16, 17

[182] S. K. Akiyama, S. S. Yamada, W.-T. Chen, and K. M. Yamada. **Analysis of fibronectin receptor function with monoclonal antibodies: roles in cell adhesion, migration, matrix assembly, and cytoskeletal organization.** *The Journal of Cell Biology*, **109**(2):863–875, 1989. 15

[183] M. V. Pulina, S. Y. Hou, A. Mittal, D. Julich, C. A. Whittaker, S. A. Holley, R. O. Hynes, and S. Astrof. **Essential roles of fibronectin in the development of the left-right embryonic body plan.** *Developmental biology*, **354**(2):208–220, 2011. 15

[184] T. Darribère and J. E. Schwarzbauer. **Fibronectin matrix composition and organization can regulate cell migration during amphibian development**. *Mechanisms of development*, **92**(2):239–250, 2000. 15

[185] R. Pankov and K. M. Yamada. **Fibronectin at a glance**. *Journal of cell science*, **115**(20):3861–3863, 2002. 15

[186] T. Sakai, K. J. Johnson, M. Murozono, K. Sakai, M. A. Magnuson, T. Wieloch, T. Cronberg, A. Isshiki, H. P. Erickson, and R. Fässler. **Plasma fibronectin supports neuronal survival and reduces brain injury following transient focal cerebral ischemia but is not essential for skin-wound healing and hemostasis.** *Nature medicine*, **7**(3):324–330, 2001. 15

[187] A. M. Salicioni, K. S. Mizelle, E. Loukinova, I. Mikhailenko, D. K. Strickland, and S. L. Gonias. **The low density lipoprotein receptor-related protein mediates fibronectin catabolism and inhibits fibronectin accumulation on cell surfaces.** *The Journal of biological chemistry*, **277**(18):16160–16166, 2002. 15, 16

[188] A. Kornblihtt, C. Pesce, C. Alonso, P. Cramer, A. Srebrow, S. Werbajh, and A. Muro. **The fibronectin gene as a model for splicing and transcription studies.** *FASEB journal : official publication of the Federation of American Societies for Experimental Biology*, **10**(2):248–257, 1996. 15, 17, 50

[189] E. S. White, F. Baralle, and A. Muro. **New insights into form and function of fibronectin splice variants**. *The Journal of pathology*, **216**(1):1–14, 2008. 15, 17, 18

[190] J. Schwarzbauer and J. Sechler. **Fibronectin fibrillogenesis: a paradigm for extracellular matrix assembly**. 1999. 15, 16

[191] P. Zago, E. Buratti, C. Stuani, and F. E. Baralle. **Evolutionary connections between coding and splicing regulatory regions in the fibronectin EDA exon.** *Journal of molecular biology*, **411**(1):1–15, 2011. 15

[192] J. Ulmer, B. Geiger, and J. P. Spatz. **Force-induced fibronectin fibrillogenesis in vitro**. *Soft Matter*, **4**(10):1998–2007, 2008. 15

[193] M. J. Humphries, A. Komoriya, S. Akiyama, K. Olden, and K. Yamada. **Identification of two distinct regions of the type III connecting segment of human plasma fibronectin that promote cell type-specific adhesion.** *Journal of Biological Chemistry*, **262**(14):6886–6892, 1987. 15

[194] A. Mould, A. Komoriya, K. Yamada, and M. Humphries. **The CS5 peptide is a second site in the IIICS region of fibronectin recognized by the integrin alpha 4 beta 1. Inhibition of alpha 4 beta 1 function by RGD peptide homologues.** *Journal of Biological Chemistry*, **266**(6):3579–3585, 1991. 15

[195] Y. Tomita, S. K. Akiyama, S.-i. Aota, K. M. Yamada, R. M. Venable, R. W. Pastor, S. Krueger, D. A. Torchia, et al. **Solution structure and dynamics of linked cell attachment modules of mouse fibronectin containing the RGD and synergy regions: comparison with the human fibronectin crystal structure**. *Journal of molecular biology*, **277**(3):663–682, 1998. 15

[196] J. L. Sechler, A. M. Cumiskey, D. M. Gazzola, and J. E. Schwarzbauer. **A novel RGD-independent fibronectin assembly pathway initiated by alpha4beta1 integrin binding to the alternatively spliced V region**. *Journal of cell science*, **113**(8):1491–1498, 2000. 15

[197] S. Miyamoto, B.-Z. Kathz, R. M. Lafrenie, and K. M. Yamada. **Fibronectin and integrins in cell adhesion, signaling, and morphogenesis**. *Annals of the New York Academy of Sciences*, **857**(1):119–129, 1998. 15

[198] S. Johansson, G. Svineng, K. Wennerberg, A. Armulik, and L. Lohikangas. **Fibronectin-integrin interactions**. *Front Biosci*, **2**:d126–d146, 1997. 15

[199] R. Pankov, E. Cukierman, B.-Z. Katz, K. Matsumoto, D. C. Lin, S. Lin, C. Hahn, and K. M. Yamada. **Integrin Dynamics and Matrix Assembly Tensin-Dependent Translocation of $\alpha 5\beta 1$ Integrins Promotes Early Fibronectin Fibrillogenesis**. *The Journal of cell biology*, **148**(5):1075–1090, 2000. 15, 16

[200] B. Geiger, A. Bershadsky, R. Pankov, and K. M. Yamada. **Transmembrane crosstalk between the extracellular matrix and the cytoskeleton**. *Nature Reviews Molecular Cell Biology*, **2**(11):793–805, 2001. 15, 16

[201] E. E. Robinson, R. A. Foty, and S. A. Corbett. **Fibronectin matrix assembly regulates $\alpha 5\beta 1$-mediated cell cohesion**. *Molecular Biology of the cell*, **15**(3):973–981, 2004. 16

[202] T. Ohashi and H. P. Erickson. **Revisiting the mystery of fibronectin multimers: the fibronectin matrix is composed of fibronectin dimers cross-linked by non-covalent bonds.** *Matrix biology : journal of the International Society for Matrix Biology*, **28**(3):170–175, 2009. 16

[203] T. B. R, D. S. Annis, and D. F. Mosher. **The N-terminal 70-kDa fragment of fibronectin binds to cell surface fibronectin assembly sites in the absence of intact fibronectin.** *Matrix biology : journal of the International Society for Matrix Biology*, **25**(5):282–293, 2006. 16

[204] D. Choquet, D. P. Felsenfeld, and M. P. Sheetz. **Extracellular matrix rigidity causes strengthening of integrin–cytoskeleton linkages**. *Cell*, **88**(1):39–48, 1997. 16, 60

[205] T. Nishizaka, Q. Shi, and M. P. Sheetz. **Position-dependent linkages of fibronectin–integrin–cytoskeleton**. *Proceedings of the National Academy of Sciences*, **97**(2):692–697, 2000. 16

[206] K. A. Brenner, S. A. Corbett, and J. E. Schwarzbauer. **Regulation of fibronectin matrix assembly by activated Ras in transformed cells.** *Oncogene*, **19**(28):3156–3163, 2000. 16

[207] F. Samantha, D. Grall, B. Cseh, and V. O. Ellen. **Regulation of fibronectin matrix assembly and capillary morphogenesis in endothelial cells by Rho family GTPases.** *Experimental cell research*, **315**(12):2092–2104, 2009. 16

[208] B. Geiger, J. P. Spatz, and A. D. Bershadsky. **Environmental sensing through focal adhesions**. *Nature Reviews Molecular Cell Biology*, **10**(1):21–33, 2009. 16

[209] Y. Sawada, M. Tamada, B. J. Dubin-Thaler, O. Cherniavskaya, R. Sakai, S. Tanaka, and M. P. Sheetz. **Force sensing by mechanical extension of the Src family kinase substrate p130Cas**. *Cell*, **127**(5):1015–1026, 2006. 16

[210] A. d Rio, R. Perez-Jimenez, R. Liu, P. Roca-Cusachs, J. M. Fernandez, and M. P. Sheetz. **Stretching single talin rod molecules activates vinculin binding**. *Science*, **323**(5914):638–641, 2009. 16

[211] Y.-K. Wang, X. Yu, D. M. Cohen, M. A. Wozniak, M. T. Yang, L. Gao, J. Eyckmans, and C. S. Chen. **Bone morphogenetic protein-2-induced signaling and osteogenesis is regulated by cell shape, RhoA/ROCK, and cytoskeletal tension**. *Stem cells and development*, **21**(7):1176–1186, 2011. 16

[212] C. Streuli. **Extracellular matrix remodelling and cellular differentiation**. *Current opinion in cell biology*, **11**(5):634–640, 1999. 16

[213] M. E. Lukashev and Z. Werb. **ECM signalling: orchestrating cell behaviour and misbehaviour**. *Trends in cell biology*, **8**(11):437–441, 1998. 16

[214] P. Huhtala, M. J. Humphries, J. B. McCarthy, P. M. Tremble, Z. Werb, and C. H. Damsky. **Cooperative signaling by alpha 5 beta 1 and alpha 4 beta 1 integrins regulates metalloproteinase gene expression in fibroblasts adhering to fibronectin.** *The Journal of cell biology*, **129**(3):867–879, 1995. 16

[215] F. Shi and J. Sottile. **MT1-MMP regulates the turnover and endocytosis of extracellular matrix fibronectin**. *Journal of cell science*, **124**(23):4039–4050, 2011. 16

[216] B. Steffensen, Z. Chen, S. Pal, M. Mikhailova, J. Su, Y. Wang, and X. Xu. **Fragmentation of fibronectin by inherent autolytic and matrix metalloproteinase activities.** *Matrix biology : journal of the International Society for Matrix Biology*, **30**(1):34–42, 2011. 16

[217] J. Sottile and J. Chandler. **Fibronectin matrix turnover occurs through a caveolin-1-dependent process.** *Molecular biology of the cell*, **16**(2):757–768, 2005. 16

[218] V. H. Lobert, A. Brech, N. M. Pedersen, J. Wesche, A. Oppelt, L. Malerd, and H. Stenmark. **Ubiquitination of alpha 5 beta 1 integrin controls fibroblast migration through lysosomal degradation of fibronectin-integrin complexes.** *Developmental cell*, **19**(1):148–159, 2010. 16

[219] V. S. Rukosuev, A. K. Nanaev, and A. P. Milovanov. **Participation of collagen types I, III, IV, V, and fibronectin in the formation of villi fibrosis in human term placenta**. *Acta histochemica*, **89**(1):11–16, 1990. 16

[220] E. Kimura, T. Kanzaki, K. Tahara, H. Hayashi, S. Hashimoto, A. Suzuki, R. Yamada, K. Yamamoto, and T. Sawada. **Identification of citrullinated cellular fibronectin in synovial fluid from patients with rheumatoid arthritis**. *Modern Rheumatology*, (0):1–4, 2014. 16

[221] R. J. Perrin, R. Craig-Schapiro, J. P. Malone, A. R. Shah, P. Gilmore, A. E. Davis, C. M. Roe, E. R. Peskind, G. Li, D. R. Galasko, et al. **Identification and validation of novel cerebrospinal fluid biomarkers for staging early Alzheimer's disease**. *PLoS One*, **6**(1):e16032, 2011. 16

[222] M. Santimaria, G. Moscatelli, G. L. Viale, L. Giovannoni, G. Neri, F. Viti, A. Leprini, L. Borsi, P. Castellani, L. Zardi, et al. **Immunoscintigraphic detection of the ED-B domain of fibronectin, a marker of angiogenesis, in patients with cancer**. *Clinical Cancer Research*, **9**(2):571–579, 2003. 17

[223] Y. Zheng, J. D. Ritzenthaler, J. Roman, and S. Han. **Nicotine stimulates human lung cancer cell growth by inducing fibronectin expression**. *American journal of respiratory cell and molecular biology*, **37**(6):681–690, 2007. 17

[224] M. Zheng, D. M. Jones, C. Horzempa, A. Prasad, and P. J. McKeown-Longo. **The first type III domain of fibronectin is associated with the expression of cytokines within the lung tumor microenvironment**. *Journal of Cancer*, **2**:478, 2011. 17

[225] H.-h. Dong, S. Xiang, H.-f. Liang, C.-h. Li, Z.-w. Zhang, and X.-p. Chen. **The niche of hepatic cancer stem cell and cancer recurrence**. *Medical hypotheses*, **80**(5):666–668, 2013. 17

[226] A. Lochter. **Involvement of extracellular matrix constituents in breast cancer**. *Lawrence Berkeley National Laboratory*, 2011. 17

[227] M. Bissell and W. Hines. **Why don't we get more cancer? A proposed role of the microenvironment in restraining cancer progression**. 2011. 17

[228] H. A. Kenny, S. Kaur, L. M. Coussens, and E. Lengyel. **The initial steps of ovarian cancer cell metastasis are mediated by MMP-2 cleavage of vitronectin and fibronectin.** *The Journal of clinical investigation*, **118**(4):1367–1379, 2008. 17

[229] A. v Au, M. Vasel, C. Glueer, S. Tiwari, M. Cecchini, and I. Nakchbandi. **Circulating fibronectin is required for blood vessel formation and tumor growth**. *Bone*, **48**, 2011. 17

[230] E. Altrock, C. Sens, C. Wuerfel, M. Vasel, N. Kawelke, S. Dooley, J. Sottile, and I. A. Nakchbandi. **Inhibition of fibronectin deposition improves experimental liver fibrosis**. *Journal of hepatology*, 2014. 17

[231] C. Samuel. **The Relevance of the Anti-Fibrotic and Other Therapeutic Actions of Relaxin to Atrial Fibrillation**. *Journal of Arrhythmia*, **27**(Supplement):SY11_4–SY11_4, 2011. 17

[232] J. Sottile, I. Nakchbandi, and B. C. Blaxall. **Treatment of fibrosis-related disorders using fibronectin binding proteins and polypeptides**, February 3 2011. US Patent App. 13/576,900. 17

[233] M. Lopez-Armada, E. Gonzalez, C. Gomez-Guerrero, and J. Egido. **The 80-kD fibronectin fragment increases the production of fibronectin and tumour necrosis factor-alpha (TNF-α) in cultured mesangial cells**. *Clinical & Experimental Immunology*, **107**(2):398–403, 1997. 17

[234] M. Yi and E. Ruoslahti. **A fibronectin fragment inhibits tumor growth, angiogenesis, and metastasis.** *Proceedings of the National Academy of Sciences of the United States of America*, **98**(2):620–624, 2001. 17

[235] R. You, R. Klein, M. Zheng, and M. P. J. **Regulation of p38 MAP kinase by anastellin is independent of anastellin's effect on matrix fibronectin.** *Matrix biology : journal of the International Society for Matrix Biology*, **28**(2):101–109, 2009. 17

[236] A. K. Chauhan, A. Iaconcig, F. E. Baralle, and A. F. Muro. **Alternative splicing of fibronectin: a mouse model demonstrates the identity of in vitro and in vivo systems and the processing autonomy of regulated exons in adult mice.** *Gene*, **324**:55–63, 2004. 17, 18, 50

[237] K. Umezawa, A. R. Kornblihtt, and F. E. Baralle. **Isolation and characterization of cDNA clones for human liver fibronectin**. *FEBS letters*, **186**(1):31–34, 1985. 18

[238] F. Han, J. R. Gilbert, G. Harrison, C. S. Adams, T. Freeman, Z. Tao, R. Zaka, H. Liang, C. Williams, R. S. Tuan, P. A. Norton, and N. J. Hickok. **Transforming growth factor-beta1 regulates fibronectin isoform expression and splicing factor SRp40 expression during ATDC5 chondrogenic maturation.** *Experimental cell research*, **313**(8):1518–1532, 2007. 18

[239] F. Oyama, S. Hirohashi, Y. Shimosato, K. Titani, and K. Sekiguchi. **Deregulation of alternative splicing of fibronectin pre-mRNA in malignant human liver tumors.** *Journal of Biological Chemistry*, **264**(18):10331–10334, 1989. 18

[240] F. Oyama, S. Hirohashi, M. Sakamoto, K. Titani, and K. Sekiguchi. **Coordinate oncodevelopmental modulation of alternative splicing of fibronectin premessenger RNA at ED-A, ED-B, and CS1 regions in human liver tumors**. *Cancer research*, **53**(9):2005–2011, 1993. 18

[241] S. Barlati, M. Colombi, and G. De Petro. **Differential expression of fibronectin and its degradation products in malignant tumors**. *Tumor Matrix Biology, CRC Press, Boca Raton, Florida*, pages 81–99, 1995. 18

[242] Y. Abe, N.-A. Bui-Thanh, C. M. Ballantyne, and A. R. Burns. **Extra domain A and type III connecting segment of fibronectin in assembly and cleavage**. *Biochemical and biophysical research communications*, **338**(3):1640–1647, 2005. 18

[243] M. Liu, M. Xie, S. Jiang, G. Liu, L. Li, D. Liu, and X. Yang. **A novel bispecific antibody targeting tumor necrosis factor α and ED-B fibronectin effectively inhibits the progression of established collagen-induce arthritis**. *Journal of biotechnology*, **186**:1–12, 2014. 18

[244] A. Gratchev, P. Guillot, N. Hakiy, O. Politz, C. Orfanos, K. Schledzewski, and S. Goerdt. **Alternatively Activated Macrophages Differentially Express Fibronectin and Its Splice Variants and the Extracellular Matrix Protein βIG-H3**. *Scandinavian journal of immunology*, **53**(4):386–392, 2001. 18

[245] D. C. Dean, C. L. Bowlus, and S. Bourgeois. **Cloning and analysis of the promotor region of the human fibronectin gene**. *Proceedings of the National Academy of Sciences*, **84**(7):1876–1880, 1987. 18, 40

[246] D. C. Dean, R. F. Newby, and S. Bourgeois. **Regulation of fibronectin biosynthesis by dexamethasone, transforming growth factor beta, and cAMP in human cell lines.** *The Journal of cell biology*, **106**(6):2159–2170, 1988. 18, 58, 61

[247] D. C. Dean, M. Blakeley, R. Newby, P. Ghazal, L. Hennighausen, and S. Bourgeois. **Forskolin inducibility and tissue-specific expression of the fibronectin promoter.** *Molecular and cellular biology*, **9**(4):1498–1506, 1989. 18

[248] C. R. Alonso, J. George, C. Pesce, D. Bissell, and A. R. Kornblihtt. **Fibronectin transcription in liver cells: promoter occupation and function in sinusoidal endothelial cells and hepatocytes.** *Biochemical and biophysical research communications*, **295**(5):1077–1084, 2002. 18

[249] D. Gradl, M. Kuhl, and D. Wedlich. **The Wnt/Wg signal transducer β-catenin controls fibronectin expression**. *Molecular and cellular biology*, **19**(8):5576–5587, 1999. 19, 58

[250] C. Yang and A. Sorokin. **Upregulation of fibronectin expression by COX-2 is mediated by interaction with ELMO1.** *Cellular signalling*, **23**(1):99–9104, 2011. 19

[251] W. Liu, T. Lan, X. Xie, K. Huang, J. Peng, J. Huang, X. Shen, P. Liu, and H. Huang. **S1P2 receptor mediates sphingosine-1-phosphate-induced fibronectin expression via MAPK signaling pathway in mesangial cells under high glucose condition.** *Experimental cell research*, **318**(8):936–943, 2012. 19, 62

[252] J. S. Tyagi, H. Hirano, and I. Pastan. **Modulation of fibronectin gene activity in chick embryo fibroblasts transformed by a temperature-sensitive strain (ts68) of Rous sarcoma virus**. *Nucleic acids research*, **13**(22):8275–8284, 1985. 19

[253] L. Devriese, A. Bosma, M. v. d Heuvel, W. Heemsbergen, E. Voest, and J. Schellens. **Circulating tumor cell detection in advanced non-small cell lung cancer patients by multi-marker QPCR analysis.** *Lung cancer (Amsterdam, Netherlands)*, **75**(2):242–247, 2012. 19

[254] S. Yang, Q. Dong, M. Yao, M. Shi, J. Ye, L. Zhao, J. Su, W. Gu, W. Xie, K. Wang, Y. Du, Y. Li, and Y. Huang. **Establishment of an experimental human lung adenocarcinoma cell line SPC-A-1BM with high bone metastases potency by (99m)Tc-MDP bone scintigraphy.** *Nuclear medicine and biology*, **36**(3):313–321, 2009. 19

[255] S. Yang, J. Shin, K. H. Park, H. C. Jeung, S. Y. Rha, S. H. Noh, W. I. Yang, and H. C. Chung. **Molecular basis of the differences between normal and tumor tissues of gastric cancer.** *Biochimica et biophysica acta*, **1772**(9):1033–1040, 2007. 19

[256] E. A. Clark, T. R. Golub, E. S. Lander, and R. O. Hynes. **Genomic analysis of metastasis reveals an essential role for RhoC**. *Nature*, **406**(6795):532–535, 2000. 19

[257] F. Wang, G. Song, M. Liu, X. Li, and H. Tang. **miRNA-1 targets fibronectin1 and suppresses the migration and invasion of the HEp2 laryngeal squamous carcinoma cell line.** *FEBS letters*, **585**(20):3263–3269, 2011. 19

[258] J. Meredith, B. Fazeli, and M. Schwartz. **The extracellular matrix as a cell survival factor.** *Molecular biology of the cell*, **4**(9):953–961, 1993. 20, 66

[259] U. K. Laemmli et al. **Cleavage of structural proteins during the assembly of the head of bacteriophage T4**. *nature*, **227**(5259):680–685, 1970. 23

[260] H. Towbin, T. Staehelin, and J. Gordon. **Electrophoretic transfer of proteins from polyacrylamide gels to nitrocellulose sheets: procedure and some applications**. *Proceedings of the National Academy of Sciences*, **76**(9):4350–4354, 1979. 23

[261] T. Heinemeyer, E. Wingender, I. Reuter, H. Hermjakob, A. Kel, O. Kel, E. Ignatieva, E. Ananko, O. Podkolodnaya, F. Kolpakov, N. Podkolodny, and N. Kolchanov. **Databases on transcriptional regulation: TRANSFAC, TRRD and COMPEL.** *Nucleic acids research*, **26**(1):362–367, 1998. 27, 39

[262] D. Farré, R. Roset, M. Huerta, J. E. Adsuara, L. Roselló, M. M. Albà, and X. Messeguer. **Identification of patterns in biological sequences at the ALGGEN server: PROMO and MALGEN**. *Nucleic acids research*, **31**(13):3651–3653, 2003. 27

[263] X. Messeguer, R. Escudero, D. Farré, O. Núñez, J. Martínez, and M. Albà. **PROMO: detection of known transcription regulatory elements using species-tailored searches.** *Bioinformatics (Oxford, England)*, **18**(2):333–334, 2002. 27

[264] N. Grabe. **AliBaba2: context specific identification of transcription factor binding sites.** *In silico biology*, **2**(1):S1–15, 2002. 27

[265] E. S.-v Olst, C. Vermeulen, R. X. d Menezes, M. Howell, E. F. Smit, and V. W. v Beusechem. **Affordable Luciferase Reporter Assay for Cell-Based High-Throughput Screening**. *Journal of biomolecular screening*, **18**(4):453–461, 2013. 28, 41

[266] K. J. Livak and T. D. Schmittgen. **Analysis of Relative Gene Expression Data Using Real-Time Quantitative PCR and the 2-$\Delta\Delta$CT Method**. *methods*, **25**(4):402–408, 2001. 33, 44, 47

[267] L. Whitesell, R. Bagatell, and R. Falsey. **The stress response: implications for the clinical development of hsp90 inhibitors**. *Current cancer drug targets*, **3**(5):349–358, 2003. 35, 64

[268] K. D. Sarge, S. P. Murphy, and R. I. Morimoto. **Activation of heat shock gene transcription by heat shock factor 1 involves oligomerization, acquisition of DNA-binding activity, and nuclear localization and can occur in the absence of stress.** *Molecular and cellular biology*, **13**(3):1392–1407, 1993. 37

[269] C. T. Harbison, D. Gordon, T. I. Lee, N. J. Rinaldi, K. D. Macisaac, T. W. Danford, N. M. Hannett, J. B. Tagne, D. B. Reynolds, J. Yoo, E. G. Jennings, J. Zeitlinger, D. K. Pokholok, M. Kellis, P. Rolfe, K. T. Takusagawa, E. S. Lander, D. K. Gifford, E. Fraenkel, and R. A. Young. **Transcriptional regulatory code of a eukaryotic genome.** *Nature*, **431**(7004):99–9104, 2004. 39

[270] S. Bolte and F. P. Cordelières. **A guided tour into subcellular colocalization analysis in light microscopy**. *Journal of microscopy*, **224**(3):213–232, 2006. 48

[271] O. Kilian, R. Dahse, V. Alt, L. Zardi, J. Rosenhahn, U. Exner, A. Battmann, R. Schnettler, and H. Kosmehl. **Expression of EDA+ and EDB+ fibronectin splice variants in bone.** *Bone*, **35**(6):1334–1345, 2004. 50, 89

[272] S. Wilkinson, O. Jim, M. Fricker, and K. M. Ryan. **Hypoxia-selective macroautophagy and cell survival signaled by autocrine PDGFR activity.** *Genes & development*, **23**(11):1283–1288, 2009. 53, 91

[273] P. Lu, V. M. Weaver, and Z. Werb. **The extracellular matrix: a dynamic niche in cancer progression.** *The Journal of cell biology*, **196**(4):395–406, 2012. 53, 91

[274] N. D. Trinklein, W. C. Chen, R. E. Kingston, and R. M. Myers. **Transcriptional regulation and binding of heat shock factor 1 and heat shock factor 2 to 32 human heat shock genes during thermal stress and differentiation**. *Cell stress & chaperones*, **9**(1):21, 2004. 58

[275] I. Birch-Machin, S. Gao, D. Huen, R. McGirr, R. A. White, and S. Russell. **Genomic analysis of heat-shock factor targets in Drosophila**. *Genome biology*, **6**(7):R63, 2005. 58

[276] A. M. Jaeger, L. N. Makley, J. E. Gestwicki, and D. J. Thiele. **Genomic Heat Shock Element Sequences Drive Cooperative Human Heat Shock Factor 1 DNA Binding and Selectivity**. *Journal of Biological Chemistry*, **289**(44):30459–30469, 2014. 58, 59

[277] J. Amin, J. Ananthan, and R. Voellmy. **Key features of heat shock regulatory elements.** *Molecular and cellular biology*, **8**(9):3761–3769, 1988. 58

[278] C. Bowlus, M. JJ, and D. Dean. **Characterization of three different elements in the 5'-flanking region of the fibronectin gene which mediate a transcriptional response to cAMP.** *The Journal of biological chemistry*, **266**(2):1122–1127, 1991. 58

[279] R. K. Vadlamudi, A. A. Sahin, L. Adam, R. A. Wang, and R. Kumar. **Heregulin and HER2 signaling selectively activates c-Src phosphorylation at tyrosine 215.** *FEBS letters*, **543**(1-3):76–80, 2003. 58

[280] P. E. Ray, L. A. Bruggeman, S. Horikoshi, G. Aguilera, and P. E. Klotman. **Angiotensin II stimulates human fetal mesangial cell proliferation and fibronectin biosynthesis by binding to AT˜ 1 receptors**. *Kidney international*, **45**:177–177, 1994. 58

[281] M. J. Guertin and J. T. Lis. **Chromatin landscape dictates HSF binding to target DNA elements.** *PLoS genetics*, **6**(9), 2010. 58

[282] D. Gratecos, C. Naidet, M. Astier, J. Thiery, and M. Semeriva. **Drosophila fibronectin: a protein that shares properties similar to those of its mammalian homologue.** *The EMBO journal*, **7**(1):215, 1988. 59

[283] H. J. Yoo, C.-N. Im, D.-Y. Youn, H. H. Yun, and J.-H. Lee. **Bis is Induced by Oxidative Stress via Activation of HSF1**. *The Korean Journal of Physiology & Pharmacology*, **18**(5):403–409, 2014. 59

[284] J. Thyberg and A. Hultgårdh-Nilsson. **Fibronectin and the basement membrane components laminin and collagen type IV influence the phenotypic properties of subcultured rat aortic smooth muscle cells differently**. *Cell and tissue research*, **276**(2):263–271, 1994. 59

[285] D. Hanahan and R. A. Weinberg. **Hallmarks of cancer: the next generation**. *Cell*, **144**(5):646–674, 2011. 60

[286] J. A. Cook, D. Gius, D. A. Wink, M. C. Krishna, A. Russo, and J. B. Mitchell. **Oxidative stress, redox, and the tumor microenvironment**. In *Seminars in radiation oncology*, **14**, pages 259–266. Elsevier, 2004. 60

[287] P. Friedl and K. Wolf. **Tumour-cell invasion and migration: diversity and escape mechanisms**. *Nature Reviews Cancer*, **3**(5):362–374, 2003. 60

[288] D. Jia, M. Yan, X. Wang, X. Hao, L. Liang, L. Liu, H. Kong, X. He, J. Li, and M. Yao. **Development of a highly metastatic model that reveals a crucial role of fibronectin in lung cancer cell migration and invasion**. *Bmc Cancer*, **10**(1):364, 2010. 60

[289] X. Meng, Y. Jin, Y. Yu, J. Bai, G. Liu, J. Zhu, Y. Zhao, Z. Wang, F. Chen, K. Lee, et al. **Characterisation of fibronectin-mediated FAK signalling pathways in lung cancer cell migration and invasion**. *British journal of cancer*, **101**(2):327–334, 2009. 60

[290] P. Friedl and S. Alexander. **Cancer invasion and the microenvironment: plasticity and reciprocity.** *Cell*, **147**(5):992–991009, 2011. 60

[291] S. Han, F. R. Khuri, and J. Roman. **Fibronectin stimulates non-small cell lung carcinoma cell growth through activation of Akt/mammalian target of rapamycin/S6 kinase and inactivation of LKB1/AMP-activated protein kinase signal pathways**. *Cancer Res.*, **66**(1):315–323, Jan 2006. 60, 62

[292] L. David, J. M. Nesland, R. Holm, and M. Sobrinho-Simões. **Expression of laminin, collagen IV, fibronectin, and type IV collagenase in gastric carcinoma**. *Cancer*, **73**(3):518–527, 1994. 60

[293] A. Östman and M. Augsten. **Cancer-associated fibroblasts and tumor growth–bystanders turning into key players**. *Current opinion in genetics & development*, **19**(1):67–73, 2009. 60

[294] C.-M. Lo, H.-B. Wang, M. Dembo, and Y.-l. Wang. **Cell movement is guided by the rigidity of the substrate**. *Biophysical journal*, **79**(1):144–152, 2000. 60

[295] D. F. Mosher. **Cross-linking of fibronectin to collagenous proteins**. In *Transglutaminase*, pages 63–68. Springer, 1984. 60

[296] M. Prager-Khoutorsky, A. Lichtenstein, R. Krishnan, K. Rajendran, A. Mayo, Z. Kam, B. Geiger, and A. D. Bershadsky. **Fibroblast polarization is a matrix-rigidity-dependent process controlled by focal adhesion mechanosensing**. *Nature cell biology*, **13**(12):1457–1465, 2011. 60

[297] R. A. Clark. **Fibronectin matrix deposition and fibronectin receptor expression in healing and normal skin**. *Journal of Investigative Dermatology*, **94**:128s–134s, 1990. 60

[298] Y. Kojima, A. Acar, E. N. Eaton, K. T. Mellody, C. Scheel, I. Ben-Porath, T. T. Onder, Z. C. Wang, A. L. Richardson, R. A. Weinberg, et al. **Autocrine TGF-β and stromal cell-derived factor-1 (SDF-1) signaling drives the evolution of tumor-promoting mammary stromal myofibroblasts**. *Proceedings of the National Academy of Sciences*, **107**(46):20009–20014, 2010. 60

[299] S. K. Calderwood, M. A. Khaleque, D. B. Sawyer, and D. R. Ciocca. **Heat shock proteins in cancer: chaperones of tumorigenesis**. *Trends in biochemical sciences*, **31**(3):164–172, 2006. 60

[300] N. L. Solimini, J. Luo, and S. J. Elledge. **Non-oncogene addiction and the stress phenotype of cancer cells**. *Cell*, **130**(6):986–988, 2007. 60

[301] T. K. Maity, M. M. Henry, M. E. Tulapurkar, N. G. Shah, J. D. Hasday, and I. S. Singh. **Distinct, gene-specific effect of heat shock on heat shock factor-1 recruitment and gene expression of CXC chemokine genes**. *Cytokine*, **54**(1):61–67, 2011. 61

[302] B. Henderson and F. Kaiser. **Do reciprocal interactions between cell stress proteins and cytokines create a new intra-/extra-cellular signalling nexus?** 2013. 61

[303] H. Sasaki, T. Sato, N. Yamauchi, T. Okamoto, D. Kobayashi, S. Iyama, J. Kato, T. Matsunaga, R. Takimoto, T. Takayama, et al. **Induction of heat shock protein 47 synthesis by TGF-β and IL-1β via enhancement of the heat shock element binding activity of heat shock transcription factor 1**. *The Journal of Immunology*, **168**(10):5178–5183, 2002. 61, 62

[304] A. Bateman. **Growing a tumor stroma: a role for granulin and the bone marrow**. *The Journal of Clinical Investigation*, **121**(2):516, 2011. 61

[305] S. S. McAllister and R. A. Weinberg. **Tumor-host interactions: a far-reaching relationship**. *Journal of Clinical Oncology*, **28**(26):4022–4028, 2010. 61

[306] R. N. Kaplan, R. D. Riba, S. Zacharoulis, A. H. Bramley, L. Vincent, C. Costa, D. D. MacDonald, D. K. Jin, K. Shido, S. A. Kerns, et al. **VEGFR1-positive haematopoietic bone marrow progenitors initiate the pre-metastatic niche**. *Nature*, **438**(7069):820–827, 2005. 61

[307] P. Kahn and S.-I. Shin. **Cellular tumorigenicity in nude mice. Test of associations among loss of cell-surface fibronectin, anchorage independence, and tumor-forming ability.** *The Journal of cell biology*, **82**(1):1–16, 1979. 61

[308] J. R. Couchman, D. A. Rees, M. R. Green, and C. G. Smith. **Fibronectin has a dual role in locomotion and anchorage of primary chick fibroblasts and can promote entry into the division cycle.** *The Journal of cell biology*, **93**(2):402–410, 1982. 61

[309] A. Yano, S. Tsutsumi, S. Soga, M.-J. Lee, J. Trepel, H. Osada, and L. Neckers. **Inhibition of Hsp90 activates osteoclast c-Src signaling and promotes growth of prostate carcinoma cells in bone**. *Proceedings of the National Academy of Sciences*, **105**(40):15541–15546, 2008. 61

[310] J. T. Price, J. M. Quinn, N. A. Sims, J. Vieusseux, K. Waldeck, S. E. Docherty, D. Myers, A. Nakamura, M. C. Waltham, M. T. Gillespie, et al. **The heat shock protein 90 inhibitor, 17-allylamino-17-demethoxygeldanamycin, enhances osteoclast formation and potentiates bone metastasis of a human breast cancer cell line**. *Cancer research*, **65**(11):4929–4938, 2005. 61

[311] A. R. Heydari, S. You, R. Takahashi, A. Gutsmann, K. D. Sarge, and A. Richardson. **Effect of caloric restriction on the expression of heat shock protein 70 and the activation of heat shock transcription factor 1**. *Developmental genetics*, **18**(2):114–124, 1996. 61

[312] M. Laplante and D. M. Sabatini. **Regulation of mTORC1 and its impact on gene expression at a glance**. *Journal of cell science*, **126**(8):1713–1719, 2013. 61

[313] F. Das, N. Ghosh-Choudhury, N. Dey, A. Bera, M. M. Mariappan, B. S. Kasinath, and G. G. Choudhury. **High Glucose Forces a Positive Feed Back Loop Connecting Akt Kinase and FoxO1 to Activate mTORC1 for Mesangial Cell Hypertrophy and Matrix Protein Expression**. *Journal of Biological Chemistry*, pages jbc–M114, 2014. 61, 62

[314] R. H. Kim, M. Peters, Y. Jang, W. Shi, M. Pintilie, G. C. Fletcher, C. DeLuca, J. Liepa, L. Zhou, B. Snow, et al. **DJ-1, a novel regulator of the tumor suppressor PTEN**. *Cancer cell*, **7**(3):263–273, 2005. 61

[315] F. Das, N. Dey, B. Venkatesan, B. S. Kasinath, N. Ghosh-Choudhury, and G. G. Choudhury. **High glucose upregulation of early-onset Parkinson's disease protein DJ-1 integrates the PRAS40/TORC1 axis to mesangial cell hypertrophy**. *Cellular signalling*, **23**(8):1311–1319, 2011. 61

[316] N. Dey, N. Ghosh-Choudhury, F. Das, X. Li, B. Venkatesan, J. L. Barnes, B. S. Kasinath, and G. Ghosh Choudhury. **PRAS40 acts as a nodal regulator of high glucose-induced TORC1 activation in glomerular mesangial cell hypertrophy**. *Journal of cellular physiology*, **225**(1):27–41, 2010. 61

[317] D. Feliers, S. Duraisamy, J. L. Faulkner, J. Duch, A. V. Lee, H. E. Abboud, G. G. Choudhury, and B. S. Kasinath. **Activation of renal signaling pathways in db/db mice with type 2 diabetes**. *Kidney international*, **60**(2):495–504, 2001. 61

[318] T. Nakamura, D. Miller, E. Ruoslahti, and W. A. Border. **Production of extracellular matrix by glomerular epithelial cells is regulated by transforming growth factor-bold beta**. *Kidney international*, **41**:1213–1221, 1992. 61

[319] Y. S. Kim, D. H. Jung, N. H. Kim, Y. M. Lee, and J. S. Kim. **Effect of magnolol on TGF-β1 and fibronectin expression in human retinal pigment epithelial cells under diabetic conditions**. *European journal of pharmacology*, **562**(1):12–19, 2007. 61

[320] D. Zhang, S. Shao, H. Shuai, Y. Ding, W. Shi, D. Wang, and X. Yu. **SDF-1α reduces fibronectin expression in rat mesangial cells induced by TGF-β1 and high glucose through PI3K/Akt pathway**. *Experimental cell research*, **319**(12):1796–1803, 2013. 61

[321] M. Steffes, D. Brown, J. Basgen, A. Matas, and S. Mauer. **Glomerular basement membrane thickness following islet transplantation in the diabetic rat.** *Laboratory investigation; a journal of technical methods and pathology*, **41**(2):116–118, 1979. 61

[322] S. H. Ayo, R. A. Radnik, J. A. Garoni, W. Glass 2nd, and J. Kreisberg. **High glucose causes an increase in extracellular matrix proteins in cultured mesangial cells.** *The American journal of pathology*, **136**(6):1339, 1990. 61

[323] S. Cherian, S. Roy, A. Pinheiro, and S. Roy. **Tight glycemic control regulates fibronectin expression and basement membrane thickening in retinal and glomerular capillaries of diabetic rats**. *Investigative ophthalmology & visual science*, **50**(2):943–949, 2009. 61

[324] X. Li, W. Liu, Q. Wang, P. Liu, Y. Deng, T. Lan, X. Zhang, B. Qiu, H. Ning, and H. Huang. **Emodin suppresses cell proliferation and fibronectin expression via p38MAPK pathway in rat mesangial cells cultured under high glucose**. *Molecular and cellular endocrinology*, **307**(1):157–162, 2009. 62

[325] C. Gelbmann, S. Mestermann, V. Gross, M. Köllinger, J. Schölmerich, and W. Falk. **Strictures in Crohns disease are characterised by an accumulation of mast cells colocalised with laminin but not with fibronectin or vitronectin**. *Gut*, **45**(2):210–217, 1999. 62

[326] F. H. Epstein, W. A. Border, and N. A. Noble. **Transforming growth factor β in tissue fibrosis**. *New England Journal of Medicine*, **331**(19):1286–1292, 1994. 62

[327] E. G. Noble and G. X. Shen. **Impact of exercise and metabolic disorders on heat shock proteins and vascular inflammation**. *Autoimmune diseases*, **2012**, 2012. 62

[328] K. E. Wellen, G. S. Hotamisligil, et al. **Inflammation, stress, and diabetes**. *Journal of Clinical Investigation*, **115**(5):1111–1119, 2005. 62

[329] R. Zhao, S. Ren, M. H. Moghadasain, J. D. Rempel, and G. X. Shen. **Involvement of fibrinolytic regulators in adhesion of monocytes to vascular endothelial cells induced by glycated LDL and to aorta from diabetic mice**. *Journal of leukocyte biology*, **95**(6):941–949, 2014. 62

[330] C. B. Collins, C. M. Aherne, A. Yeckes, K. Pound, H. K. Eltzschig, P. Jedlicka, and E. F. d Zoeten. **Inhibition of N-terminal ATPase on HSP90 attenuates colitis through enhanced Treg function**. *Mucosal immunology*, **6**(5):960–971, 2013. 62, 65

[331] J. D. Hasday and I. S. Singh. **Fever and the heat shock response: distinct, partially overlapping processes**. *Cell stress & chaperones*, **5**(5):471, 2000. 62

[332] S. Dai, Z. Tang, J. Cao, W. Zhou, H. Li, S. Sampson, and C. Dai. **Suppression of the HSF1-mediated proteotoxic stress response by the metabolic stress sensor AMPK**. *The EMBO journal*, 2014. 62

[333] C. R. Kliment and T. D. Oury. **Oxidative stress, extracellular matrix targets, and idiopathic pulmonary fibrosis**. *Free Radical Biology and Medicine*, **49**(5):707–717, 2010. 62

[334] M. Li, D. Georgakopoulos, G. Lu, L. Hester, D. A. Kass, J. Hasday, and Y. Wang. **p38 MAP kinase mediates inflammatory cytokine induction in cardiomyocytes and extracellular matrix remodeling in heart**. *Circulation*, **111**(19):2494–2502, 2005. 62

[335] U. Kucich, J. C. Rosenbloom, G. Shen, W. R. Abrams, A. D. Hamilton, S. M. Sebti, and J. Rosenbloom. **TGF-β1 stimulation of fibronectin transcription in cultured human lung fibroblasts requires active geranylgeranyl transferase I, phosphatidylcholine-specific phospholipase C, protein kinase C-δ, and p38, but not erk1/erk2**. *Archives of biochemistry and biophysics*, **374**(2):313–324, 2000. 62

[336] P. Widłak, M. Gramatyka, and M. Kimmel. **Crosstalk between stress-induced NF-κB, p53 and HSF1 signaling pathways–review.** 2014. 62

[337] S. M. Greenberg. **Cerebral amyloid angiopathy Prospects for clinical diagnosis and treatment**. *Neurology*, **51**(3):690–694, 1998. 62

[338] H. Akiyama, T. Arai, H. Kondo, E. Tanno, C. Haga, and K. Ikeda. **Cell mediators of inflammation in the Alzheimer disease brain**. *Alzheimer Disease & Associated Disorders*, **14**(1):S47–S53, 2000. 62

[339] H. Akiyama, S. Barger, S. Barnum, B. Bradt, J. Bauer, G. M. Cole, N. R. Cooper, P. Eikelenboom, M. Emmerling, B. L. Fiebich, et al. **Inflammation and Alzheimers disease**. *Neurobiology of aging*, **21**(3):383–421, 2000. 62

[340] J. A. Burlison, C. Avila, G. Vielhauer, D. J. Lubbers, J. Holzbeierlein, and B. S. Blagg. **Development of novobiocin analogues that manifest antiproliferative activity against several cancer cell lines**. *The Journal of organic chemistry*, **73**(6):2130–2137, 2008. 64

[341] S. Kummar, M. E. Gutierrez, E. R. Gardner, X. Chen, W. D. Figg, M. Zajac-Kaye, M. Chen, S. M. Steinberg, C. A. Muir, M. A. Yancey, et al. **Phase I trial of 17-dimethylaminoethylamino-17-demethoxygeldanamycin (17-DMAG), a heat shock protein inhibitor, administered twice weekly in patients with advanced malignancies**. *European Journal of Cancer*, **46**(2):340–347, 2010. 64

[342] M. A. Smith, C. L. Morton, D. A. Phelps, E. A. Kolb, R. Lock, H. Carol, C. P. Reynolds, J. M. Maris, S. T. Keir, J. Wu, et al. **Stage 1 testing and pharmacodynamic evaluation of the HSP90 inhibitor alvespimycin (17-DMAG, KOS-1022) by the pediatric preclinical testing program**. *Pediatric blood & cancer*, **51**(1):34–41, 2008. 64

[343] S. Pacey, R. H. Wilson, M. Walton, M. M. Eatock, A. Hardcastle, A. Zetterlund, H.-T. Arkenau, J. Moreno-Farre, U. Banerji, B. Roels, et al. **A phase I study of the heat shock protein 90 inhibitor alvespimycin (17-DMAG) given intravenously to patients with advanced solid tumors**. *Clinical Cancer Research*, **17**(6):1561–1570, 2011. 64

[344] E. A. Sausville, J. E. Tomaszewski, and P. Ivy. **Clinical development of 17-allylamino, 17-demethoxygeldanamycin**. *Current cancer drug targets*, **3**(5):377–383, 2003. 64

[345] A. Donnelly and B. Blagg. **Novobiocin and additional inhibitors of the Hsp90 C-terminal nucleotide-binding pocket**. 2008. 64

[346] J.-H. Lee, J. Gao, P. A. Kosinski, S. J. Elliman, T. E. Hughes, J. Gromada, and D. M. Kemp. **Heat shock protein 90 (HSP90) inhibitors activate the heat shock factor 1 (HSF1) stress response pathway and improve glucose regulation in diabetic mice**. *Biochemical and biophysical research communications*, **430**(3):1109–1113, 2013. 65

[347] Y. Chen, B. Wang, D. Liu, J. J. Li, Y. Xue, K. Sakata, L. Q. Zhu, S. A. Heldt, H. Xu, and F. F. Liao. **Hsp90 chaperone inhibitor 17-AAG attenuates A-induced synaptic toxicity and memory impairment**. *J. Neurosci.*, **34**(7):2464–2470, Feb 2014. 65

[348] G. Donmez, A. Arun, C.-Y. Chung, P. J. McLean, S. Lindquist, and L. Guarente. **SIRT1 protects against α-synuclein aggregation by activating molecular chaperones**. *The Journal of Neuroscience*, **32**(1):124–132, 2012. 65

[349] A. R. Heydari, S. You, R. Takahashi, A. Gutsmann-Conrad, K. D. Sarge, and A. Richardson. **Age-related alterations in the activation of heat shock transcription factor 1 in rat hepatocytes**. *Experimental cell research*, **256**(1):83–93, 2000. 65

[350] K. Kilpatrick, J. A. Novoa, T. Hancock, C. J. Guerriero, P. Wipf, J. L. Brodsky, and L. Segatori. **Chemical induction of Hsp70 reduces α-synuclein aggregation in neuroglioma cells**. *ACS chemical biology*, **8**(7):1460–1468, 2013. 65

[351] Y.-Q. Jiang, X.-L. Wang, X.-H. Cao, Z.-Y. Ye, L. Li, and W.-Q. Cai. **Increased heat shock transcription factor 1 in the cerebellum reverses the deficiency of Purkinje cells in Alzheimer's disease**. *Brain research*, **1519**:105–111, 2013. 65

[352] X. Liangliang, H. Yonghui, E. Shunmei, G. Shoufang, Z. Wei, and Z. Jiangying. **Dominant-positive HSF1 decreases alpha-synuclein level and alpha-synuclein-induced toxicity**. *Molecular biology reports*, **37**(4):1875–1881, 2010. 65

[353] J. Muenchhoff, A. Poljak, F. Song, M. Raftery, H. Brodaty, M. Duncan, M. McEvoy, J. Attia, P. W. Schofield, and P. S. Sachdev. **Plasma Protein Profiling of Mild Cognitive Impairment and Alzheimer's Disease Across Two Independent Cohorts**. *J. Alzheimers Dis.*, Aug 2014. 65

[354] J. Wang and R. Milner. **Fibronectin promotes brain capillary endothelial cell survival and proliferation through α5β1 and αvβ3 integrins via MAP kinase signalling**. *Journal of neurochemistry*, **96**(1):148–159, 2006. 66

[355] R. C. Rintoul and T. Sethi. **Extracellular matrix regulation of drug resistance in small-cell lung cancer**. *Clinical Science*, **102**(4):417–424, 2002. 66

[356] H. Xing, D. Weng, G. Chen, W. Tao, T. Zhu, X. Yang, L. Meng, S. Wang, Y. Lu, and D. Ma. **Activation of fibronectin/PI-3K/Akt2 leads to chemoresistance to docetaxel by regulating survivin protein expression in ovarian and breast cancer cells**. *Cancer letters*, **261**(1):108–119, 2008. 66

5

Appendix

5.1 Cytotoxicity assays

In order to determine the concentration at which different compounds used in this study were toxic to Hs578T cells, WST-1 cell proliferation assays were conducted. Hs578T cells were treated with different concentrations of GA, NOV and rapamycin. WST-1 reagent was added to each well after 48 h of treatment and was incubated for for 4 h at 37 °C. Absorbance was then measured and the data obtained were analysed in GraphPad Prism 4 and EC_{50} values were calculated. Data for each compound are displayed as dose response curves, with percentage cell survival plotted against the log treatment concentration.

GA treatment of Hs578T cells for 48 h yielded an EC_{50} value of 4925 nM, NOV had 282.5 μM in the same assay conditions. Rapamycin treatment showed an EC_{50} value of 8.838 μM. These concentration values were all at least 5-fold higher than the concentrations used in the various experiments during the present study.

5.2 qPCR housekeeping gene validation

In order to conduct qPCR analysis using the $\Delta\Delta$Ct method, two housekeeping genes must be assayed in addition to the gene of interest. As outlined in the calculation section below, these are used as normalising (or non-targeting) controls to which the gene of interest can be compared. For optimal analysis, the levels housekeeping genes should not change significantly between the control and experimental conditions.

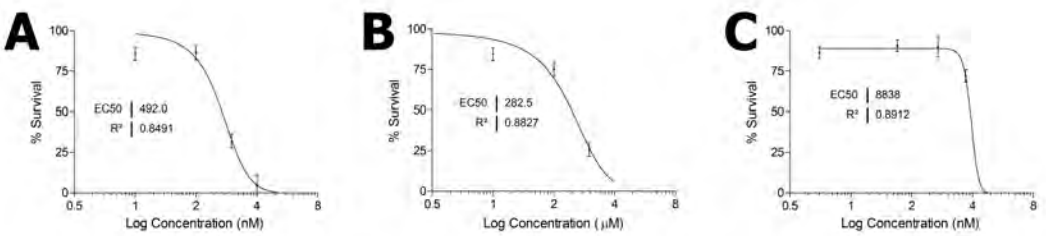

Figure 5.1: WST1 cytotoxicity assays - Hs578T cells were treated with concentrations of geldanamycin from 0 nM - 100 μM, novobiocin between 0 μM - 10 mM or rapamycin between 0 nM - 50 μM. WST-1 reagent was added to each well after 48 h of treatment and was incubated for for 4 h at 37 °C. Absorbance was then measured and the data obtained were analysed in GraphPad Prism 4. EC_{50} values of 492 nM (R^2: 0.8491) for geldanamycin (**A**), 282.5 μM (R^2: 0.8827) for novobiocin (**B**), and 8.838 μM (R^2: 0.8912) for rapamycin (**C**) were determined.

Four genes for proteins that conduct cellular housekeeping functions were selected for analysis; *ACTB*, *GAPDH*, *HRPT* and *PPIA*. Hs578T cells were treated with 100 μM NOV, 10 nM GA or DMSO. Total RNA was extracted 24 hours after treatment and cDNA synthesis was conducted. cDNA from equal amounts of RNA from each treatment were assayed for housekeeping gene levels by qPCR. Data were analysed in BioRAD CFX Manager 3.1 Software, and is displayed in Figure 5.2.

ACTB and *PPIA* were the two genes to change the least upon treatment of cells with Hsp90 inhibitors compared with DMSO treatment, with a standard deviation of the average Ct values of 0.372201 and 0.425245 respectively. *GAPDH* did not change greatly following treatment with GA, however a loss of GAPDH RNA upon NOV treatment made this gene unsuitable for use as a non-targeting control. HRPT showed great variability upon GA treatment and had a large average Ct standard deviation (1.865083) across treatments, and was therefore similarly unsuitable for use as a housekeeping gene in subsequent qPCR assays. As an additional control for qPCR assays making use of the ΔCt method, a housekeeping gene was also analysed, in order to ensure equal cDNA loading. Interestingly during experiments in which cells were treated with rapamycin, PPIA RNA varied greatly between control and test conditions. PPIA plays an important role in metabolic regulation in hepatic cells, and therefore changes in RNA levels upon mTOR inhibition might be expected. ACTB was therefore used

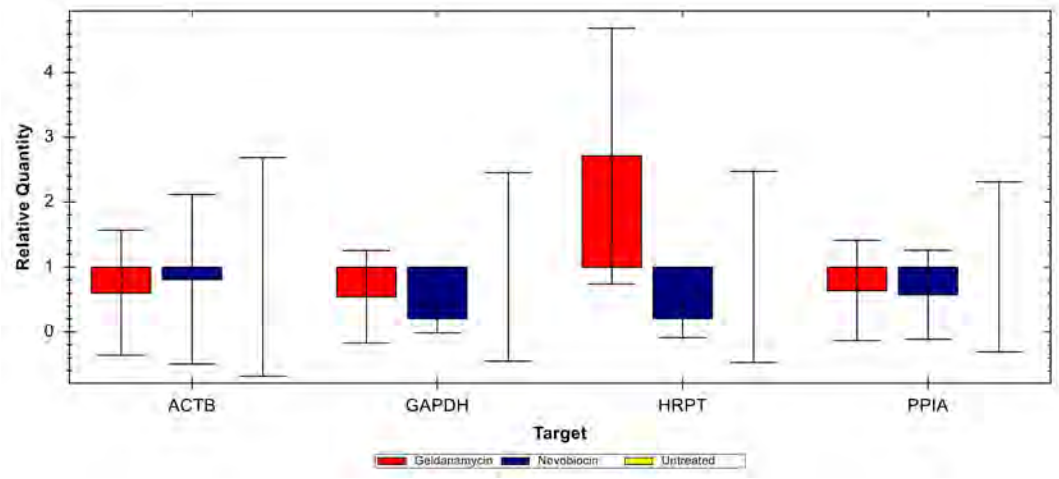

Figure 5.2: ACTB and PPIA are the most stable housekeeping genes under Hsp90 inhibition test conditions - Hs578T cells were treated with 100 μM NOV, 10 nM GA or DMSO. total RNA was extracted and cDNA synthesis was conducted as previously described. qPCR analyses of the levels of housekeeping genes under treatment relative to the untreated samples are displayed. The standard deviation in the average Ct values across treatments were determined: *ACTB* (0.372201), *GAPDH* (1.155177), *HRPT* (1.865083) and *PPIA* (0.425245).

for these experiments.

5.3 Cloning of pGL4-pFN1

The *FN1* promoter was synthesised and obtained in the pUC57 vector. The *FN1* promoter sequence was modified at the 5' end to contain an *Nhe*I restriction site, and at the 3' end to contain a *Bgl*II restriction site. As outlined in the schematic diagram in Figure 5.3 A, these two enzymes were used to digest the FN promoter insert out from the pUC57 vector. The same sites were found in the multiple cloning site on the pGL4.17 vector, upstream of the *luc2* luciferase reported gene. These sites were exploited in order to ligate the FN promoter insert into the pGL4.17 vector in the correct orientation.

In order to confirm the successful sub-cloning of the FN promoter insert to create the pGL4-pFN1 vector, the vector produced was digested with *Acc*65I alone, and with *Bgl*II and *Nhe*I in combination. These digests were resolved and visualised on an agarose gel (Figure 5.3 B) in order to confirm the insertion. The correct orientation of

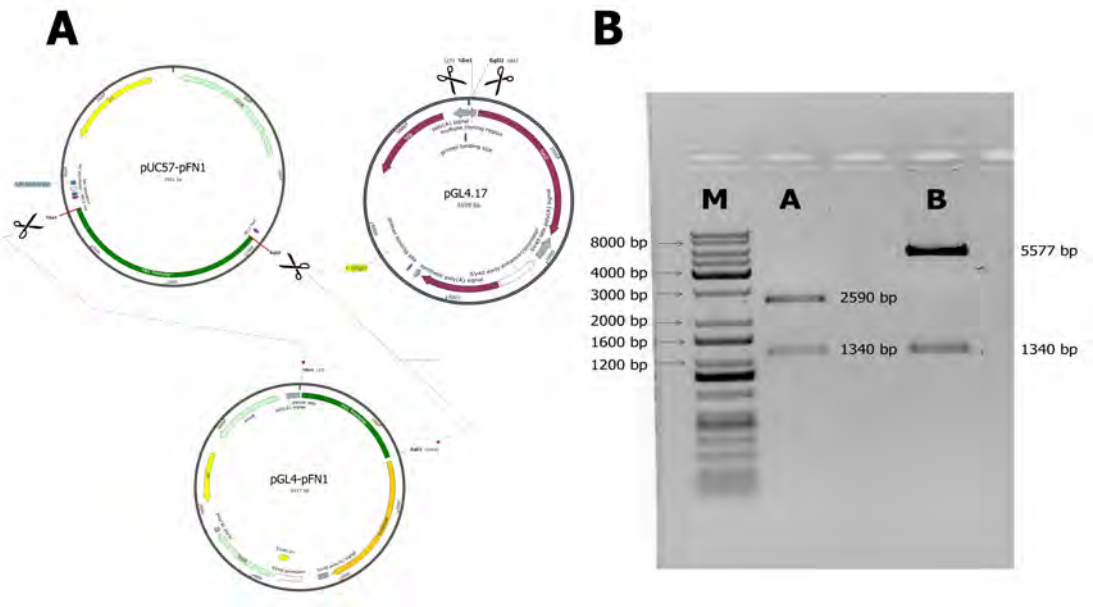

Figure 5.3: The strategy and confirmation restriction digest for sub-cloning of the *FN1* promoter sequence into the promoterless luciferase reporter vector pGL4.17 - **A** The synthesised *FN1* promoter was contained in the pUC57 vector with a 5' *Nhe*I and a 3' *Bgl*II restriction site at either end of the *FN1* promoter. The pGL4.17 promoterless reporter vector (Promega) was digested using *Nhe*I and *Bgl*II prior to ligation of the pFN1 promoter insert into the pGL4.17 backbone. The pGL4-pFN1 reporter vector was confirmed by sequencing. **B** Successful sub-cloning of the FN promoter insert to create the pGL4-pFN1 vector was confirmed using restriction digestion of the original pUC57-pFN1 vector and the product vector and resolution on a 1 % (w/v) agarose gel. pUC57-pFN1 was digested with both *Bgl*II and *Nhe*I to yield the pUC57 backbone (2590 bp) and the pFN1 insert (1340 bp)(**A**). The pFN1 insert was subcloned into the pGL4 promoterless reporter vector and the construct pGL4-pFN1 was confirmed with a digestion using both *Bgl*II and *Nhe*I to yield the pGL4 backbone (5577 bp) and the pFN1 insert (1340 bp)(**B**). (**M**) was the KAPA Universal DNA Ladder.

the insert was confirmed by sequencing. The pGL4.17 vector was 5,599 bp in size and the insert was 1,340 bp in size.

5.4 Chromatin shearing optimisation

The optimal duration for digestion of chromatin with DNAseI was determined. Cross-linked chromatin was extracted from Hs578T cells as previously described. The chromatin was then used in a digestion reaction using 0.05 U DNAseI per μg of chromatin at 37 °C. At 10 min intervals, aliquots of the digestion were removed and the reaction was stopped by the addition of EDTA to 5 mM. After 100 mins, all of the chromatin digest aliquots were further heat-inactivated at 95 °C for 60 mins. This heat treatment also reversed the formaldehyde cross-linking. The resulting prepared chromatin was resolved on a 2 % (m/v) agarose gel (Figure 5.4). Digestion using DNAseI resulted in an increasing amount of DNA fragments with a length smaller than 500 bp with increasing reaction time. After only 10 min of incubation with DNAseI, a substantial amount of chromatin degradation can be observed (Figure 5.4), with a loss in intensity in the low MW region as treatment time increases. A persistent high MW band is visible across all treatment times.

Some chromatin remains inaccessible to DNAseI during the digestion reaction as is apparent from the visible high MW band in all lanes in Figure 5.4. This is likely due to proteins cross-linked to the DNA. Total degradation of the smaller DNA fragments is visible at the 90 and 100 min time points, whereas earlier time points show an abundance of 500 bp to 100 bp DNA fragments.

Occupancy of purported HSE1 (pHSE1) by HSF1 was tested using a ChIP assay. Hs578T cells were treated with either DMSO or 100 nM GA ChIP was conducted using an Imprint UltraChromatin Immunoprecipitation kit (Sigma-Aldrich). The product of the pHSE1 qPCR product was sent for sequencing in order to confirm its identity as the relevant region upstream of *FN1*. The sequencing results were analysed using BLASTn and the sequence identities of all results are summarised in Table 5.1. The only matching DNA identified by the alignment tool were from 1295 bp on the 5' side of *FN1* on chromosome 2 (216307679 bp to 216307756 bp), confirming the HSF1 bound DNA as HSE1; -965 bp to -951 bp on the *FN1* promoter.

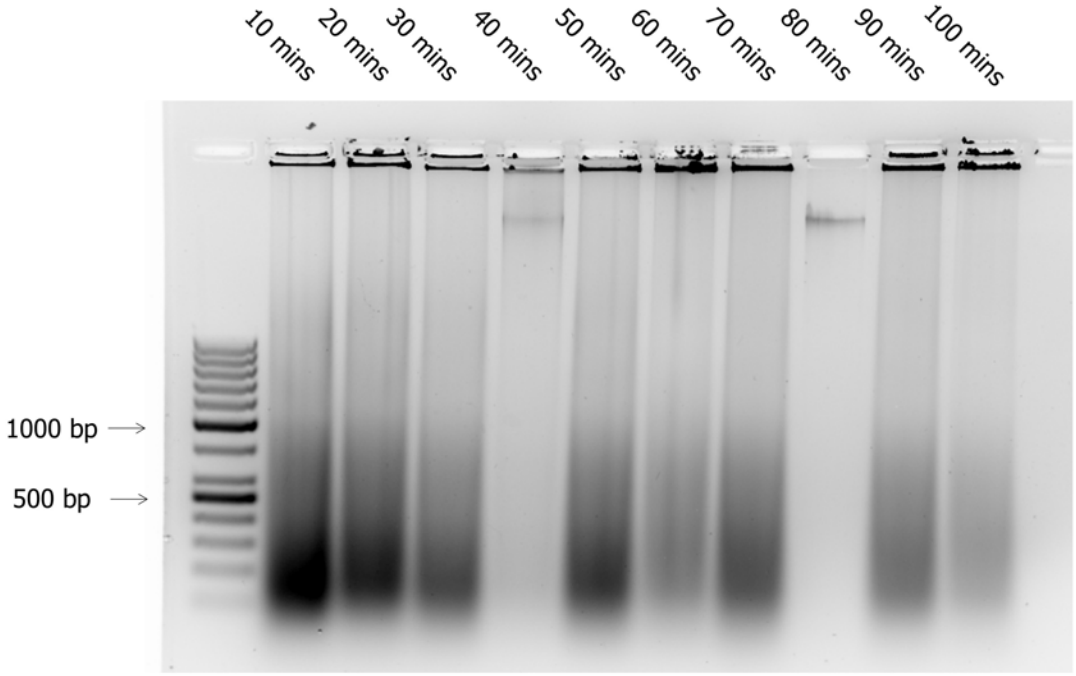

Figure 5.4: Validation of chromatin preparation using DNAseI digestion - Hs578T cells were treated with either 100 nM GA or the vehicle control. 24 hours post-treatment the cells were harvested and formaldehyde (1 %) was used to cross-link DNA and protein. The chromatin was sheared using DNAseI treatment (0.05 U/μg DNA) at 37 °C for different periods of time after which the fragmentation reaction was arrested using EDTA (5 mM) and heat inactivation for 1 hour at 95 °C which also served to reverse the cross-linking. Products were run on a 2 % (w/v) agarose gel.

Table 5.1: BLAST results pHSE1 sequence.

Description	Identity	E-value	Accession
HS chr2, Alt. Ass. CHM1_1.1 - 1176 bp at 5' side of FN isoform 7 preproprotein	100 %	2e-32	NC018913.2
HS chr2, Alt. Ass. HuRef - 1176 bp at 5' side: FN isoform 7 preproprotein	100 %	2e-32	AC000134.1
HS chr2, GRCh38 Pri. Ass. - 1180 bp at 5' side: FN isoform 7 preproprotein	100 %	2e-32	NC000002.12

5.5 RT-PCR of FN mRNA transcript splice variants

The relative proportions of FN mRNA splice variants was investigated by RT-PCR analysis of FN mRNA using exon flanking primers adapted from Kilian *et al.* (2004)(271). Hs578T cells were treated with Hsp90 inhibitors and RNA processed as previously described. The primers were used five separate PCR reactions per cDNA sample and were conducted such that the reactions were non saturated. Primer pairs were each expected to yield a number of bands and these anticipated products are detailed in Table 5.2.

The PCR products were resolved and visualised using agarose gel electrophoresis and a representative example of the resulting bands are shown in Figure 5.5. A single band at 419 bp is visible in the III9 lane, corresponding to an exon in the FN primary transcript which is included in all FN splice variants. In the ED-B and ED-A lanes, higher and lower MW bands correspond to extra domain exon inclusive, and exclusive splice variants respectively. Primers CS1 and CS2 produce products from the area of exon 39 including IIICS 360 bp, IIICS 267 bp, IIICS 192 bp and IIICS 0 bp. Primers CS1 and CS3 produce two products corresponding to IIICS 360 bp and IIICS 267 bp. Primer pair CS2 and CS4 also produce two products corresponding to the IIICS 360 bp and IIICS 285 bp splice variants. The relative band intensities of bands in the same lane were analysed using densitometry in ImageJ 1.42I and the percentage composition of each alternately spliced exon as a proportion of total FN, as detected by the III9 exon which is present in all FN splice variants. Calculations are outlined in the calculation section below.

The PCR products corresponding to the IIICS variable region splice variants were isolated by gel excision and analysed by direct sequencing. These sequences were then aligned with the full length FN mRNA transcript (NM_212482) in order to identify the locations of splice junctions within the IIICS exon. These results are summarised in Figure 5.6.

Exon 39 of the *FN1* primary transcript is 360 bp long and has five splice variants designated IIICS 0 bp, IIICS 192 bp, IIICS 267 bp, IIICS 285 bp and IIICS 360 bp, according to the size of the included fragment (Figure 3.9 D). IIICS 0 bp is the complete exclusion of the exon, and IIICS 360 bp is the complete inclusion. The three partially included fragments are structured as follows: IIICS 192 bp has both a 5' 72 bp and a

Table 5.2: The expected band sizes from primer pairs used in the RT-PCR analysis of FN splice variant mRNA composition upon treatment with Hsp90 inhibitors

Variant	Exon Location	Size	Primers	Expected Products
III9	Exon 27 (4609bp to 4878bp)	270bp	III9F & III9R	419bp
ED-B+	Exon 24 (4063bp to 4335bp)	273bp	EDBF & EDBR	775bp
ED-B-		0bp		502bp
ED-A+	Exon 32 (5431bp to 5700bp	270bp	EDAF & EDAR	604bp
ED-A-		0bp		334bp
IIICS 360bp	Exon 39 (6514bp to 6980bp)	360bp	CS1 & CS2, CS1 & CS3, CS2 & CS4	796bp, 710bp, 393bp
IIICS 285bp		285bp	CS2 & CS4	318bp
IIICS 267bp		267bp	CS1 & CS2, CS1 & CS3	703bp, 617bp
IIICS 192bp		192bp	CS1 & CS2	628bp
IIICS 0bp		0bp	CS1 & CS2	436bp

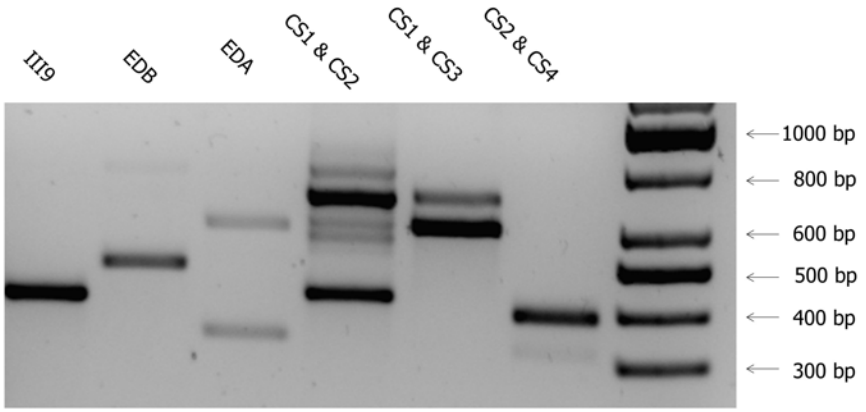

Figure 5.5: Example of RT-PCR analysis of a single sample - Hs578T cells were treated and extracted mRNA was analysed according to the RT-PCR splice variant experiments described. The band sizes visualised using agarose gel (1.5 % w/v) electrophoresis from primer pairs listed in Table 2.5 match the expected products as described in Table 5.2. Band identities were confirmed using direct sequencing.

3' 90 bp truncation. The IIICS 267 bp splice variant has only the 3' 90 bp truncation, and the IIICS 285 bp splice variant has only the 5' 72 bp truncation (Figure 5.6).

5.6 Promoter HSE analysis

We investigated potential responsiveness of a number of other extracellular matrix proteins (ECMs) to GA treatment. The -2000 bp to +1 bp promoter regions of known heat-shock inducible genes (*HSP90AA1*, *HSPA1A*, *HSPB1*(55), stress related transcription factors (*HSF1*, *HIF1A*)(30)(272) and a subset of key extracellular matrix protein genes (lamanin beta 3 [*LAMB3*], lamanin gamma 2 [*LAMC2*], collagen 4 alpha 2 [*COL4A2*], collagen 4 alpha 3 [*COL4A3*], elastin [*ELN*], vitronectin [*VTN*] and osteopontin [*SPP1*])(141)(140)(273) were obtained from the Ensemble database and screened for potential HSEs using TFSearch. The results from this analysis are presented in Table 5.3.

5.7 Calculations

5.7.1 qPCR calculations

$$\Delta\text{Ct} = \text{Ct Target Gene} \quad \text{Ct Reference Gene}$$

Figure 5.6: Sequence for *FN1* exon 39 (IIICS / variable region) - Primers CS1 & CS2, CS1 & CS3, and CS2 & CS4 were used to produce PCR products from the sequence encoding FN exon 39. These had different MW corresponding to splice variants of the IIICS variable region; IIICS 360 bp, IIICS 285 bp, IIICS 267 bp, IIICS 192 bp and IIICS 0 bp (Table 5.2 & Figure 5.5). The PCR products corresponding to each splice variant were isolated and sequenced. Alignment of these products to a full length FN mRNA transcript was used in order to identify the locations of IIICS splice junctions. IIICS 0 bp is the complete exclusion of the exon, except the 5' sequence in bold font which is present in all isoforms tested. IIICS 360 bp is the complete inclusion of the full sequence given. The three partially included fragments are structured as follows: IIICS 192 bp has both a 5' 72 bp and a 3' 90 bp truncation, including only the underlined sequence and the sequence in bold font. The IIICS 267 bp splice variant has only the 3' 90 bp truncation, thus including the whole sequence given beginning with the underlined sequence. The IIICS 285 bp splice variant has only the 5' 72 bp truncation, thus excluding only the sequence between the underlined sequence and the sequence in bold font.

Table 5.3: Promoter purported HSE analysis

Gene Name	Ensemble ID	Total pHSEs	Distinct pHSE Sites	Locations Relative to TSS				
FN1	ENSG00000115414	7	3	-1353	-1101	-855		
LAMB3	ENSG00000196878	4	1	-1142				
LAMC2	ENSG00000058085	15	5	-1780	-1353	-1341	-246	-15
COL4A2	ENSG00000134871	8	3	-1408	-1369	-329		
COL4A3	ENSG00000169031	1	1	-1780				
ELN	ENSG00000049540	1	1	-1527				
VTN	ENSG00000109072	2	2	-1599	-1100			
SPP1	ENSG00000118785	5	3	-1952	-1695	-971		
HSF1	ENSG00000185122	1	1	-1107				
HIF1A	ENSG00000100644	1	1	-1164				
HSP90AA1	ENSG00000080824	4	2	-1590	-867			
HSP90AB1	ENSG00000096384	2	2	-841	-794			
HSPA1A	ENSG00000204389	14	6	-1581	-871	-653	-241	-120 -27
HSPB1	ENSG00000106211	3	1	-19				

$$\Delta\text{Ct Control} = \text{Ct Target Gene} - \text{Ct Reference Gene}$$
$$\Delta\text{Ct Test} = \text{Ct Target Gene} - \text{Ct Reference Gene}$$
$$\Delta\Delta\text{Ct} = \Delta\text{Ct Test} - \Delta\text{Ct Control}$$
$$\text{Normalised Expression Ratio (NER)} = 2^{-\Delta\Delta Ct}$$

Example:

$$\Delta\text{Ct} = \text{Ct (FN1)} - \text{Ct (ACTB)}$$
$$\Delta\text{Ct DMSO} = \text{Ct (FN1)} - \text{Ct (ACTB)}$$
$$\Delta\text{Ct GA (10 nM)} = \text{Ct (FN1)} - \text{Ct (ACTB)}$$
$$\Delta\Delta\text{Ct} = \Delta\text{Ct GA (10 nM)} - \Delta\text{Ct DMSO}$$
$$\text{NER} = 2^{-\Delta\Delta Ct} = \text{Fold change of FN1 with GA, relative to DMSO.}$$

5.7.2 ChIP calculations

Differences in chromatin sample preparation between experiments were accounted for by normalising to the Ct value of the same qPCR reaction conducted on the input DNA:

$$\Delta\text{Ct Normalised} = (\text{Ct Target ChIP} - \text{Ct Input DNA} - \text{Log}_2(\text{Input Dilution Factor}))$$

Where the Input Dilution Factor = (fraction of the input chromatin reserved)$^{-1}$. e.g. 1 % corresponds to a dilution factor of 100.

The normalized Ct values for each replicate PCR were then averaged for each ChIP, and these average normalised Ct values were then adjusted to account for signal background as determined by the isotype control for each ChIP antibody:

$$\Delta\Delta\text{Ct} = \Delta\text{Ct ChIP} - \Delta\text{Ct Isotype Control}$$

The fold enrichment for the target over the background signal was then calculated:

$$\text{Fold Enrichment} = 2^{-(\Delta\Delta)Ct}$$

Finally the fold enrichment of each treated ChIP sample was normalised to the vehicle control:

$$\text{Normalised Fold Enrichment} = \text{Fold Enrichment (GA ChIP)} / \text{Fold Enrichment (DMSO ChIP)}$$

5.7.3 RT-PCR splice variant calculations

The relative band intensities of bands in the same lane were analysed using densitometry in ImageJ 1.42I and the percentage composition of each alternately spliced exon as a proportion of total FN was determined as follows:

Extra Domain Exons -

$$\% \text{ ED+} = (\text{Band Area ED+} / (\text{Band Area ED+} + \text{Band Area ED-})) \times 100$$
$$\% \text{ ED-} = (\text{Band Area ED-} / (\text{Band Area ED+} + \text{Band Area ED-})) \times 100$$

Variable Region Exons -

Each band was normalised to the IIICS 360 bp band for that lane. The proportion of the sum of these values accounted for by a particular band, corresponded to the proportion of the transcripts containing the corresponding IIICS splice variant.

E.g.:

% IIICS 0 bp = [(436 bp Band Area / IIICS 360 bp Band Area) / (IIICS 285 bp Band Area + IIICS 267 bp Band Area + IIICS 192 bp Band Area + IIICS 0 bp Band Area) / IIICS 360 bp Band Area] $\times$ 100